

THESIS

GEOLOGY, ALTERATION AND PRECIOUS METAL RECONNAISSANCE
OF THE NOGAL CANYON AREA, SAN MATEO MTS., N.M.

Submitted by

Jon Foruria

Department of Earth Resources

In partial fulfillment of the requirements
for the Degree of Master of Science
Colorado State University
Fort Collins, Colorado
Summer 1984

ABSTRACT OF THESIS
GEOLOGY, ALTERATION AND PRECIOUS METAL RECONNAISSANCE
OF THE NOGAL CANYON AREA, SAN MATEO MTS., N.M.

The Nogal Canyon area lies within the southern San Mateo mountains and displays epithermal, volcanic hosted precious metal occurrences in the San Jose and Quartz Hill districts and in the Aragon Hill area. The San Mateos represent an isolated, north trending, eastward tilted, structural block located in the northeastern portion of the Cenozoic Mogollon-Datil volcanic field.

Mid-Tertiary, calc-alkalic andesites to high silica rhyolites and minor volcanoclastics dominate the lithologies exposed in the Nogal Canyon area. The Oligocene Spears Formation, the oldest unit present, consists of andesitic to latitic flows, breccias, and ash-flow tuff and sporadic volcanoclastic sandstone. The Hells Mesa rhyolite ash-flow tuff overlies the Spears Formation and is sequentially superimposed by the Unit of Luna Park which includes andesitic flows, dacite flow breccias, rhyolite tuff, and minor volcanoclastics. The majority of the upper felsic sequence exposed in the southern San Mateos consists of the Oligocene Vicks Peak Tuff, a thick, densely to partially welded rhyolite ash-flow tuff, and the overlying Springtime Canyon Quartz Latite. Younger

porphyritic rhyolite intrusives, rhyolite flow-dome rocks, and intrusive breccia appear localized along major structural trends within the southern foothills of the San Mateo mountains.

Major northeast and northwest trending, steeply dipping, normal faults crosscut the Vicks Peak Tuff and host "fissure-type" precious metal occurrences in the San Jose district. Structural preparation relates either to the proposed Nogal Canyon cauldron or to mid-late Tertiary regional extensional tectonism. Hydrothermal alteration effects contemporaneous with precious metal mineralization consist of pervasive and veinlet silicification, pervasive intermediate argillic alteration, and quartz-alunite replacement alteration. Silica alteration is strongly localized along fracture and breccia zones consisting of vein-infillings, pervasive wall rock alteration, and quartz network-stockwork type occurrences. The gangue mineral assemblage accompanying vein-infilling silicification includes adularia, sericite, calcite, pyrolusite, and cryptomelane. Intermediate argillic alteration consists of montmorillonite, montmorillonite-illite mixed layer, illite, kaolinite, and pyrite systematically zoned as reaction aureoles about major structures. Argillic alteration broadens beneath the Vicks Peak Tuff-Springtime Canyon Quartz Latite contact which acted as a permeability barrier to ascending hydrothermal solutions. Quartz-alunite alteration occurs as areally restricted, pervasive replacement deposits with accessory pyrite, specularite, kaolinite, and chalcedony. Mineralization accompanying vein-related silicification

Figure 9. Variable textural features displayed by the Vicks Peak ash-flow Tuff. (A) is partially welded showing eutaxitic structure development. (B) is partially welded exhibiting fluidal compaction of pumice fragments. (C) is densely welded showing complete loss of pore space resulting in a dense, porcelain-like texture.

consists of native silver, native gold, cerargyrite, and pyrite and appears modified by supergene oxidation processes. Trace element studies indicate the mineralization exhibits low arsenic and antimony signatures and lacks base metal introduction at present erosional levels. A single hydrothermal episode which generated structurally confined boiling appears responsible for the development of hypogene alteration and insignificant silver-gold mineralization centered over the Nogal Canyon area.

Precious metal occurrences at Aragon Hill consist of gold bearing, quartz-calcite-barite fracture fillings crosscutting the Aragon Hill intrusive breccia. Pervasive phyllic alteration, contemporaneous with breccia emplacement, occurs throughout the pipe-like intrusive breccia and concentrically envelopes the surrounding rhyolite flow-dome rocks. Phyllic alteration consists of sericite, montmorillonite-chlorite mixed layer clay, quartz, pyrite, and kaolinite products. The precious metal bearing fracture fillings probably represent leaching and minor metal deposition during the late waning stages of breccia emplacement, or possibly high level expression of epigenetic breccia-hosted silver-gold mineralization at depth.

Jon Foruria
Department of Earth Resources
Colorado State University
Fort Collins, Colorado 80523
Summer, 1984

ACKNOWLEDGMENTS

Numerous people deserve recognition for the inception and assistance in completing this thesis study. Continental Mining and Minerals Corp. furnished financial support during all phases of this endeavor and generously supplied logistical field provisions. Special thanks are extended to Robert J. Pulfrey of Continental who proposed the precious metal evaluation project and provided direction, ideas, and incentive during the duration of the study. G.R. Osburn of the New Mexico Bureau of Mines indoctrinated the author to the volcanic stratigraphy of the San Mateo mountains and provided valuable constructive criticism on stratigraphic aspects during field studies of the project.

My graduate committee, especially Dr. Tommy B. Thompson, provided constant support throughout the entire effort. Tommy, who always had an open door, continuously supplied guidance, expertise, and encouragement during both the thesis study and throughout my entire stay at C.S.U. Dr. M. McCallum provided valuable advise during numerous consultation sessions. Thanks go to Dr. Dale Winder for participating in yet another geological endeavor.

Many fellow graduate students at C.S.U. contributed both directly and indirectly to this thesis by extending the mutual help and educational comradery necessary outside the classroom.

Special thanks go to Jeff Edwards, John Rice, and Al Trippel. I am also indebted to John Memmi and Bill Larsen for offering endless assistance in tackling computer work.

My family, especially my dad, deserves special mention for always offering support, encouragement, and stressing the benefits of education. Finally, deepest thanks are extended to my wife, Kim, who probably often wondered whether I was married to her or my thesis. Her understanding, patience, and enduring fortitude throughout this major project played an important role in its successful completion.

TABLE OF CONTENTS

<u>Chapter</u>		<u>Page</u>
I	INTRODUCTION	
	Location and Geography	1
	Purpose	3
	Previous Work	4
	Methods of Investigation	6
II	REGIONAL GEOLOGY	
	Geologic Setting and Petrogenesis	8
	Economic Geology	14
III	STRATIGRAPHY AND PETROLOGY	
	Tertiary Extrusive and Sedimentary Rocks	15
	Spears Formation	15
	Lower Member	16
	Upper Member	17
	Hells Mesa Tuff	21
	Unit of Luna Park	25
	Vicks Peak Tuff	28
	Springtime Canyon Quartz Latite	34
	Rhyolite Flow-dome Rocks	37
	Tertiary Intrusive Rocks	41
	Porphyritic Rhyolite Intrusive Rocks	41
	Intrusive Breccia	42
	Quaternary Alluvium and Colluvium Deposits	47
IV	STRUCTURE	
	Introduction	48
	Local Structure	49
	Faults	49
	Joints	52
	Aragon Hill Structure Zone	53
	Nogal Canyon Cauldron	55

<u>Chapter</u>	<u>Page</u>	
V	ALTERATION	
	Introduction	58
	Intermediate Argillic Alteration	59
	Pyrite Alteration	67
	Advanced Argillic Alteration	69
	Silica Alteration	74
	Phyllic Alteration	79
	Supergene Alteration	85
VI	MINERALIZATION AND TRACE ELEMENT GEOCHEMICAL STUDIES	
	Introduction	87
	Pankey Mine	89
	Trace Element Geochemistry	93
	Gold	93
	Silver	100
	Arsenic	108
	Antimony	111
	Base Metals	113
VII	DISCUSSION AND CONCLUSIONS	
	Nogal Canyon Area	115
	Aragon Hill Area	125
	Seferino, Fifty-fifty Hill Area	130
REFERENCES	131
APPENDIX	139

LIST OF TABLES

<u>Table</u>		<u>Page</u>
1	Modal analyses of volcanic rocks in the Nogal Canyon study area	24
2	Modal analyses of volcanic rocks in the Nogal Canyon study area	40
3	Correlation coefficients of hydrothermally altered rock samples from the Vicks Peak Tuff	103

LIST OF FIGURES

<u>Figure</u>		<u>Page</u>
1	Location map of the Nogal Canyon study area .	2
2	Location of the Mogollon-Datil field in relation to the mid-Tertiary volcanic province of western North America	9
3	Diagrammatic cross section depicting stratigraphic relationships from the Rock Springs Canyon area southward to the Red Rock arroyo area	19
4	Heterolithic latite flow breccia of the upper Spears Formation exposed near Rock Springs Canyon	20
5	Photomicrograph of the Heterolithic latite flow breccia	20
6	Hells Mesa Tuff slabbed hand specimen	23
7	Heterolithic dacite flow breccia of the Unit of Luna Park exposed east of Red Rock Ranch arroyo	27
8	Exposures of Vicks Peak Tuff along the west side of San Jose arroyo	30
9	Variable textural features displayed by the Vicks Peak Tuff	33
10	Photomicrograph of Vicks Peak Tuff exhibiting eutaxitic texture defined by flattened, devitrified pumice fragments	35
11	Slabbed hand specimens of the rhyolite flow-dome unit and the porphyritic rhyolite intrusive	38
12	Vertical contact between Aragon Hill intrusive breccia and rhyolite flow-dome rocks	44
13	Aragon Hill intrusive breccia slabbed hand specimen	46

<u>Figure</u>		<u>Page</u>
14	Location map of the proposed Nogal Canyon cauldron in the southern San Mateo mountains .	56
15	Pervasive intermediate argillic alteration exposed in the Taylor Shaft area	60
16	Intermediate argillic alteration confined beneath the Vicks Peak Tuff-Springtime Canyon Quartz Latite contact	62
17	Photomicrograph of microcrystalline kaolinite aggregates replacing feldspar phenocryst . . .	64
18	Phyllosilicate alteration zoning relationships along the Pankey fault in the Pankey mine area	66
19	Photomicrograph of quartz-alunite replacement of pumice fragment within partially welded Vicks Peak Tuff	71
20	Diagrammatic cross section through the Indian Peak area showing spatial zoning relationships of alteration types	73
21	Geology and alteration of the Seferino, Fifty-fifty Hill area	75
22	Vein-infilling silica displaying crustification textures and fine grained, banded adularia . .	77
23	Subparallel quartz veinlet networks peripheral to the Pankey fault in the Pankey mine area .	80
24	Photomicrograph of the Aragon Hill intrusive breccia matrix material	82
25	Sericite pervasively replacing feldspar phenocryst and groundmass of the rhyolite flow-dome unit	84
26	Exposure of the Pankey fault on the north side of Springtime Canyon	90
27	Paragenesis of the Pankey mine mineralization	91
28	Summary of gold and silver population parameters from hydrothermally altered rock samples in the Nogal Canyon study area	94

<u>Figure</u>		<u>Page</u>
29	Bimodal cumulative probability plots of gold and silver in hydrothermally altered rock samples from the Nogal Canyon study area . . .	95
30	Geochemical distribution of gold, silver, and arsenic from the Pankey mine area	97
31	Geochemical distribution of gold, silver, and antimony from the Taylor Shaft and Rhyolite mine areas	98
32	Geochemical distribution of gold and silver from the Seferino, Fifty-fifty Hill area . . .	99
33	Geochemical distribution of gold and silver from the Henckley mine, Aragon Hill	101
34	Geochemical distribution of gold and silver from the Aragon Hill area	102
35	Geochemical distribution of silver, and arsenic from the Indian Peak and Indian Trail Canyon areas	106
36	Summary of arsenic distribution from the Vicks Peak Tuff, and comparison to other precious metal occurrences in the Mogollon-Datil volcanic field	109
37	Cumulative probability plots for arsenic, antimony, and base metals from the Nogal Canyon study area	110
38	Summary of antimony and base metal population parameters of Vicks Peak Tuff from the Nogal Canyon study area	112
39	Diagrammatic illustration depicting exposure levels of various Nogal Canyon precious metal occurrences in reference to an idealized epithermal fissure-type system	122

LIST OF APPENDIX

	<u>Page</u>
APPENDIX A	138

LIST OF PLATES

<u>Plate</u>		<u>Page</u>
1	Reconnaissance geologic and alteration map of the Nogal Canyon area	in back .pocket
2	Cross sections A-A', B-B', and C-C' of the Nogal Canyon area	in back .pocket
3	Rock chip geochemistry sample location map in the Nogal Canyon study area	in back .pocket

CHAPTER I

INTRODUCTION

Location and Geography

The San Mateo mountains form a north trending, eastward tilted structural block located in southwestern Socorro and northern Sierra counties. The isolated range lies in the northeastern portion of the Mogollon-Datil volcanic field and is surrounded by fault-bounded desert basins including the Rio Grande rift valley to the east. The mountains stretch approximately 64 km in length and 29 km in width and include over 2500 m of mid-Tertiary volcanic rocks unconformably overlying sporadically exposed Paleozoic sediments.

The Nogal Canyon study area is situated in the southern portion of the San Mateo mountains located approximately 95 km southwest of Socorro, New Mexico (Fig. 1). The area covers 89 square km which includes portions of the Vicks Peak, Steel Hill, Monticello, and Sierra Fijardo 7.5 minute U.S.G.S. topographic quadrangles. The study area includes the San Jose and Quartz Hill districts and the Aragon Hill area which host precious metal occurrences. The San Jose district is located in the northern portion of the map area bounded by Springtime Canyon to the north and San Jose arroyo to the south (Plate 1). The Aragon Hill

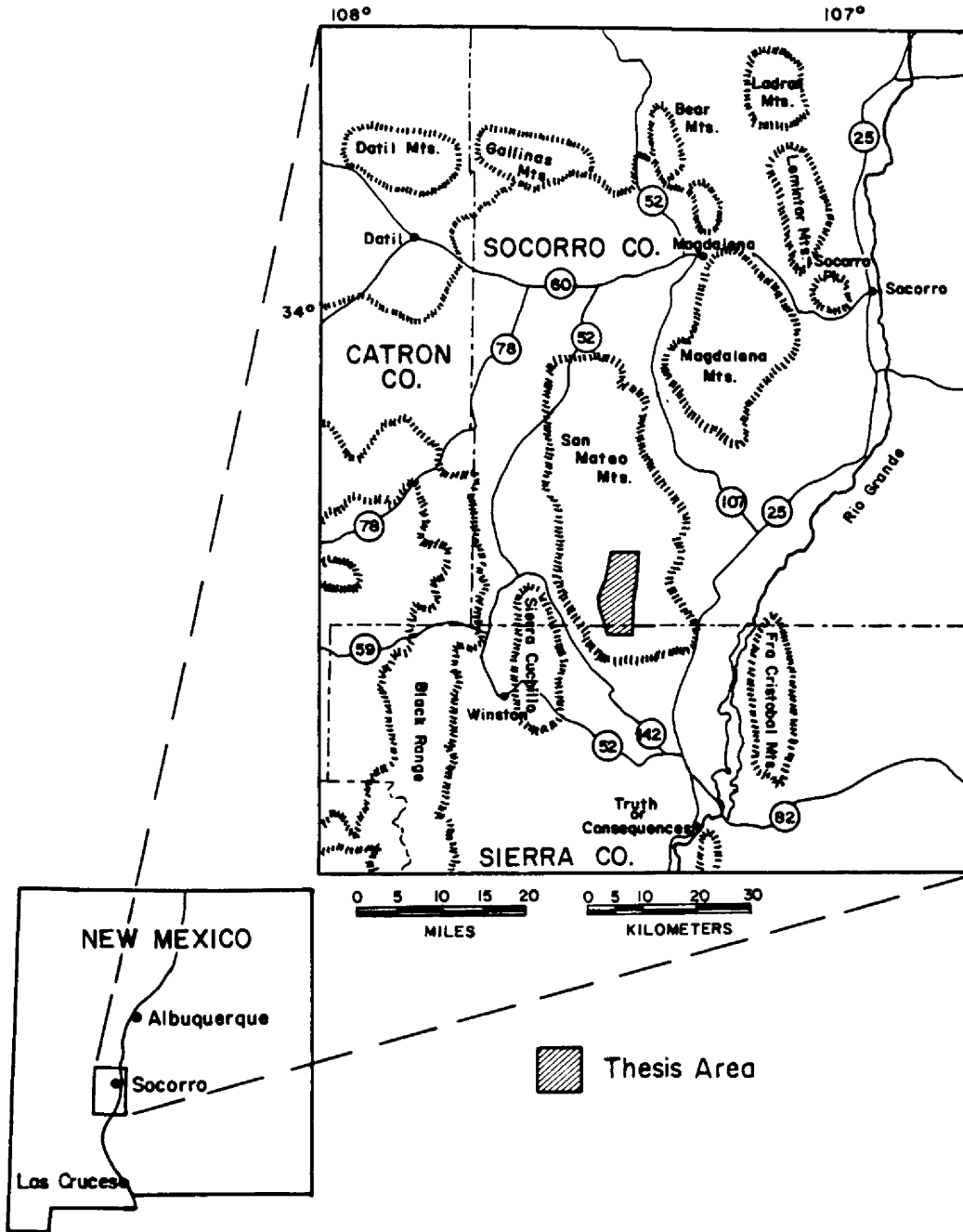


Figure 1. Location map of the Nopal Canyon study area.

occurrence appears in the southern portion of the map area adjacent to the Socorro-Sierra county line and is areally restricted to Aragon Hill (Plate 1). The Quartz Hill district lies off the map area proper, 9 km south of Aragon Hill within the eastern portion of the Monticello quadrangle (Sec 31, T10S, R5W).

Topography varies from gentle in the lower southern foothills to rugged in the mountainous northern areas. Total relief in the map area is over 600 m with elevations varying from approximately 1830 m to 2500 m. The lower foothills support sparse vegetation consisting of grasses, juniper, and man-eating cacti. Upper elevations host abundant pine, cedar, and juniper. Winter snow and summer thunderstorms average approximately 51 cm of precipitation a year; thundershowers are most abundant from late July to early September.

Purpose and Scope

Previously published geologic investigations have never addressed the mineral resource potential of the southern San Mateo mountains. The region possesses numerous precious metal occurrences within the San Jose and Quartz Hill mining districts and in the Aragon Hill area. Review of the existing literature and preliminary reconnaissance shows locally widespread bleaching and alteration, the proposed existence of a major ash-flow tuff cauldron, and numerous historic mines with very limited production. The region has never undergone heavy prospecting. Bob Pulfrey of Continental Mining and Minerals Corp. recognized

the possible precious metal potential and proposed a comprehensive evaluation be performed of the area.

The purpose and objectives of this thesis study include the following:

- 1) to describe the general geology of the southern portion of the San Mateo mountains.
- 2) to delineate and gain insight into the spatial and temporal relationships of mineral deposits, and hydrothermal alteration.
- 3) to evaluate areas of potential precious metal mineralization on a detailed reconnaissance basis.

Previous Work

Previous geologic investigations within the San Mateo mountains consist primarily of stratigraphic and volcano-tectonic structural studies. Only limited published studies concerning economic geology exist.

Early reconnaissance work on the volcanic stratigraphy by Willard (1957), Dane and Bachman (1965), and Weber (1963) utilized the broad stratigraphic nomenclature initially defined by Winchester (1920) and Tonking (1957). Regional stratigraphic and structural studies in the southern San Mateo mountains include work by Furlow (1965) and Farkas (1969).

Furlow mapped the San Mateo Peak area in the southcentral portion of the range and utilized Winchester's (1920) obsolete stratigraphic nomenclature. Farkas documented the general geology of the entire southern San Mateo mountains and subdivided lower volcanic stratigraphic units with informal nomenclature. Deal (1973) working in the northern San Mateo mountains revised the general geology and documented the existence of the Mt. Withington cauldron. Reconnaissance work by Deal and Rhodes (1976) documented the stratigraphic and structural relations of the San Mateo mountains and proposed the existence of the Nogal Canyon cauldron within the southern region. Atwood (1982) studying the San Juan Peak area established the volcanic stratigraphy utilizing formalized designations and examined peralkaline riebeckite-bearing rhyolites in the area. Recently Osburn and Chapin (1983) summarized the accepted nomenclature for Cenozoic rocks of the northeast Mogollon-Datil volcanic field. Kottlowski (1960, 1963) and Kelly and Furlow (1965) document the Paleozoic stratigraphy exposed along the southwestern and eastern flanks of the San Mateo mountains.

Published mineral occurrence investigations in the San Mateo mountains include county ore deposit reports by Lasky (1932) and Harley (1934). Griffitts et al., (1971) of the U.S. Geological Survey conducted a regional stream sediment survey examining the Pb, Zn, Mo, Ag, Au, Sn, La, B, Sb, and Nb distribution in the southeastern San Mateo mountains. Berry et al., (1981) conducted a regional uranium resource evaluation of the Tularosa quadrangle in southwestern New Mexico.

Methods of Investigation

Geologic, alteration, and geochemical studies were conducted from late May to late August 1982 in the Nogal Canyon study area. Mapping utilized 1:20,000 scale U.S. Forest Service color aerial photographs of the Cibola National Forest.

Laboratory investigations included examination of 105 thin sections for lithologic and alteration information and 10 polished sections for opaque mineral petrography. Modal analyses on 15 specimens utilized both potassium feldspar stained slabs and thin sections; a minimum of 1000 points were counted for each specimen. All modal analyses include inclusion free calculations and represent volumetric percentages. Sodium cobaltinitrite staining methods, described by Bailey and Stevens (1960), were utilized to examine samples suspected of potassium metasomatic phases, and stain for K-feldspar. Plagioclase compositions were determined optically using the Michel-Levy method described by Kerr (1977). Percent SiO₂ determinations on selected rock types utilized refractive index - silica bead tests described by George (1924) and Kittleman (1963). Standard XRD methods, supplemented by optical means, identified hypogene and supergene alteration products. cursory fluid inclusion work using petrographic thin sections examined general features of fluid inclusions, specifically liquid-vapor ratio characteristics.

Cone Geochemical Inc. of Lakewood, Colorado performed trace element geochemical analyses on 251 rock samples employing

atomic absorption spectrometry methods. Rock samples totalling 2 kg of chip material were collected within a 3 m radius of the outcrop location. Underground samples represent continuous chip intervals at waist height; material was manually mixed and split.

CHAPTER II

REGIONAL GEOLOGY

Geologic Setting and Petrogenesis

The San Mateo mountains lie in the northeastern portion of the mid-Tertiary to Quaternary Mogollon-Datil volcanic field. The volcanic pile consists of a composite, 1000-3000 m thick, mafic to felsic sequence covering 25,000 square km of southwestern New Mexico. The Mogollon-Datil volcanics occur in the southcentral Basin and Range province and represent a portion of the extensive Cenozoic volcanic occurrences of the western U.S. and Mexico (Fig. 2). Pre-Tertiary rocks underlying the Mogollon-Datil field include Precambrian igneous and metamorphic rocks, Paleozoic and Triassic sedimentary rocks, and Cretaceous sedimentary and volcanic rocks. Mid-Miocene to Quaternary clastic sedimentary rocks, primarily sandstones and conglomerates, overlie and obscure large areas of the volcanic field. No pre-Tertiary units appear in the Nogal Canyon study area; however, the Pennsylvanian Magdalena group conformably overlain by the Permian Abo formation crops out along the southwestern and eastern flanks of the San Mateo mountains (Farkas, 1969).

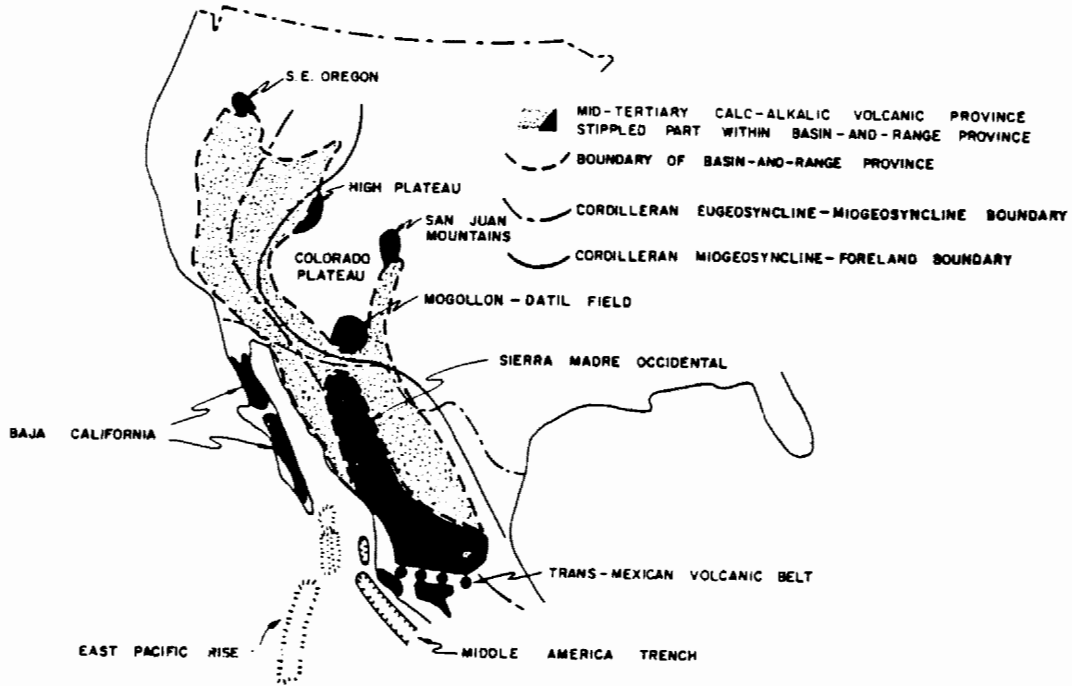


Figure 2. Location of the Mogollon-Datil field in relation to the mid-Tertiary volcanic province of western North America (from Elston, 1976a).

The mid-Tertiary to Quaternary volcanic rocks of the Mogollon-Datil field subdivide into two magmatic associations based on age and petrochemistry. The associations consist of the following: 1) mid-Tertiary, high-K, calc-alkalic basalt to high silica rhyolite, and 2) post mid-Miocene, weakly bimodal, alkalic to tholeiitic basalt and calc-alkalic rhyolite (Bornhorst, 1980; Elston et al., 1976b). Only rocks of the first association appear in the study area. The mid-Tertiary association consists of early, fundamentally andesitic rocks and later, voluminous, weakly bimodal silicic rocks; however, Bornhorst (1980) subdivided the mid-Tertiary association into the following suites: 1) predominantly andesitic, noncauldron associated, calc-alkalic basalt to rhyolite (42-18 m.y.), and 2) predominantly rhyolitic, cauldron associated, calc-alkalic dacite to high silica rhyolite (40-18 m.y.).

Mid-Tertiary calc-alkalic volcanism began about 42 m.y.b.p. corresponding to the end of the Laramide orogeny (Coney, 1972) and became widespread at about 37 m.y. The noncauldron suite represents the volumetrically most abundant extrusive phase during 42-33 m.y. and 25-18 m.y. (Bornhorst, 1980). Units corresponding to the 33-25 m.y. period are not widespread and appear concentrated in the southern and western portions of the volcanic field (Bornhorst, 1980). Unaligned, central vent volcanic centers and fissures appear as the sources for magma eruptions and are poorly documented except for the younger extrusive centers (Elston et al., 1976b). The noncauldron rocks primarily consist of intermediate to dark colored andesitic lava

flows and breccias composed dominantly of plagioclase and hydrous ferromagnesian minerals. The suite varies chemically and petrologically through time evolving to a younger (33-18 m.y.) basaltic character (Bornhorst, 1980). This transition also occurs in other calc-alkalic associations within regions of the western U.S. (Lipman et al., 1972). The calc-alkalic basalt to rhyolite magmas originated from hydrous partial melting of upper mantle (50-100 km) peridotite (Elston, 1976a; Bornhorst, 1980).

The mid-Tertiary, calc-alkalic dacite to high silica rhyolite suite consists predominantly of cauldron derived rhyolites and includes sparse peralkaline occurrences (Bornhorst, 1980). This series includes ash-flow tuffs, ring fracture and moat deposits, and flow-banded rhyolites consisting of a quartz, sanidine, plagioclase, and biotite leucocratic assemblage. The units represent the volumetrically most abundant rock suite emplaced between 34-25 m.y.a. and appear confined to the central core of the volcanic field, the Mogollon plateau (Elston et al., 1976b). The oldest high silica rhyolites occur along the outer margin of the plateau and the age of eruptive centers decreases toward the core (Elston et al., 1976b). Rhodes (1976) and Elston et al., (1976b) postulate the existence of a Mogollon plateau granitic pluton underlying the presently exposed high level volcanic complex. Magma formed at least in part by partial melting of the intermediate to siliceous granulite and gneiss fractions of the lower crust (20-40 km)(Bornhorst, 1980; Elston et al., 1976b).

The mid-Tertiary magmatic system appears associated with convergent, subduction-related tectonics active during the early Cenozoic in western North America (Elston et al., 1976b; Bornhorst, 1980). The Mogollon-Datil volcanism closely compares with the general features present in other Cenozoic volcanic fields inland from convergent ocean-continent plate boundaries on continental crust (Bornhorst, 1980). Magma generation occurred within the upper mantle and lower crust with probably minor contribution from the subducted oceanic lithosphere (Bornhorst, 1980). Rhodes (1976) and Elston et al., (1976b) theorize the rise or crystallization of calc-alkalic noncauldron magmas possibly caused partial melting of the upper lithosphere to form the dacite to high silica rhyolite magmas.

The post mid-Miocene magmatic association consists of: 1) cone and fissure derived, alkalic and tholeiitic basalts associated sporadically with rhyolitic lavas, and 2) cauldron-derived high silica, calc-alkalic rhyolites (Bornhorst, 1980). Mildly bimodal volcanism occurs from 14 m.y.a. to the present and primarily exists throughout the outer portions of the volcanic field (Bornhorst, 1980). The volumetrically prevalent basaltic lavas typically consist of olivine, plagioclase, clinopyroxene, and opaque oxide dominant lithologies and overlies or occur interbedded with Basin and Range related sedimentary fill sequences. Post mid-Miocene volcanic activity represents magmatism associated with brittle, extensional continental rifting and fundamentally differs from the earlier calc-alkalic basalt to high silica rhyolite association (Bornhorst, 1980).

The regional structure of the Mogollon-Datil volcanic province developed in response to east-west extensional tectonism, emplacement of plutons, and ash-flow tuff cauldron collapse and resurgence. Early ductile extension began about 32-28 m.y.a. in the Socorro-southern Rio Grande region (Chapin, 1979; Seager et al., 1984) and developed due to convergence-related intra-arc and back-arc extension within the Basin and Range province (Zoback et al., 1981; Eaton, 1982). Calc-alkalic magmatism occurred contemporaneously with back-arc extensional tectonism which assisted the ascent of magmas and corresponding intrusive body emplacement (Elston et al., 1976; Zoback et al., 1981). Early extension resulted in the development of broad, relatively deep, northwest-trending basins, shallow brittle deformation including tilting ($30-70^{\circ}$) along northwest listric normal faults, and incipient uplift of some of the region's fault-block mountains (Seager et al., 1984). Structural controls on the major volcanic centers and the Mogollon plateau pluton are yet undetermined. Many structures formed within ash-flow cauldron localities in response to cauldron collapse and resurgence (Elston et al., 1976b). The more recent late-Miocene to Pliocene extensional episode, transitional with earlier extension through Miocene time, produced the north to north-northeast trending rift basins and uplifts, and developed due to extensional tectonism along the modern Rio Grande rift (Lipman, 1981; Zoback et al., 1981; Seager et al., 1984).

Economic Geology

The distribution of mid-Tertiary age mining districts in southwestern New Mexico shows a common spatial association with mid-Tertiary cauldron-related ring fracture zones and central resurgent domes (Elston, 1978). Specific types of mineralization typically coincide with rocks of particular volcanic suites. The mid-Tertiary, calc-alkalic basalt to rhyolite suite corresponds with chalcophile (Ag, Cu, Pb, Zn) base metal mineralization; whereas, lithophile deposits (Sn, W, Mo, Be) coincide with calc-alkalic high silica rhyolite occurrences (Elston et al., 1976b). Both volcanic suites exhibit late stage precious metal and fluorspar mineralization (Elston, 1978). Volcanic hosted "fissure-type" gold-silver vein deposits constitute the majority of mid-Tertiary precious metal districts. Although spatial association of precious metal fissure veins to cauldron related fracture zones is almost ubiquitous, age of mineralization in select cases is considerably younger than volcanism (Kent, 1983).

Known mineral occurrences in the San Mateo mountains include the volcanic hosted "fissure-type" gold-silver veins within the Rosedale, San Jose, and Quartz Hill districts. Uranium occurrences exist in the Placitas Canyon area and in the San Juan Peak area; the latter is associated with peralkaline silicic rocks (Berry et al., 1981; Atwood, 1982).

CHAPTER III

STRATIGRAPHY AND PETROLOGY

Tertiary Extrusive and Sedimentary Rocks

Spears Formation

The Spears Formation is the basal series of the Tertiary volcanic sequence in the southern San Mateo mountains and occurs throughout the northeastern Mogollon-Datil volcanic field. Initially designated by Tonking (1957) as the Spears Member of the Datil Formation, Chapin (1971) later raised the Spears unit to formational status. The type section, measuring 415 m thick, occurs on the northeast side of the Bear mountains and consists of intermediate extrusives and volcanoclastics lying between the Eocene Baca Formation and the Oligocene Hells Mesa Tuff. In the southern San Mateo mountains, Farkas' (1969) Red Rock Ranch Formation and the lower portion of the Rock Springs Formation corresponds to the Spears Formation. Age dates range from 39.6 to 33.1 m.y. based on K-Ar and fission track methods (Osburn and Chapin, 1983). Tonking (1957) and Brown (1972) describe occurrences in other areas of the northeastern Mogollon-Datil volcanic field. In the Nogal Canyon study area, the Spears Formation consists of andesite flows and flow breccias, latitic flows and ash-flow tuffs, and minor volcanoclastics. The unit

has been informally divided into lower and upper lithologic members.

Lower Member

The lower member crops out in the foothills of the Luna Park and Red Rock arroyo region located in the southwestern portion of the map area (Plate 1). Estimated minimum thicknesses reach 220 m with an indeterminate maximum thickness due to an unexposed base within the map area. The unit contains a monotonous series of dark greenish-grey andesite flows, flow breccias, with minor interlayered rhyolite air-fall tuff. The andesite flows and breccias consist of plagioclase, amphibole, and pyroxene bearing porphyritic to fine grained lithologies; trachytic and vesicular subordinate textures are common. Plagioclase is most abundant in the intermediate flows, and magnetite exists ubiquitously in accessory amounts. The flow breccias contain cobble-sized porphyritic andesite and latite fragments in a dense, greenish-grey aphanitic igneous matrix. Thicknesses of individual flows range from 10 to 25 m and all units exhibit pervasive chlorite-epidote weathering products.

A distinct porphyritic andesite flow exists near the top of the member corresponding to the Luna Park andesite of Farkas (1969) and is possibly correlative with Atwood's (1982) andesite dike member of the Spears Formation. The flow shows strong similarities with Knewedl's (1974) "turkey track andesite" of the Spears Formation in the Magdalena mountains. The unit

exhibits a porphyritic, holocrystalline texture with a fine grained, equigranular groundmass. Subhedral plagioclase phenocrysts range in size from 3-15 mm averaging 10 mm and constitute 43 percent of the rock. Anhedral amphibole phenocrysts, probably hornblende, make up 3 percent of the rock and average 1.5 mm across.

In the Seferino, Fifty-fifty Hill area (Sec 31, T10S, R5W), a distinctive silicified laharic breccia overlies andesite flows of the lower member; however, exact stratigraphic relationships are unclear. Farkas (1969) positioned his Seferino Hill unit at the top of the Red Rock Ranch sequence which corresponds to the upper portion of the lower Spears member. The laharic breccia consists of unsorted, subangular to subrounded, heterolithic clasts varying from lapilli to boulder sizes. These matrix-supported clasts consist dominantly of tuffaceous rhyolite fragments, intermediate porphyritic rocks, and coarsely crystalline quartz clasts. The massive, unstratified deposits sporadically exhibit elongate pebble imbrication within the tuffaceous volcanoclastic matrix. Alteration will be discussed in Chapter V.

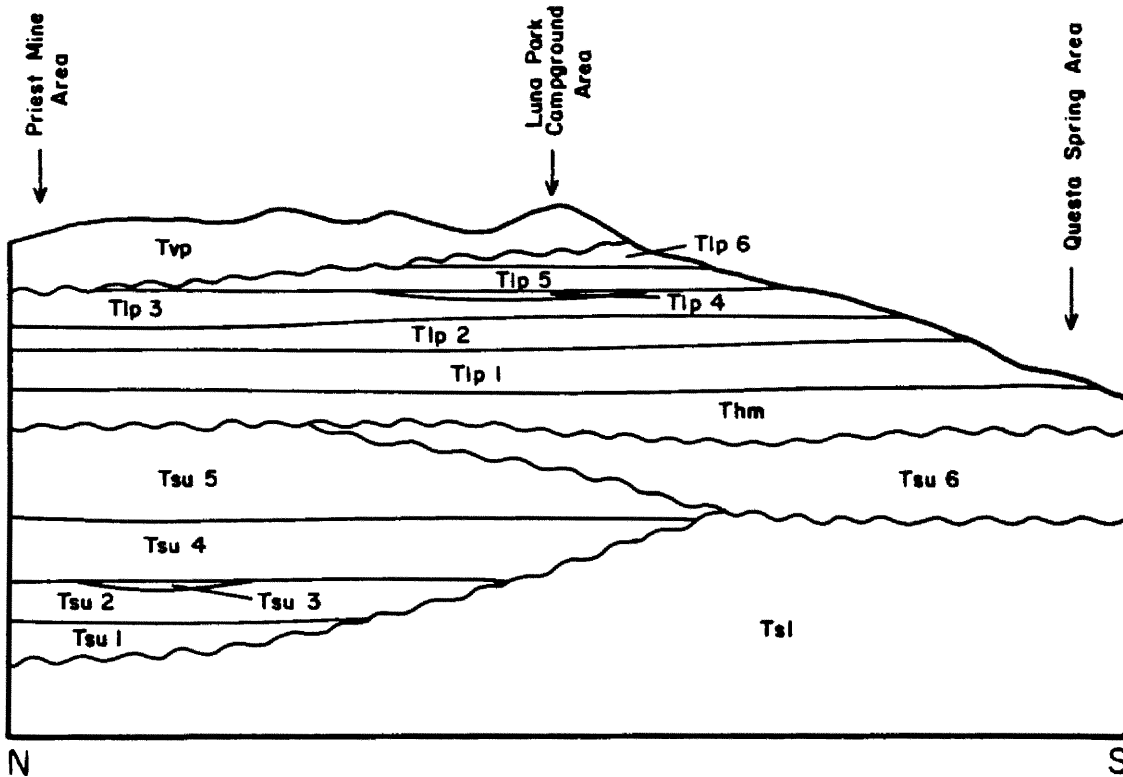
Upper Member

The upper member of the Spears Formation, unconformably overlying the lower member, crops out in the southern portion of the study area and consists of a series of intermediate flows, breccias, sporadic volcanoclastic sandstones, and a latite

ash-flow tuff. Stratigraphic relations indicate the flows and volcaniclastics occur in the Rock Springs Canyon/Luna Park areas and pinch out southward past the Luna Park campground area. The latite ash-flow, the stratigraphically uppermost rock type, is the only upper member unit dispersed over the entire southern portion of the map area. Stratigraphic relations appear in Figure 3. Thicknesses vary from 55 m in the Aragon Hill area to 180 m in the Luna Park area.

The lower 125 m consists of interlayered latite and andesite flows, flow breccias, discontinuous beds of tuffaceous sandstone, and heterolithic latite flow breccias progressing from base to top. The andesite flows typically exhibit porphyritic textures, plagioclase-pyroxene-hornblende essential phases, and a fine grained holocrystalline to felty groundmass. Latite flows consist of a plagioclase-biotite crystal vitrophyre and a coarse monolithic flow breccia with well developed fluidal structures. The flow breccia grades vertically into a massive latite flow. The heterolithic latite flow breccia is a reddish-brown, lithic and vitric fragment bearing porphyritic latite lithology which typically exhibits a dense, massive structure (Fig. 4). Microscopic examination reveals a hypocrySTALLINE groundmass of brown glass with trachytic plagioclase microlites commonly aligned around abundant accidental clasts and crystals in a fluidal pattern (Fig. 5).

The upper 55 m consists of a conspicuous, aerially extensive, crystal rich, latite ash-flow tuff. The deep reddish-grey tuff grades upward from a lithic-poor, pumice-rich, densely to



STRATIGRAPHIC COLUMN

	Tvp	Vicks Peak Tuff
Unit of Luna Park	Tlp 6	Rhyolite ash-flow tuff
	Tlp 5	Andesite flow
	Tlp 4	Volcaniclastic Conglomerate
	Tlp 3	Andesite flows
	Tlp 2	Dacite heterolithic flow breccia
	Tlp 1	Andesite flows
	Thm	Hells Mesa Tuff
Upper Spears Formation	Tsu 6	Latite ash-flow tuff
	Tsu 5	Latite heterolithic flow breccia
	Tsu 4	Latite flows
	Tsu 3	Volcaniclastic sandstone
	Tsu 2	Andesite flow
	Tsu 1	Latite flow
	Tsl	Lower Spears Formation

— Contact

~ Unconformable Contact

Figure 3. Diagrammatic cross section depicting stratigraphic relationships from the Rocks Springs Canyon area southward to the Red Rock arroyo area.



Figure 4. Heterolithic latite flow breccia of the upper Spears Formation which crops out near Rock Springs Canyon; lens cap is 6 cm across.

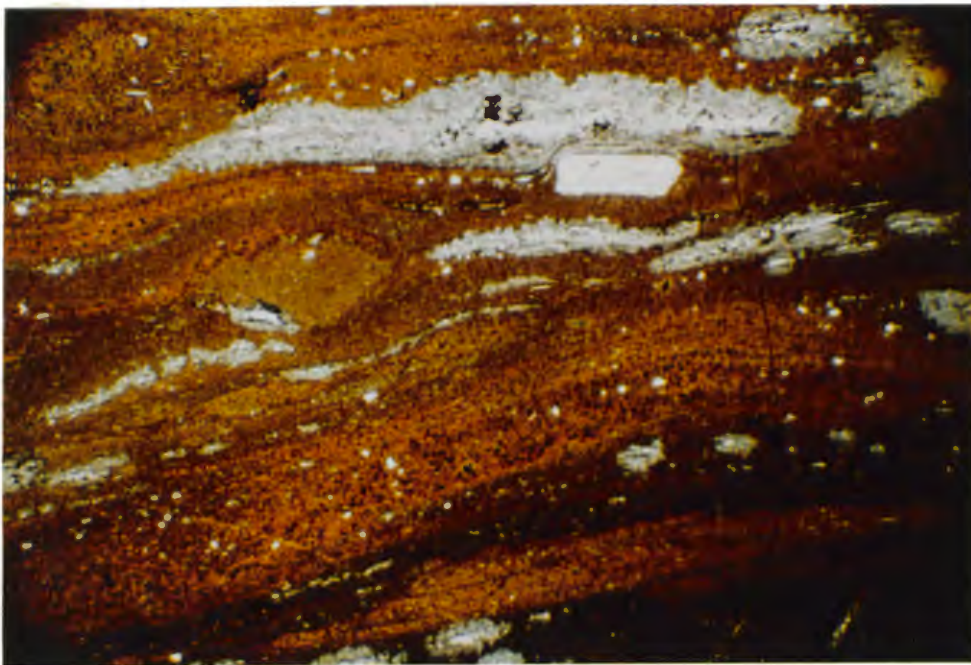


Figure 5. Photomicrograph of the heterolithic latite flow breccia showing fluidal texture development; the scale along the bottom dimension is 11 mm, uncrossed nicols.

partially welded lower zone to a lithic-rich, pumice-poor, partially welded upper zone. The ash-flow tuff displays characteristic eutaxitic structures in outcrop and exhibits crystal zoning from 23-30 percent in the lower interval to 15-22 percent in the upper interval. The unit contains plagioclase, sanidine, and biotite phenocrysts with traces of sphene. Plagioclase (An_{58-45}) occurs as fine to medium grained, subhedral, progressively zoned phenocrysts ranging in content from 12-17 percent, whereas subhedral sanidine ranges from 8-12 percent. This rock type shows strong similarities to the Tuff of Granite Mountain (personal communication, G.R. Osburn, 1982). Supergene weathering products consist of weak calcite and montmorillonite after feldspar crystals and groundmass. Sericite and iron oxides weakly replace biotite phenocrysts.

Hells Mesa Tuff

The Hells Mesa Tuff is a thick, multiple flow, crystal rich quartz latite to rhyolite ash-flow tuff cropping out throughout the northeast Mogollon-Datil volcanic field. Originally defined by Tonking (1957) as the Hells Mesa Member of the Datil Formation, Chapin (1971) later designated the Hells Mesa to formational status. Deal (1973) confined the usage to the first crystal rich rhyolite ash-flow tuff overlying the Spears Formation. Within the northern San Mateo mountains, Deal (1973) noted discontinuous occurrences along the south side of Estalin Canyon and on the east side of Grassy mountain. Exposures in the

San Juan Peak area occur along the northern side of East Red Canyon (Atwood, 1982). The Hells Mesa Tuff crops out as pale white, marginal cliffs in the Red Rock arroyo area, and as low profile exposures northwest of Aragon Hill in the southern San Mateos. Erupted from the Socorro cauldron in the Magdalena mountains, age dates of the Hells Mesa Tuff average 33.1 m.y. based on K-Ar dates on biotite (Osburn and Chapin, 1983). Brown (1972) and Simon (1973) discuss the unit in the Bear mountains region. The Hells Mesa separates underlying quartz phenocryst deficient, intermediate rock types from younger quartz bearing ash-flow tuffs in the Mogollon-Datil region (Osburn and Chapin, 1983).

In the southern San Mateo mountains, the Hells Mesa Tuff consists of a pale pink to buff white, crystal rich, partially welded ash-flow tuff. Outcrops commonly display a massive structure; however, locally they exhibit a poorly developed eutaxitic foliation defined by minor amounts of flattened pumice. Thicknesses range up to 37 m in the Questa de Trujillo area and thin toward the southeast eventually pinching out near Aragon Hill.

Microscopically the Hells Mesa possesses phenocrysts of sanidine, quartz, plagioclase, biotite with trace amounts of zircon dispersed within the strongly devitrified groundmass (Fig. 6, Table 1). Subhedral, progressively zoned plagioclase crystal fragments (An_{46-33}) range from 0.4-1.0 mm and typically host kaolinite and montmorillonite alteration. Quartz occurs as moderately resorbed, anhedral crystals which range from 0.3-2.5 mm and average 1.2 mm. Sanidine phenocrysts exhibit



Figure 6. Slabbed hand specimen of the Hells Mesa Rhyolite Tuff.

TABLE 1. Modal Analyses of Volcanic Rocks in the Nogal Canyon Study Area.

	1	2	3	4	5	6	7	8
Matrix	66.1	72.5	99.1	99.1	97.1	96.8	68.4	76.2
Quartz	8.2	4.8	0.1	---	0.2	---	---	---
Sanidine	11.1	9.5	0.8	0.9	2.0	2.9	26.6	22.5
Plagioclase	12.6	11.1	---	---	0.6	0.1	0.7	0.1
Biotite	1.5	1.4	tr	tr	0.1	0.2	---	---
Apatite	---	---	---	---	tr	---	---	---
Zircon	tr	tr	tr	tr	tr	tr	0.2	---
Opaque Fe Oxides	0.5	0.6	tr	---	---	---	4.1	1.1
Total	100.0	99.9	100.0	100.0	100.0	100.0	100.0	99.9
Points Counted	1051	1003	1307	1045	1227	1157	1296	1041
Original % Lithics	1.1	2.9	0.5	---	---	---	---	---

1,2 - Hells Mesa Tuff
 3,4,5,6 - Vicks Peak Tuff
 7,8 - Springtime Canyon Quartz Latite

anhedral, embayed crystal forms and average 1.0 mm. Subhedral, bronzy biotite crystals typically parallel the compaction foliation and exhibit weak sericite plus opaque iron oxide alteration products. Strong devitrification overprinted by supergene clay alteration obscures the original vitroclastic textures; however, sporadic axiolitic textures and relict glass shards are present locally.

Unit of Luna Park

The informal name Unit of Luna Park is proposed for a series of interlayered intermediate flows, flow breccias, volcanoclastic sediments, and rhyolite tuff exposed in the southern portion of the study area. The unit continuously crops out as gentle slopes along the east side of Rock Springs Canyon and as rugged hills in the Luna Park and Street Canyon areas. Conformably overlying the Hells Mesa Tuff, the rock types correspond to the upper portion of the Rock Springs Formation described by Farkas (1969) and range from 75 to 135 m thick. Relative ages utilizing the underlying Hells Mesa and overlying Vicks Peak brackets the unit between 33.1 to 31.3 ± 2.6 m.y.

The lower 105 m consists of interlayered andesite flows and a heterolithic dacite flow breccia. The andesite flows exhibit medium to dark grey, finely porphyritic to trachytic lithologies and appear massive in outcrop. The groundmass typically varies from fine grained, holocrystalline to hypocrySTALLINE, pilotaxitic varieties. Plagioclase (An_{60-35}) is the dominant

phenocryst phase with subordinate pyroxene and traces of magnetite disseminated in the groundmass. The heterolithic dacite flow breccia consists of poorly sorted, angular to sub-rounded fragments primarily composed of intermediate porphyritic and aphanitic rock types and commonly range up to 1.5 m in size. The matrix supportive groundmass is a dense, fine grained to microcrystalline, felsic material with fragmented lithic and crystal constituents (Fig. 7). Continuous exposures extend approximately one mile in the Street Canyon and Luna Park locality with relatively uniform thicknesses.

The upper 30 m consists of a volcanic conglomerate, andesite flow, and rhyolite ash-flow tuff from base to top (Fig. 3). The framework-supported volcanoclastic conglomerate consists of cobble to granule size, moderate to well rounded, heterolithic clasts engulfed in an iron oxide stained, siliceous matrix. Thicknesses range from 0-9 m with weakly developed fining upward sequences the only sedimentary structures locally preserved. The andesite flow consists of a dark grey-green, finely porphyritic rock with chlorite-bearing vesicular cavities. In thin section, the pilotaxitic groundmass contains trace amounts of disseminated magnetite and hosts propylitic alteration products. The rhyolite ash-flow tuff crops out sporadically as thin exposures below the Vicks Peak Tuff (NW 1/4 of Sec 31, T9S, R5W), and consists of a pale maroon, densely welded, crystal poor tuff. The porcelain-like, massive tuff contains fine grained sanidine, quartz, and biotite phenocrysts totalling less than 4 percent; pumiceous and lithic materials are absent. In thin



Figure 7. Dacite heterolithic flow breccia of the Unit of Luna Park which crops out east of Red Rock arroyo; hammer handle is 35 cm long.

section, alignment of biotite crystals defines poorly developed fluidal/eutaxitic structures. The unit shows similarities to the La Jencia Tuff.

Vicks Peak Tuff

The Vicks Peak Tuff is a multiple ash-flow, simple cooling unit of high silica alkali rhyolite composition occurring throughout the northeast Mogollon-Datil volcanic field. Occurrences span from southern-most exposures in the northern Black Range northward to the Datil and Bear mountains and the Joyita Hills. The unit is 31.3 ± 2.6 m.y. based on zircon fission track dates (Bornhorst et al., 1982) and overlies the La Jencia Tuff and underlies the Lemintar Tuff. The principal reference section described by Brown (1972) appears in the southern Bear mountains. Farkas (1969) originally named the unit for exposures at Vicks Peak in the southern San Mateos. Deal and Rhodes (1976) interpreted the unit as a major ash-flow tuff sequence erupted from the proposed Nogal Canyon cauldron based on reconnaissance work. In the southern San Mateo mountains, the Vicks Peak Tuff is the most widespread and volumetrically most abundant rock type with maximum thicknesses reaching approximately 590 m at Vicks Peak. It crops out continuously from Roberts Canyon southward to Lumber Canyon constituting the precipitous cliffs, valleys, and rugged hills of the northern and central portions of the Nogal Canyon study area. In the southern region, the Vicks Peak occurs as isolated outcrops capping knobs

and hills. An angular unconformity separates the underlying Unit of Luna Park from the Vicks Peak Tuff (Fig. 3).

The Vicks Peak Tuff exhibits characteristic and systematic features which correspond to traits defined by Smith (1960) and Ross and Smith (1961) within thick ash-flow sheets. A basal vitrophyre zone, ranging up to 3 m thick, consists of a dark, greyish-green holohyaline lithology with local spherulites as much as 0.3 m in diameter. Above the basal vitrophyre, the lower portion of the ash-flow tuff possesses a densely welded character defined by the near complete loss of pore space resulting in a dense, massive, porcelain-like rock type. Flattened lithophysal cavities, developed from entrapped or exsolved gases, appear as flat wisp-like cavities without vapor-phase constituents and characterize the densely welded portion of the tuff. The zone also exhibits massive structures varying to moderately developed columnar jointing and typically forms the precipitous cliffs and valley walls within the study area (Fig. 8). The lower interval is crystal poor with phenocrysts totalling 1-3 percent, and no pumice or lithic material is present. The upper portion of the Vicks Peak Tuff is partially welded and possesses well defined eutaxitic structures defined by flattened pumice fragments and lithophysal cavities. Columnar jointing is typically poorly developed or absent in this zone. This interval shows a greater diversity of welding textures and a variable degree of pumice fragment collapse. Amethystine quartz vapor-phase material commonly infills flattened lithophysal cavities as fine, euhedral mosaics.



Figure 8. Exposures of the Vicks Peak Tuff along the west side of San Jose arroyo. The scarp shows columnar jointing developed within the densely to partially welded intervals of the Tuff.

Phenocryst totals remain less than 3 percent, but increase vertically with contents locally totalling 8 percent. Figure 9 shows the variable textural features displayed by the rhyolite tuff. Non-welded intervals of the ash-flow tuff do not crop out in the study area.

Hand specimen and microscopic examination of the Vicks Peak Tuff reveals a finely porphyritic texture with strong devitrification of both densely and partially welded intervals. Phenocrysts consist of sanidine, quartz, plagioclase, and biotite with trace amounts of apatite, zircon, and sporadic pyrite in the groundmass. Subhedral sanidine, ranging from 1-3 percent, occurs as embayed, unzoned crystals and ranges between 0.7 and 2.5 mm averaging 1.3 mm in size. Quartz amounts to less than 1 percent and occurs as anhedral, resorbed crystals averaging 1.0 mm. Plagioclase appears as subhedral, corroded and abraded laths averaging 0.9 mm in size. Subhedral biotite phenocrysts, occurring in trace amounts, average 0.4 mm and range from 0.3-0.5 mm. Trace amounts of pyrite appear as fine grained (< 0.2 mm) disseminated anhedral which occur sporadically within the densely welded, unaltered, lower portions of the tuff. Pyrite is not systematically associated with phenocrysts, lithophysal cavities, or primary iron oxides. Pyrite probably formed during post- emplacement, deuteric processes related to equilibration of entrapped or exsolved H₂S bearing gases which underwent incomplete oxidation during ash- flow eruption and emplacement. Modal analysis data of samples located within the densely welded, lower portion appear in Table 1. Flattened, strongly



(A)



(B)



(C)

devitrified pumice fragments as much as 10 cm long appear microscopically as very fine grained, interlocking xenomorphic mosaics of quartz-alkali feldspar (Fig. 10). Vitroclastic textures are only preserved in localities from the upper sections. The tuff's characteristic pale to deep maroon color occurs due to abundant cryptocrystalline goethite/hematite disseminations throughout the matrix; discoloration results from hypogene and/or supergene alteration of the tuff.

The Vicks Peak Tuff hosts epithermal "fissure-type" precious metal occurrences within the San Jose district. Areas of local and extensive hydrothermal alteration most prevalent in the Nogal Canyon region are addressed in Chapter V.

Springtime Canyon Quartz Latite

The Springtime Canyon Quartz Latite consists of massive, crystal rich quartz latite lava flows unconformably overlying the Vicks Peak Tuff and crops out extensively in the southern San Mateo mountains. Furlow (1965) originally named the unit for exposures in Springtime Canyon within the southern San Mateo mountains, but described it as a rhyolite welded tuff. Farkas (1969) characterized the rock type as a rhyolite sill intruded between the Vicks Peak Tuff and overlying rhyolitic extrusives. Deal and Rhodes (1976) reinterpreted the Springtime Canyon Quartz Latite as a cauldron lava flow erupted from the Nogal Canyon ring fracture zone. Relative ages with the rhyolite

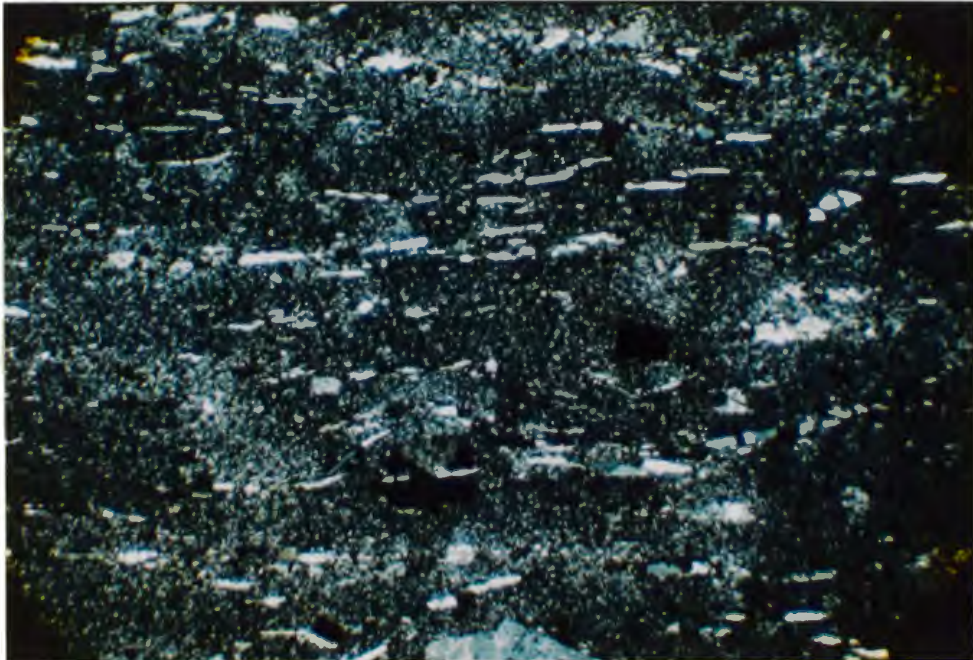


Figure 10. Photomicrograph of Vicks Peak Tuff showing eutaxitic structure defined by flattened, devitrified pumice fragments; the scale along the bottom dimension is 11 mm, x-nicols.

flow-dome unit and porphyritic rhyolite intrusive rocks in the study area's southern region are not known.

Within the Nogal Canyon study area, the Springtime Canyon Quartz Latite caps isolated hills and ridges as knobby outcrops in the Nogal Canyon, Springtime Canyon, and Taylor Shaft areas. Its southern-most exposures lie north of San Jose arroyo (Plate 1). Thicknesses range from 9 to 190 m based on cross section data. The formation consists of a basal vitrophyric quartz latite flow overlain by a holocrystalline quartz latite sequence. The quartz latite vitrophyre ranging from 0-25 m thick consists of a pale brownish-black, hypocrySTALLINE lithology commonly exhibiting fluidal flow textures. Phenocrysts of plagioclase, sanidine, and biotite ranging from 12-14 percent occur within the weakly devitrified, spherulitic groundmass. The matrix contains trace amounts of disseminated, anhedral magnetite with 4-10 percent accidental lithic fragments. The overlying quartz latite is pale to dark greenish-grey, holocrystalline, and coarsely porphyritic exhibiting a weakly fractured, massive structure. The dense, aphanitic groundmass exhibits no internal structures or phenocryst alignments. Phenocrysts include dominant sanidine with lesser plagioclase and biotite; magnetite and zircon occur as very fine grained accessories. Modal analysis data of the Springtime Canyon unit appear in Table 1. Sanidine occurs as weakly zoned, subhedral crystals with weakly resorbed outlines; no strongly developed disequilibrium relationships exist. Sizes range from 2.0-8.0 mm and average 4.0 mm. Subhedral

plagioclase crystals exhibit strong progressive zoning and range from 1.0-2.5 mm averaging 1.8 mm. Subhedral to anhedral, fine grained (< 0.3 mm) magnetite is ubiquitous. Supergene weathering products include minor amounts of calcite, chlorite, kaolinite, montmorillonite, and goethite; discussion of hypogene alteration appears in Chapter V.

Rhyolite Flow-Dome Rocks

The rhyolite flow-dome rocks consist of a massive, crystal rich sequence cropping out at Aragon Hill in the southern portion of the study area. The rhyolite ranging from 25-110 m thick unconformably overlies the upper member of the Spears Formation and covers approximately a quarter square mile. Relative age relationships with nearby porphyritic intrusive rocks and with the Springtime Canyon Quartz Latite flow rocks exposed to the north are uncertain. Farkas (1969) grouped the rhyolite at Aragon Hill with the intrusive "quartz rhyolite porphyry" rock types exposed in the southern San Mateo mountains. However, the phenocryst abundances, phenocryst ratios, phenocryst size ranges, accessory mineral differences, overall lithologic appearance, and field relationships distinguish the rhyolite flow-dome rocks from the intrusives (Fig. 11). A flow origin rather than an intrusive mode of emplacement is implied by thick, tongue-like forms with local steep sided rounded exposures and by typically flat basal contacts with a locally irregular floor. Results of refractive index/silica bead tests on three rhyolite

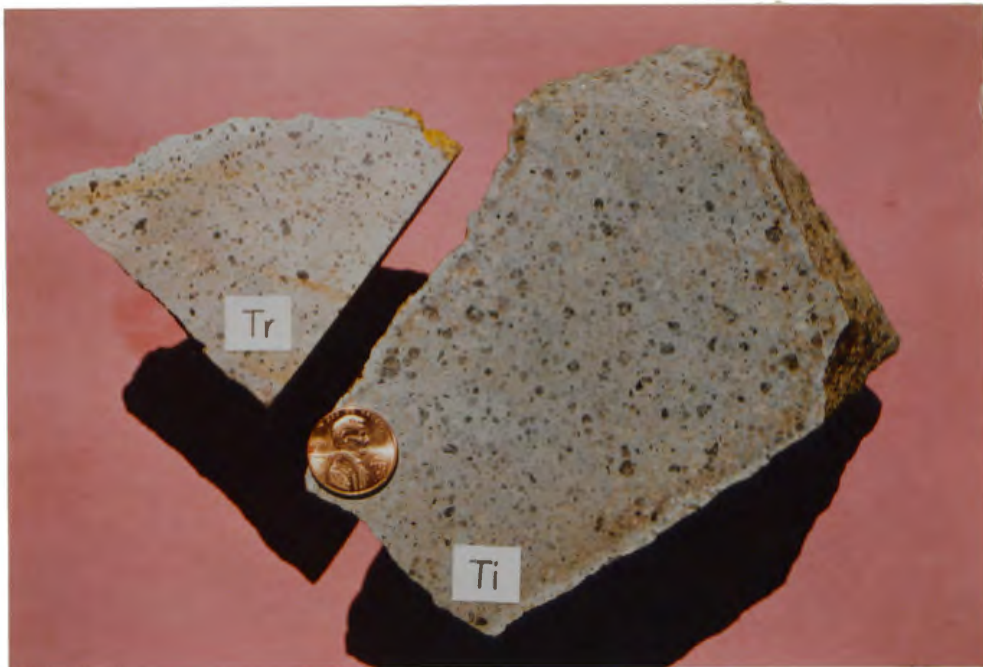


Figure 11. Slabbed hand specimens of the rhyolite flow-dome unit (Tr) and the porphyritic rhyolite intrusive (Ti).

flow-dome samples document a 75 ± 2 wt% SiO_2 content based on plots from Kittleman (1963, Fig. 2). These cursory determinations place the rock in the rhyolite category (70-75 wt% SiO_2) based on a calc-alkalic rock classification applicable to the Mogollon-Datil volcanic field (Bornhorst, 1980, p. 429).

The buff to creamy white rhyolite displays thick, massive, medium porphyritic features and exhibits local near vertical columnar jointing. Megascopically the unit contains quartz, sanidine, plagioclase, and biotite phenocrysts within a microcrystalline groundmass. Modal analysis results appear in Table 2. Subhedral to anhedral quartz exhibits resorbed crystal outlines and varies from 0.4-4.0 mm averaging 1.5 mm in size. Local secondary silica overgrowths on quartz phenocrysts probably result from silica nucleation generated after desilication alteration reactions. Sanidine occurs as progressively zoned, resorbed crystals averaging 2.0 mm. Subhedral plagioclase displays strong progressive zoning but clay alteration commonly obscures other detailed features. Feldspar phenocrysts locally possess trace to moderate amounts of sericite, kaolinite, and montmorillonite alteration. Biotite consists of subhedral grains ranging from 0.4-1.5 mm in size. Mosaic-like aggregates of sericite plus irregular iron oxide material constitute biotite alteration products. The groundmass is a dense, microcrystalline quartz-feldspar mosaic altering locally to plumose sericite and kaolinite aggregates.

TABLE 2. Modal Analyses of Volcanic Rocks in the Nogal Canyon Study Area.

	1	2	3	4	5	6	7
Matrix	79.8	75.8	82.3	64.9	70.5	66.8	60.9
Quartz	3.2	5.0	4.5	8.0	13.6	12.0	8.4
Sanidine	3.4	4.6	4.1	6.6	9.8	19.3	21.7
Plagioclase	13.3	14.3	8.6	19.1	5.5	1.7	8.6
Biotite	0.3	tr	0.3	0.8	0.5	0.1	0.2
Zircon	---	tr	---	tr	---	tr	tr
Opaque Fe Oxides	tr	0.3	0.2	0.6	0.1	0.1	0.1
Total	100.0	100.0	100.0	100.0	100.0	100.0	99.9
Points Counted	1164	1124	1033	1274	1134	1022	1217

1,2,3,4 - Rhyolite flow-dome unit
 5,6,7 - Porphyritic Rhyolite Intrusive

Tertiary Intrusive Rocks

Porphyritic Rhyolite Intrusive Rocks

Porphyritic rhyolite intrusives crop out as scattered occurrences in the southwestern portion of the map area and intrude the lower and upper members of the Spears Formation. Farkas (1969) observed "quartz rhyolite porphyry" stocks and dikes in the same locality with occurrences continuing eastward to the Eagles Roost/Penasco Peak area (Sec 11, T10S, R5W). Deal and Rhodes (1976) recognized small porphyritic quartz latite stocks ranging to rhyolitic compositions around the southern and southeastern margin of the San Mateos which postdate the Vicks Peak Tuff. They interpreted the intrusions as defluidized magma emplaced along the ring fracture zone of the Nogal Canyon cauldron. SiO_2 determinations based on refractive index/silica bead tests suggest a 73 ± 2 wt% SiO_2 utilizing diagrams from Kittleman (1963, Fig. 2) and documents a rhyolite composition.

The intrusives consist of dikes, plugs, and small irregular stocks up to 1 km long scattered along a west-northwest trending structural zone and extend over a known 5 km distance (Plate 1). Contacts with the Spears Formation appear sinuous in nature, and joints within the rhyolite are poorly developed except for sporadic columnar sets. Exposures consist of prominent, rounded knobby hills and low profile outcrops with poorly preserved fluidal structures locally present on weathered surfaces. The rhyolite is generally buff white to pale brown, massive, and medium to coarsely porphyritic with a dense,

microcrystalline groundmass (Fig. 11). Phenocrysts consist of quartz, sanidine, plagioclase, and biotite crystals with accessory zircon and local traces of pyrite. Modal analysis data appear in Table 2. Anhedral to subhedral quartz ranges from 0.4-5.5 mm averaging 2.5 mm and exhibits moderately resorbed crystal outlines. Sanidine occurs as subhedral, unzoned crystals ranging from 0.5-5.0 mm and averages 3.0 mm in size. Plagioclase phenocrysts consist of progressively zoned, glomeroporphyritic aggregates, or less commonly as single crystals ranging from 0.8-6.0 mm. Biotite crystals exhibit subhedral outlines and average 1.0 mm in size. Trace amounts of zircon occur as poikilitically enclosed euhedral crystals within quartz and biotite. Primary cubic, euhedral pyrite averages 0.8 mm and occurs locally in accessory amounts. Supergene alteration products include sericite, kaolinite, and montmorillonite after feldspar phenocrysts and groundmass material. Pyrite weathers to opaque iron oxides, whereas biotite alters to trace amounts of chlorite plus iron oxide alteration.

Intrusive Breccia

The term intrusive breccia used here follows the definition proposed by Wright and Bowes (1963, p. 84) who state "...intrusive breccia forms by the fragmentation of a rock and its mobilization by magma or gases and intrusion with or without an igneous matrix". The Aragon Hill intrusive breccia in the southern portion of the map area crops out as a roughly

ellipsoid-shaped, low profile, non-resistant exposure approximately 75 by 230 m in size (Plate 1). Steeply dipping to vertical crosscutting contact relationships with the surrounding rhyolite flow-dome rock implies a near vertical pipe-like form extending at depth (Fig. 12). The breccia extends to a minimum exposed depth of approximately 30 m; however, vertical movement of fragments derived from lower stratigraphic levels is at least 125 meters and may be considerably greater. Contact margin zones exhibit moderately to strongly sheared intervals varying from 1-9 m in width. These friable, fragment-poor, clay-gouge zones commonly display weakly defined, near vertical, closely spaced shear fractures. The rhyolite flow rocks adjacent to the breccia contact zone possess orthogonal fracture patterns oblique to the contact orientation. Weak pervasive silica alteration and sporadic crystalline, drusy quartz veinlets constitute an alteration phase strictly confined to the contact zone. The intimate association of the intrusive breccia with the rhyolite flow-dome rocks possibly suggests a close genetic relationship between the breccia and igneous activity. The breccia occurs within a broad, west-northwest trending structural zone defined by the occurrence of intrusive porphyritic rhyolites and rhyolite flow-dome rocks; no specific structure or structural intersections crosscut Aragon Hill.

Fragments within the matrix-supported intrusive breccia include lapilli to block size clasts ranging to as much as 1.5 m in diameter. They are subangular to rounded, poorly to moderately sorted and consist of heterolithic lithologies. The fragments



Figure 12. Vertical contact between the Aragon Hill intrusive breccia (left) and the rhyolite flow-dome unit (right) exposed on the west side of Aragon Hill; hammer handle is 35 cm long.

include latite ash-flow tuff, rhyolite flow, andesite flow, and andesite flow breccia rock types derived primarily from the underlying Spears Formation; glassy, pumiceous, scoriaceous, or mineralized fragments are absent. Occurrence of andesitic fragments from the lower Spears Formations suggests vertical movement of at least 125 m. No systematic variation of fragment size or morphology occurs within the limits of the pipe-like body. The shape and size of fragments is a function of rock competency, transport distance, and amount of turbulence. The fragments exhibit differing types and degrees of alteration primarily reflecting the dissimilar clast lithologies.

The intrusive breccia matrix consists of a moderate pale green, fine grained (< 0.025 mm) rock flour which contains minute comminuted rock fragments and abraded quartz and feldspar crystal fragments (Fig. 13). No indications of an igneous matrix were observed. The matrix consists predominantly of sericite with lesser amounts of mixed-layer montmorillonite-chlorite, kaolinite, quartz, and pyrite with late calcite. Sericite occurs as plumose to flake-like aggregates throughout the matrix, whereas, kaolinite and quartz appear as irregular microcrystalline masses. Fine grained pyrite is disseminated in trace amounts throughout the matrix. Calcite occurs as patchwork masses replacing abraded feldspar phenocrysts and matrix material. No systematic fragment distribution, flowage structures, lineations, or eddy patterns peripheral to fragments were observed within the breccia.



Figure 13. Slabbed hand specimen of the Aragon Hill intrusive breccia.

Sporadic northeast-trending, steeply-dipping fractures crosscut the intrusive breccia and host euhedral, tabular barite blades intergrown with calcite and crystalline quartz infilling open spaces. The fractures also contain moderate amounts of goethite and pyrolusite and appear best exposed within the Henckley mine on the northeast side of Aragon Hill.

Within the intrusive breccia, the fragment and matrix alteration assemblage results from syngenetic hypogene processes associated with intrusive breccia emplacement. Descriptive details and evidence supporting this conclusion appear in Chapter V.

Quaternary Alluvium and Colluvium Deposits

Alluvium and colluvium deposits occur in present day canyons, stream channels, and arroyos throughout the Nogal Canyon study area. The deposits include poorly sorted, unconsolidated, fine to coarse grained clastics consisting of locally derived volcanic lithologies. These chaotic to coarsely bedded units generally occur as elevated stream terrace deposits best developed in Nogal Canyon, Luna Park, Red Rock Canyon, and Springtime Canyon.

CHAPTER IV

STRUCTURE

Introduction

The San Mateo mountains represent a north trending, uplifted structural block located within the southcentral Basin and Range province. Early extensional tectonism in the southwestern U.S. led to the development of northwest-trending structural features which commenced about 32-28 m.y.a. in the Socorro - southern Rio Grande rift region (Chapin, 1979; Seager et al., 1984). Late Miocene-Pliocene Basin and Range block faulting generated the northerly structural and topographic fabric present throughout the modern southern Rio Grande rift region (Seager et al., 1984).

In the southern San Mateo mountains, the mid-Tertiary intermediate to felsic volcanic sequence dips homoclinally 5-15 degrees to the east probably due to Basin and Range block-faulting. Fault, joint, and lineament orientations throughout the map area define dominant northeast and northwest structural trends. The east-west trending Aragon Hill structure zone located in the southern border area represents an anomalous structural feature discordant to the predominant northerly structural fabric. Large scale folding is absent within the

area. Deal and Rhodes (1976) proposed the existence of the Nogal Canyon cauldron centered over the southern San Mateo mountains. Evidence supporting a major volcano-tectonic depression is based primarily on reconnaissance work and is not conclusive.

Local Structure

Faults

In the Nogal Canyon study area, fault systems generally consist of high angle normal faults showing predominant dip-slip throw. Major structures crossing the Springtime Canyon, Nogal Canyon, and San Jose arroyo areas host silver-gold vein occurrences of the San Jose district.

In the northern and central portions of the map area, a subparallel series of high angle normal faults postdate the Springtime Canyon Quartz Latite (Plate 1). Lack of stratigraphic control precludes specific time constraints on faulting. The structures trend primarily N20°E and to a lesser extent N35°W. The faults downdrop a series of en echelon blocks to the west with local intervening downdropped eastern blocks resulting in horst and graben-like structural offsets (Plate 2). Relative ages between the northeast and northwest fracture systems is presently unconfirmed; however, poorly documented fault terminations tentatively suggest a contemporaneous relationship. Evidence for faulting includes displacement of contiguous basal contacts of the Springtime Canyon Quartz Latite, continuous gouge and breccia zones, and linear

silicified outcrops infilling and replacing fractured areas. Stratigraphic offset played a minor role in the recognition of structures cutting the extensive Vicks Peak Tuff due to the lack of discernable stratigraphic horizons. Structures documented by alteration features commonly consist of discontinuous silicified outcrops aligned in linear arrays with or without surrounding argillic alteration. Structure zone widths, defined by lateral gouge extent, range from 0.3 m to 4 m.

In the northern area, the northeast-trending Pankey fault dips approximately 80 degrees to the east. Its sense of displacement is down to the east with stratigraphic throw of the Vicks Peak Tuff-Springtime Canyon Quartz Latite contact measuring 83 m. Exposure length of the fault is approximately 2.5 km, and its surface trace in the Pankey mine area exhibits a sinuous pattern (Plate 1). The lack of brecciation of the late-silica vein material suggests negligible post-mineralization movement. The Indian Peak fault, a northeast trending, steeply northwest dipping fracture, exhibits prominent silicified ribs with as much as 15 m of relief on the southwest side of Indian Peak. The structure is exposed along a 3.5 km length and possesses an unknown amount of displacement. Local quartz-alunite replacement bodies and intermediate argillic alteration are spatially related to the Indian Peak fault. The Rhyolite fault represents the most continuous structure in the area, and is exposed over an 8 km length from the Rhyolite mine northward to the Springtime Canyon area. Stratigraphic throw along this fault probably exceeds 110 m with relative displacement being down to the west.

Fault trace-topography relationships indicate a steep westward dip varying from 75-80 degrees north of Nogal Canyon but steepening to near vertical south of Nogal Canyon.

In the southern portion of the map area, a conjugate set of northeast- and northwest-trending faults displace the Vicks Peak Tuff against older units lower in the stratigraphic section (Plate 1). Fault trends are concordant with the structural pattern in the northern portion of the study area and probably represent a contiguous fracture fabric. The majority of faults consist of high angle normal faults with dip-slip throws varying from tens to hundreds of meters (Plate 2). Fault age relationships are poorly documented in the southern area; however, near Aragon Hill, northeast and/or east-west faults offset northwest-trending faults. Age relations between east-west faults related to the Aragon Hill structure zone and northeast faults are unknown. The northwest-trending faults consistently display a down to the northeast pattern without any substantial tilting (Plate 1). Offset along the conjugate northeast- and northwest-trending fault system exposes a window of lower stratigraphic units north of the Aragon Hill structure zone, which possibly represents doming or structural uplift generated by an underlying intrusive. Faults within the southern map area lack alteration and mineralization features at present erosional levels.

Origin of the northeast- and northwest-trending fault systems within the Nogal Canyon study area is uncertain. The high angle, northwest faults share similarities in trend and

timing with mid-Tertiary pre-Basin and Range structures which formed during regional WSW-ENE extensional tectonism. The Nogal Canyon fault, discussed by Farkas (1969) and Atwood (1982), is located along the eastern flank of the southern San Mateo mountains and strongly resembles mid-Tertiary faults in style, timing, and strike orientation. However, northwest faults appear both coeval and older than northeast-trending faults, and therefore suggest a different state of stress responsible for simultaneous faulting. If present, cauldron development in concert with regional WSW-ENE extension could account for the modified stress field that generated coeval, obliquely oriented fracture patterns. The northeast-trending faults, although possibly cauldron related, strongly resemble Basin and Range faults based on similar trends, anastomosing pattern, style, and age characteristics.

Joins

Joins appear as moderately developed, planar discontinuities in the majority of rock types exposed in the Nogal Canyon study area. Observational data are primarily confined to joint occurrences within the Vicks Peak Tuff which locally hosts silver-gold vein mineralization. The majority of the smooth-surfaced, through-going structures originated during a cooling extensional processes as suggested by their strong development and distributional confinement to the densely welded, lower portion of the Vicks Peak rhyolite. Jointing is typically

poorly developed to non-existent in the partially to less welded, upper intervals of the tuff. Joint patterns show consistent, well developed northeast and northwest trends with near vertical dips and a poorly developed north-south trend based on qualitative inspection of 147 data points (Plate 1). Northeast and northwest orientations average $N25^{\circ}E$, $80^{\circ}NW$ and $N40^{\circ}SW$, $75^{\circ}S$, respectively. The majority of joints predate northeast and northwest trending faults and exhibit no genetic relation apart from possible control on the orientation of fault planes. Tectonic joints genetically related to normal faulting were superimposed upon the preexisting structural fabric and probably resulted in the reactivation of previous discontinuities. Hydrothermal alteration postdates the development of both joints and faults as all observed orientations exhibit hypogene alteration effects.

Aragon Hill Structure Zone

A series of structural, intrusive, and alteration features characterize the Aragon Hill structure zone located along the southern border of the map area. Farkas (1969, p. 68) noted "...an intensely faulted area two to three miles in width which runs parallel to the southern edge of the San Mateo mountains for more than ten miles". In the Aragon Hill - Red Rock arroyo area, the west-northwest trending structural zone approaches 1.5 km widths and consists of rhyolitic intrusives and extrusives aligned along intersecting structural trends. Northeast and

northwest trending faults of the southern area intersect steeply dipping east-west trending faults defining the structure zone. Structural intersections localized porphyritic rhyolite intrusive activity, intrusive breccia emplacement, and rhyolite flow-dome extrusion. The intrusives clearly postdate the structural episode evidenced by the dike-shaped porphyritic rhyolite intrusives elongated in northwest-southeast and east-west orientations (Plate 1). Further evidence includes the lack of brecciation or other tectonic features present within intrusive bodies or along country rock contacts. The Aragon Hill intrusive breccia occurring along this zone consists of a west-northwest elongated ellipsoid-shaped pipe. The breccia parallels the east-west structural trend and does not appear to be localized along structural intersections. Areal distribution of the rhyolite flow-dome rocks appears confined to the width of the structure zone. Although no vent or vents were observed, proximity of a near-by vent is probable.

Exposures within and immediately north of the Aragon Hill structure zone display east-west compaction foliations with gentle northerly dips, and are discordant to the consistent northwest-trending, northeast-dipping structural pattern throughout the southern San Mateos. Orientational deviations of the foliations may result from surface irregularities prior to ash-flow deposition, but probably reflect intrusion and consequent doming along the structure zone. The west-northwest-trending Aragon Hill structure zone is discordant with the regional structural fabric developed during mid-Tertiary to

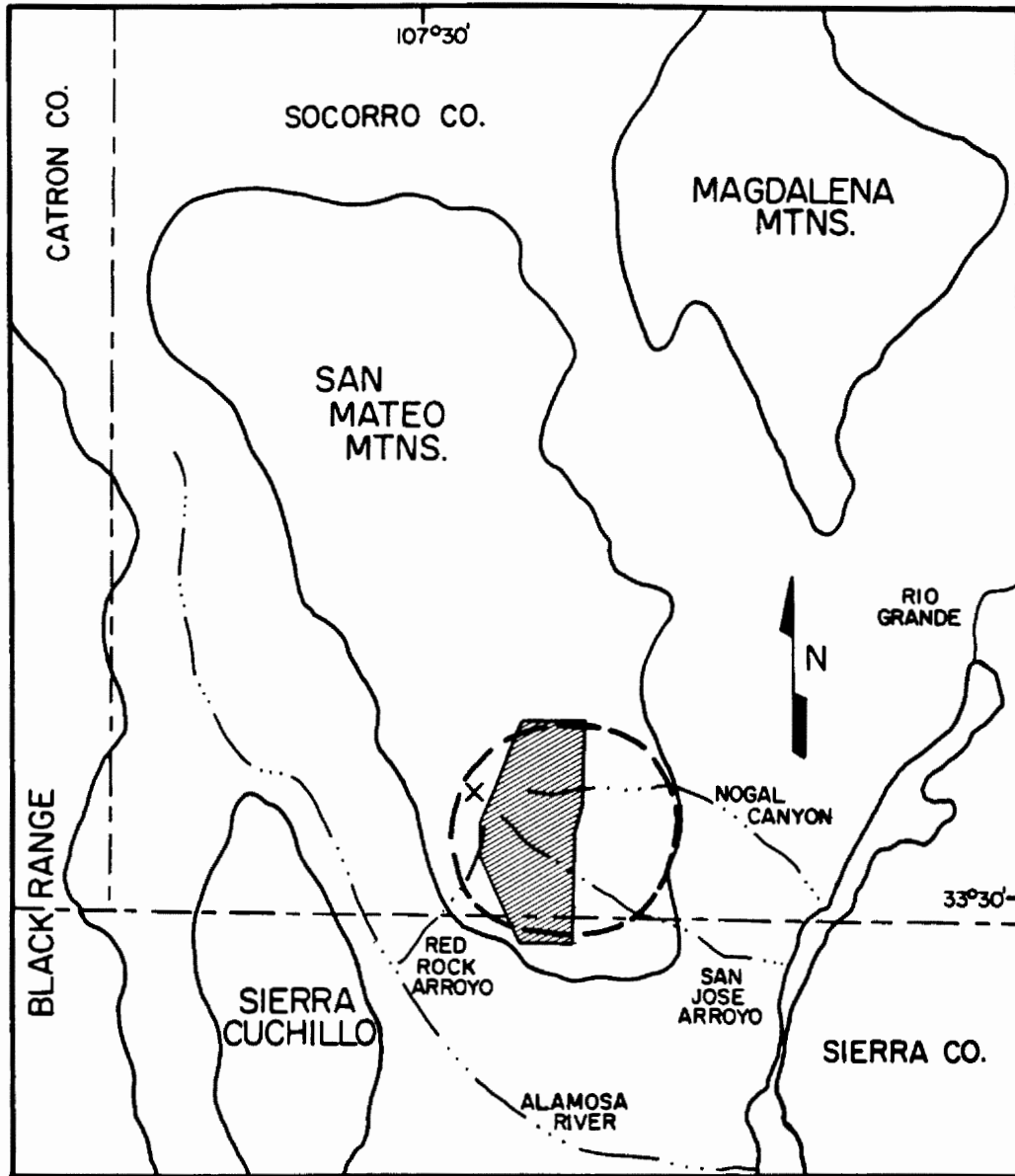
Quaternary extension within the southern Rio Grande rift area. Deal and Rhodes (1976) interpreted this structure zone as the southern margin of the Nogal Canyon cauldron.

Nogal Canyon Cauldron

Deal and Rhodes (1976) proposed the existence of the Nogal Canyon cauldron located in the southern San Mateo mountains (Fig. 14) based on reconnaissance results and reinterpretation of previous work. Evidence cited includes structural, stratigraphic, and intrusive features used to define the ring-fracture zones, the cauldron-filling ash-flow tuff, and other inherent features of volcano-tectonic depressions. Deal and Rhodes (1976, p. 56) suggest that

"... the southern margin of the cauldron is outlined by a series of small stocks that intrude the Vicks Peak Rhyolite, ..., an arcuate fault pattern also is present around the southern margin of the cauldron".

The structure zone appears well documented along the southern border area; however, arcuate continuity of the fracture zone to the northeast and northwest has not yet been established by detailed mapping. Deal and Rhodes (1976) interpreted the Springtime Canyon Quartz Latite as a post-cauldron lava erupted along the northern portion of the ring-fracture zone. Mapping in the northern region of the study area did not document eruptive centers for the quartz latite, nor the existence of a structural segment possibly correlative with a ring fracture zone. If present, the fractures associated with the northern margin



EXPLANATION

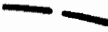
-  NOGAL CANYON CAULDRON MARGIN
-  NOGAL CANYON STUDY AREA
-  VICKS PEAK



Figure 14. Location map of the proposed Nogal Canyon cauldron in the southern San Mateo mountains (modified after Deal and Rhodes, 1976).

should appear north of Roberts Canyon. According to Deal and Rhodes (1976), the Vicks Peak Tuff which erupted from the Noyal Canyon cauldron reaches 650 m thicknesses in the southern San Mateo mountains and thinner "outflow facies" occur in the Sierra Cuchillo and Magdalena mountains. However, ash-flow tuff thicknesses exceeding 620 m do exist in non-cauldron fill ash-flows under appropriate topographic conditions. A cauldron-fill volcanoclastic and extrusive sequence overlying the Vicks Peak Tuff is not present within the map area possibly reflecting the erosional level of the volcanic pile. Detailed evidence for the existence of a cauldron is not conclusive, but inference supporting its presence is strong.

CHAPTER V

ALTERATION

Introduction

Hydrothermal alteration effects within the Nogal Canyon study area enclose "fissure-type" silver-gold occurrences in the San Jose and Quartz Hill districts and intrusive breccia at Aragon Hill. Wall rock alteration occurring as local and extensive mineralogical and textural changes exhibits characteristic and systematic zonation commonly observed within epithermal systems. Alteration assemblages associated with precious metal vein occurrences consist of silicification, intermediate argillic and advanced argillic alteration. Hypogene alteration connected with the Aragon Hill intrusive breccia includes phyllic alteration apparently unrelated to "fissure-type" occurrences elsewhere. Supergene argillization locally overprints intermediate argillic assemblages in the Nogal and Springtime Canyon areas. Alteration mapping served to delineate alteration assemblages, their distribution, and their spatial and temporal relationships. Mapping specifically gained insight into zoning characteristics in order to establish exposure levels of the epithermal vein systems. XRD analyses supplemented the establishment of phyllosilicate zonation

within intermediate argillic intervals adjacent to the Pankey mine area and elsewhere within the San Jose district.

Intermediate Argillic Alteration

Intermediate argillic alteration, as defined for the San Jose district occurrences, consists of essential kaolinite, illite, montmorillonite-illite mixed layer clay, and montmorillonite with accessory pyrite and quartz. Argillic assemblages occur within the Vicks Peak Tuff and basal portions of the Springtime Canyon Quartz Latite and represent the areally and volumetrically most extensive alteration grade within the San Jose district. Distribution is restricted to areas north of San Jose arroyo and appears spatially related to major structures cross-cutting the Springtime Canyon, Nogal Canyon, and San Jose arroyo areas (Plate 1). In outcrop, argillized rocks vary from irregularly distributed selvages enveloping fracture systems to broad, pervasive, blanket-like occurrences confined to intervals beneath the Vicks Peak Tuff and Springtime Canyon Quartz Latite contact (Fig. 15). Controls on the distribution and intensity of argillic alteration include proximity to structures, structure width, wall rock porosity and permeability (i.e., welding characteristics), fracture intensity, wall rock grain size and mineralogy, and location of permeability barriers. The massive, impermeable Springtime Canyon Quartz Latite exerted an important role in affecting the distribution of intermediately argillized rocks. Locally argillic alteration



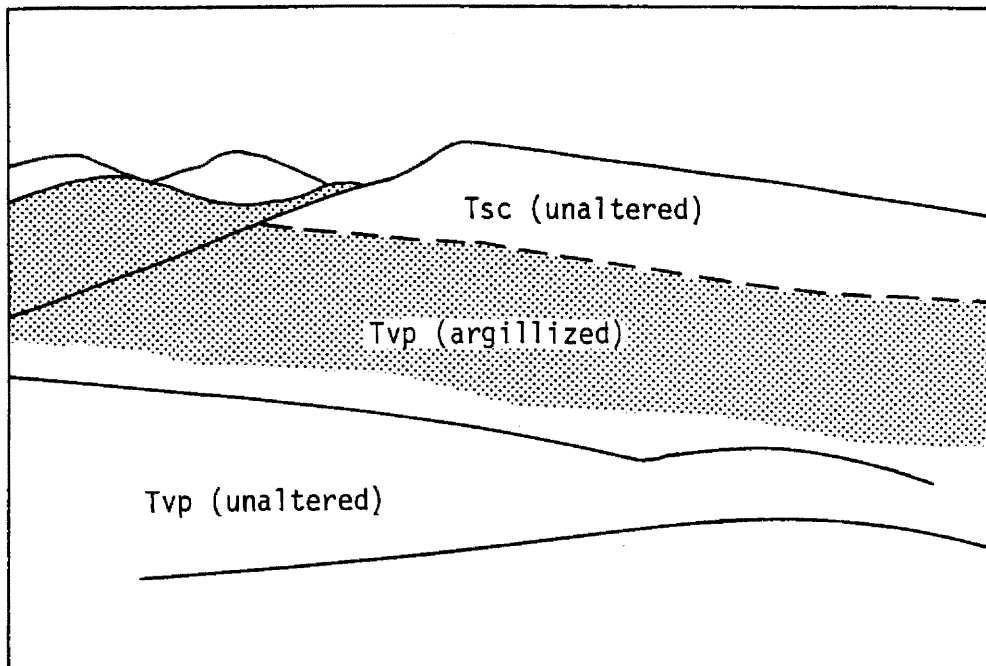
Figure 15. Pervasive intermediate argillic alteration of the Vicks Peak Tuff cropping out in the Taylor Shaft area; clip board is 30 cm across.

extends vertically upward from the Vicks Peak-Springtime Canyon contact and gradationally diminishes in intensity over tens of feet into the quartz latite flow. The upper intervals of the flow exhibit weak supergene propylitic effects. These field relations appear best developed in exposures located in the southwest quarter of Sec. 27, T8S, R5W. Therefore, argillic alteration postdates the emplacement of quartz latite flows, and the unit behaved as a vertical permeability barrier to ascending hydrothermal fluids resulting in lateral migration and "blanket type" intermediate argillization (Fig. 16).

Weak to moderate argillic alteration typically envelopes structures varying from 0-40 m outward. Clay abundances total 1-10 percent for weak grades and 10-50 percent for moderate grades with kaolinite, illite, montmorillonite, and montmorillonite-illite mixed-layer clays present. Porphyritic and eutaxitic primary structures and textures are commonly well preserved. Strong argillic alteration appears confined to intervals beneath the Vicks Peak-Springtime Canyon contact occurring in sporadic amounts. Phyllosilicate contents, dominantly montmorillonite and montmorillonite-illite mixed-layer clays, vary from 50 to 65 percent. These alteration zones exhibit obliteration of primary textures and generally display a porous, friable, buff white appearance. Kaolinite occurs as microcrystalline, mosaic-like aggregates replacing both phenocrysts and groundmass in the rhyolite host. It preferentially replaces plagioclase in relation to sanidine phenocrysts and appears as irregular, patchwork intergrowths



(A)



(B)

Figure 16. (A) displays intermediate argillic alteration restricted beneath the Vicks Peak Tuff - Springtime Canyon Quartz Latite contact in the Frank's Well area. (B) depicts the distribution of rock types and hydrothermal alteration in the above photo.

within the groundmass (Fig. 17). Montmorillonite and illite occur as microcrystalline anhedral to bladed aggregates dispersed throughout the matrix. They locally form patchwork masses replacing feldspar phenocrysts. XRD studies indicate montmorillonite-illite randomly mixed-layered clays vary from illitic rich, calcium montmorillonite end members to illitic poor, montmorillonite varieties. The mixed-layer clays locally appear intergrown with either kaolinite or montmorillonite and occur as microcrystalline aggregates replacing both sanidine and matrix material. Quartz, primarily generated from desilication reactions during argillization, occurs as dispersed aggregates commonly lining open spaces. Argillic zone pyrite is discussed in the following section.

A sequential phyllosilicate zoning pattern exists peripheral to structures in the Nogal Canyon area and is best exemplified adjacent to the Pankey fault on the north side of Springtime Canyon (Fig. 18). Relative to the largest abundance of clay minerals present, the following zones occur successively outward from the structure: 1) kaolinite, 2) montmorillonite-illite, and 3) montmorillonite. Kaolinite is locally absent from the inner alteration zones in which case the montmorillonite-illite grade occurs adjacent to the structure. Within the mixed-layer subzone, a sequential enrichment in the illitic component and corresponding depletion of the montmorillonitic portion occurs within the randomly mixed-layer clays as the structure zone is approached. Overall phyllosilicate zoning patterns, specifically cation variation

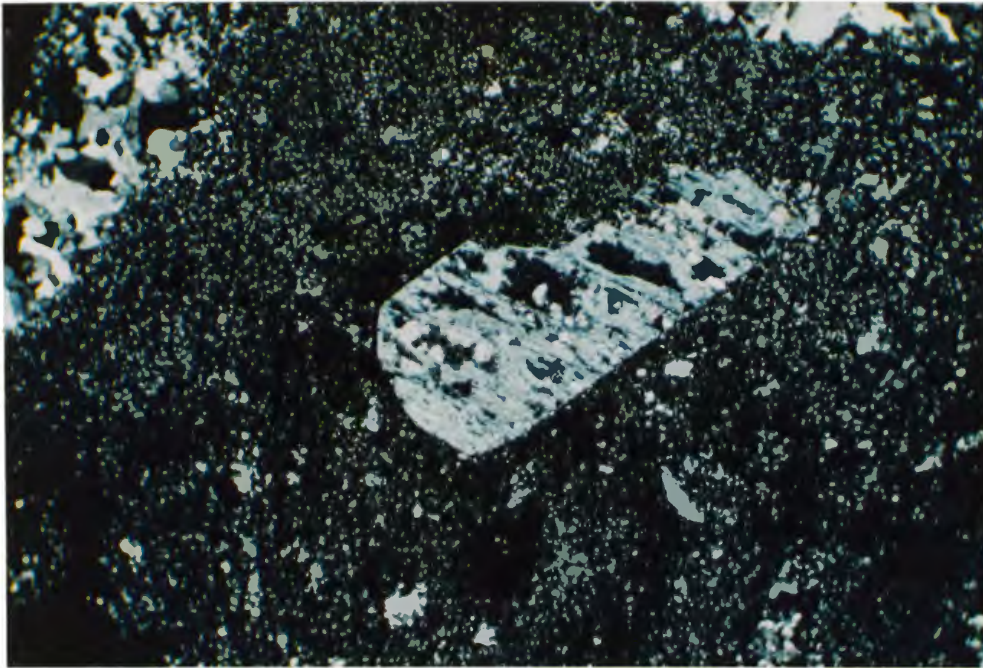


Figure 17. Photomicrograph of microcrystalline kaolinite aggregates replacing feldspar phenocryst within the Vicks Peak Tuff; the scale along the bottom dimension is 4.4 mm, x-nicols.

EXPLANATION

INTERMEDIATE ARGILLIC ALTERATION

 KAOLINITE ZONE

 MONTMORILLONITE-ILLITE ZONE

 MONTMORILLONITE ZONE

 <1 VOLUME % PYRITE  1-2 VOLUME % PYRITE

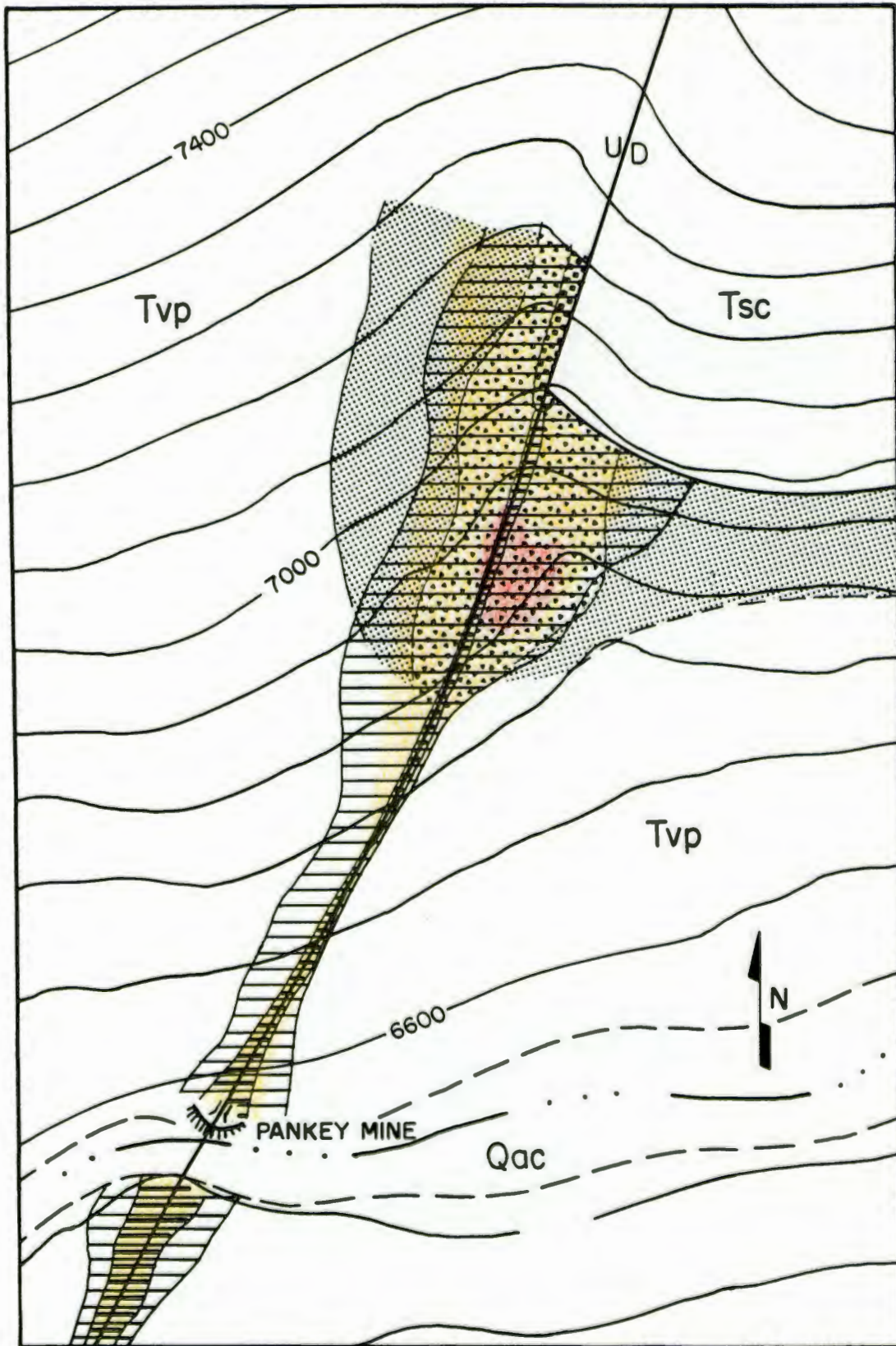
SILICA ALTERATION

 VEIN-INFILLINGS AND PERVASIVE

 VEINLET NETWORK AND STOCKWORK


0 250 500 FEET

Figure 18. Phyllosilicate alteration zoning relationships along the Pankey fault in the Pankey mine area. Refer to Plate 1 for complete rock type and symbol explanation.



of the mixed-layer clays, reflects varying degrees of hydrolytic attack and consequent cation leaching as function of fluid hydrogen ion ratios and temperature. Discussion of the chemical and stability aspects in hydrothermal alteration processes appear in Hemley and Jones (1964), Creasey (1966), and Rose and Burt (1979).

Argillic alteration grades laterally outward into fresh rock away from the structure or controlling channelway, and where present, inward into silica alteration. Field relations indicate argillic alteration is in part contemporaneous with but typically predates silicification. Evidence includes the existence of pervasive silica fronts adjacent to the structure which encroach through argillized wall rock. Also within the Pankey structure zone, late stage silica cement encapsulates argillized breccia fragments.

Pyrite Alteration

Throughout much of the San Jose district, variable amounts of accessory pyrite occurs as the stable sulfide phase within the intermediate argillic alteration assemblage hosted in the Vicks Peak Tuff. Although genetically associated with intermediate argillization, pyrite is discussed separately in this section due to the presence of both epigenetic and post-depositional/deuteric pyrite within the Vicks Peak rhyolite. Pyrite is also associated with silica alteration, phyllic alteration, and

advanced argillic alteration which are discussed separately in the following sections.

Epigenetic pyrite coeval with argillic alteration occurs as fine grained (0.05-0.3 mm) disseminations varying from traces to as much as 2 percent in volume. Average abundances are less than 1 volume percent. Pyrite always exhibits discrete, cubic euhedral forms and occurs ubiquitously throughout argillized areas. Pyrite abundances commonly increase vertically within argillized intervals, and zones beneath the Vicks Peak Tuff-Springtime Canyon Quartz Latite commonly exhibit the highest pyrite percentages as evidenced in the Pankey mine area (Fig. 18). The majority of field occurrences display an oxidized cubic pyrite boxwork in hand specimen generated by weathering processes. However, local unoxidized pyrite occurrences within argillized samples reflect a hypogene origin. Successive supergene stages of magnetite replacing pyrite are followed by hematite replacements of secondary magnetite. Final weathering products include goethite/hematite and manganese oxide which typically impart reddish-brown stains to the argillized units. Liberation of H_2SO_4 during the pyrite degeneration process is a strong control affecting the distribution of supergene argillic alteration. Hypogene pyrite forms due to sulfidization of the original iron silicates and/or oxides during argillization (Creasey, 1966).

In contrast to epigenetic pyrite, post-depositional/deuteric pyrite occurs within the unaltered, densely welded lower intervals of the Vicks Peak Tuff. The pyrite

characteristically appears as distinct, subhedral to anhedral crystals only occurring sporadically throughout the massive tuff. Grain sizes are less than 0.20 mm in size.

Advanced Argillic Alteration

Advanced argillic alteration occurrences in the San Jose district contain essential quartz and alunite with accessory pyrite, specularite, kaolinite, and chalcedony. The quartz-alunite assemblage is the least widespread alteration type present in the study area and crops out as bold, resistant knobs on Indian Peak (Plate 1). Advanced argillic alteration occurs as intense, pervasive replacement deposits hosted within the transition from densely to partially welded intervals of the Vicks Peak Tuff. The replacement bodies characteristically feature flat bottoms conformable to the host rock compaction foliations and occur adjacent to the Indian Peak fault. Host rock porosity, permeability, and fracture intensity exerted only a minor effect on the distribution and intensity of this alteration grade. Localization was controlled primarily by proximity to the major structure and the generation of acidic, oxidizing fluids during hydrothermal alteration.

The quartz-alunite replacement deposits consist of a fine grained, massive to vuggy, buff white lithology varying to pale reddish-brown where stained by iron-oxides. Pre-alteration textures are poorly preserved in the lower densely welded host rock intervals and typically well preserved in the upper

partially welded portions of the Vicks Peak Tuff. Sporadic quartz phenocrysts exhibiting secondary silica overgrowths and bladed alunite aggregates pseudomorphing sanidine phenocrysts reflects relict porphyritic textures of the rhyolite. Relict eutaxitic structures, best preserved in the upper partially welded zones, are characterized by tabular alunite intergrowths replacing flattened pumice fragments and lining lithophysal cavities (Fig. 19). Fine grained quartz (mean grain size 0.2 mm) appears as seriate, xenomorphic aggregates ranging from 80-94 volume percent. Quartz abundance is greatest in the lower portions of the replacement bodies. Alunite ranging from 6-20 volume percent occurs as fine grained anhedral forms (0.3-1.5 mm) xenomorphically intergrown with quartz. Euhedral, hexagonal, plate-like mosaics of alunite replace sanidine phenocrysts and pumice fragments, and infill lithophysal cavities. XRD analysis confirms the potassium rich end member of the alunite group. Opaque minerals include both pyrite and specularite present as fine grained (< 0.025 mm) crystals disseminated throughout the quartz-alunite rock. Subhedral to anhedral pyrite, occurring in trace amounts, consistently appear enclosed poikilitically within quartz and never spatially associated with alunite phases. Trace amounts of specularite exist as subhedral forms dispersed primarily within alunite aggregates and to a lesser extent enclosed in quartz. Specularite is a distinct primary phase. Kaolinite appears as sporadic microcrystalline aggregate masses lining vuggy cavities. Textural relations indicate that kaolinite postdates alunite/specularite

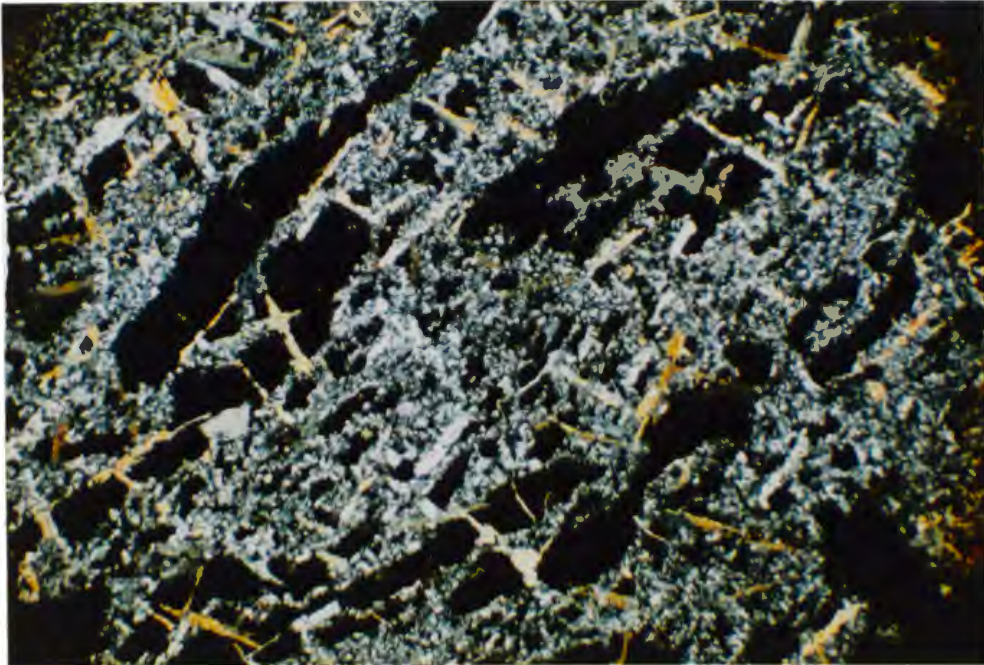
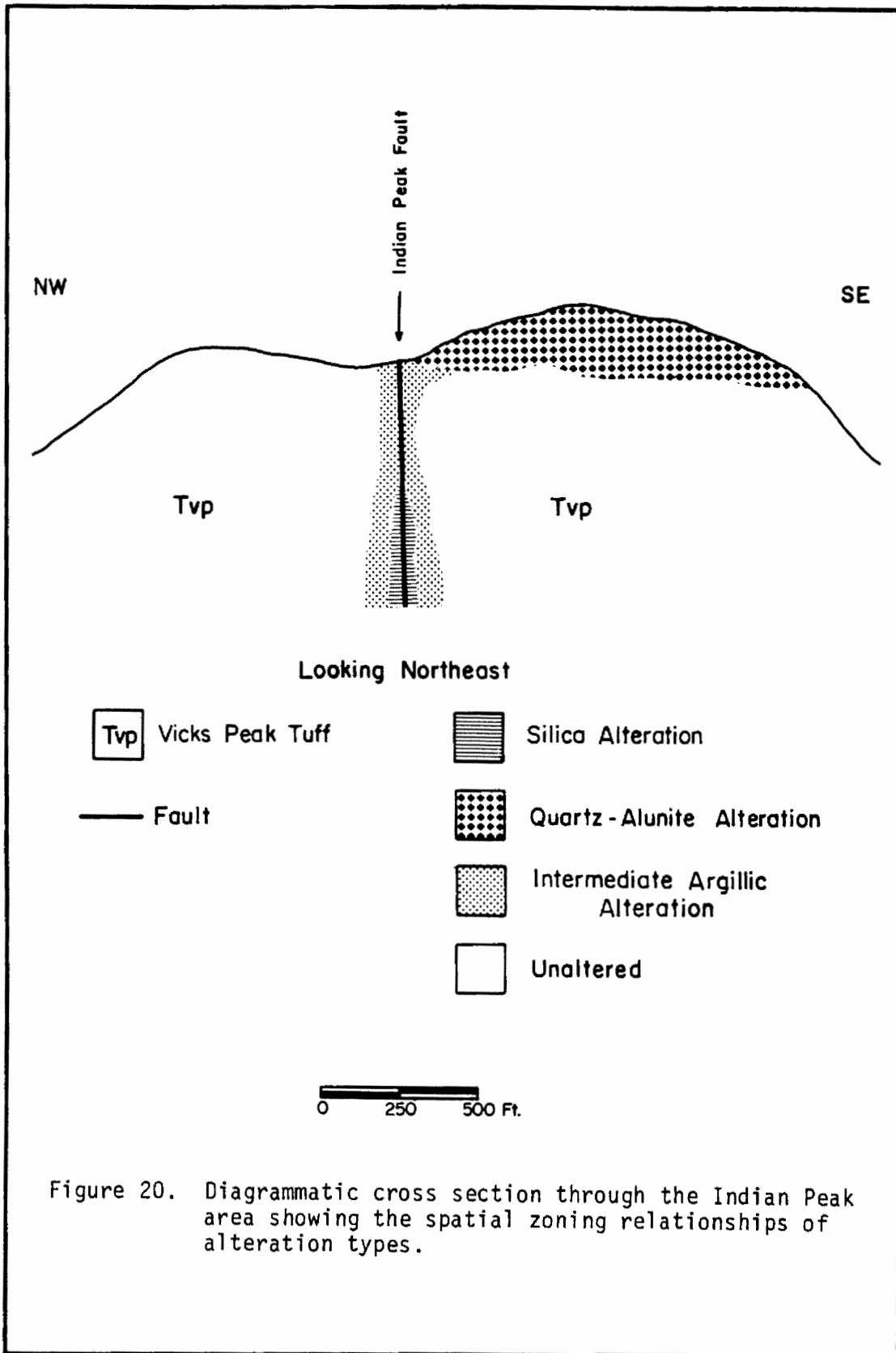


Figure 19. Photomicrograph of quartz-alunite replacement of a pumice fragment within the partially welded Vicks Peak Tuff; the scale along the bottom dimension is 11 mm, x-nicols.

deposition. Trace amounts of primary zircon exist as unaltered, subhedral forms averaging less than 0.025 mm. Chalcedony occurs as amorphous vug and void infillings associated with supergene silica dissolution and precipitation.

The advanced argillic deposits extend downward into unaltered Vicks Peak rhyolite. Basal contacts with unaltered tuff appear sharply contacted over intervals of less than 6 m. Alteration stratigraphically below the quartz-alunite deposits along the Indian Peak fault consists of strong pervasive wall rock silicification with thin argillic envelopes peripheral to the fault. Vertical relations are diagrammatically displayed in Figure 20. Surrounding argillic alteration assemblages commonly exhibit non-discernable primary textures in contrast to preserved textures within the quartz-alunite deposits.

Replacement alunite deposits commonly indicate a near surface, shallow environment in which oxidation of hypogene H_2S -bearing fluids play an important genetic role. Near surface oxidation of hypogene fluids usually occurs due to boiling and/or mixing with meteoric waters above the paleowater table. High acidity is necessary for alunite-silicate equilibrium assemblages under elevated temperatures and kaolinite is stable instead of alunite under the same sulfate and potassium activities when pH increases (Hemley et al., 1969). Mineral stability relationships of coexisting alunite and specularite pairs at 250°C indicate highly oxidizing conditions and pH's of less than 4 (Kesler et al., 1981). Chemical aspects of advanced argillic

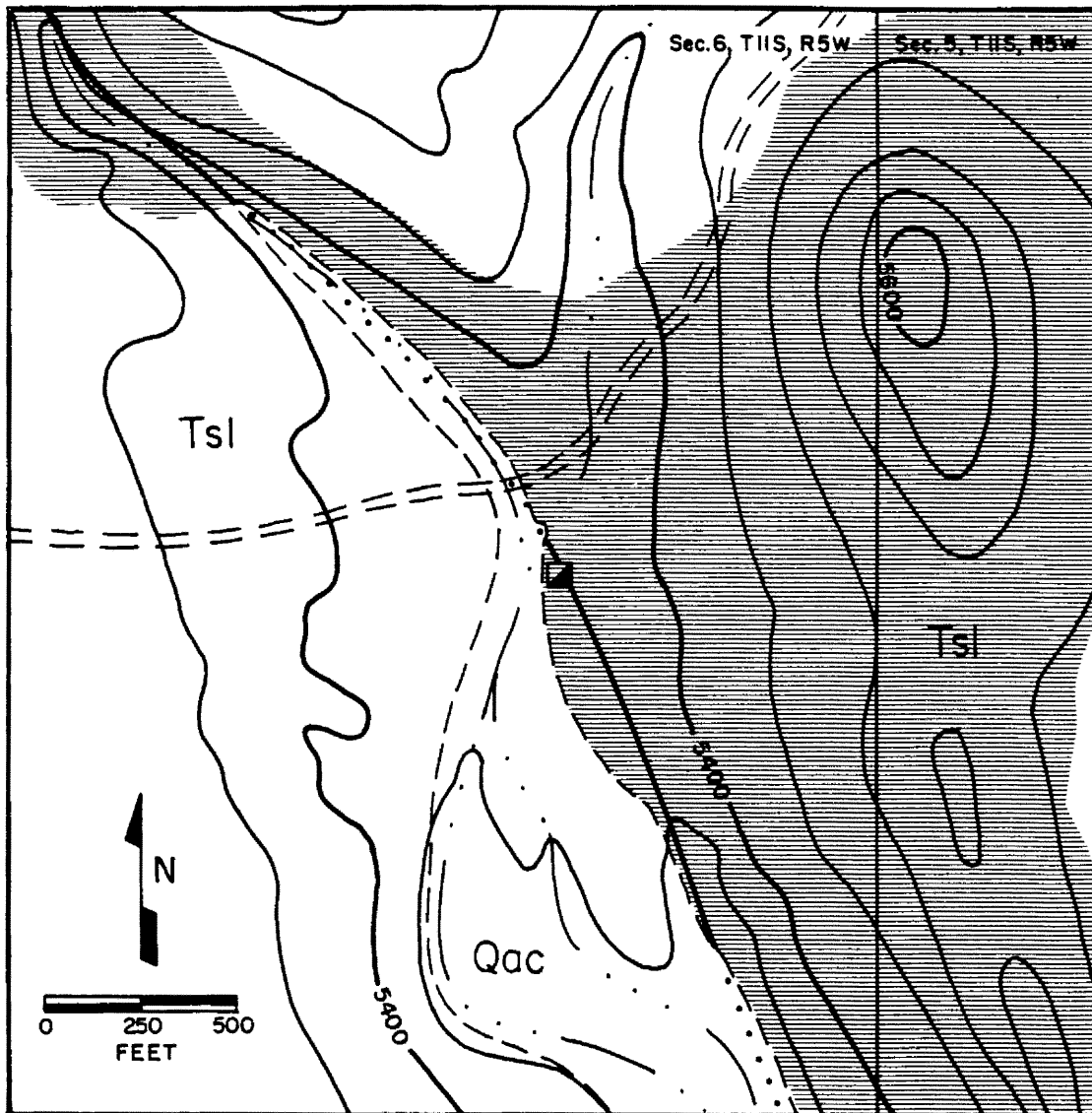


alteration are well defined by Hemley and Jones (1964) and Knight (1977).

Silica Alteration

Silicification refers to wallrock alteration containing hydrothermally introduced quartz as its major component and occurs spatially associated with major structures. Quartz also exists as abundant products within advanced argillic zones and as minor quantities within intermediate argillic intervals described previously in this chapter. Precious metal (silver-gold) mineralization is contemporaneous with vein-infilling silica in the San Jose and Quartz Hill districts.

Silica alteration, as defined herein, includes essential crystalline quartz with or without accessory to trace amounts of pyrite, calcite, adularia, sericite, pyrolusite, and cryptomelane. Silica introduction occurs associated with major structures in the San Jose district hosted within the Vicks Peak Tuff. Extensive silica alteration also appears in the Seferino Fifty-fifty Hill area within the lower Spears laharc breccia (Fig. 21). Silica alteration subdivides into the following three occurrence types: 1) vein infillings and breccia replacements within structure zones, 2) pervasive wallrock replacement bordering structures, and 3) quartz veinlet networks or stockworks varying from subparallel to random orientations adjacent to structures. Factors controlling intensity and type of silica alteration include primary porosity and permeability, wall rock



EXPLANATION

— — — CONTACT	Qac ALLUVIUM AND COLLUVIUM DEPOSITS
$\frac{U}{D}$ — — — FAULT	Tsl LOWER MEMBER OF THE SPEARS FORMATION
▣ SHAFT	 SILICIFICATION
CONTOUR INTERVAL IS 40 FT.	

Figure 21. Reconnaissance geologic and alteration map of the Seferino, Fifty-fifty Hill area, Nogal Canyon study area.

mineralogy and grain size, fracture abundance, structure zone width, and duration of the alteration episode. Vein infilling silica occurrences consist of fine to medium grained quartz (> 0.05 mm) exhibiting a variety of open space textures. Crustification features including cockscomb and colloform banding textures appear ubiquitously in this silica alteration type, and massive to vuggy textures also occur. Drusy quartz commonly surrounds argillized or silicified breccia fragments within the structure zone. Amethystine cockscomb quartz and colloform chalcedonic quartz commonly appear as alternating bands along with quartz pseudomorphs after bladed calcite. Adularia, present in the Pankey vein, occurs as fine grained, drusy crustiform bands alternating with quartz-rich layers (Fig. 22). Plumose to bladed sericite, also present in the Pankey vein, ranges in size from 0.05-0.5 mm and is intergrown with massive quartz and manganese minerals. Adularia and sericite deposition occurs as vein infilling silicification in the lower exposure levels at the Pankey mine. Calcite occurs as euhedral lamellae intergrown with quartz and adularia gangue; however, due to post-depositional replacement, quartz pseudomorphing calcite forms now exist. Pyrite consists of fine grained (mean size 0.3 mm), euhedral to subhedral crystals disseminated within massive quartz vein material. Pyrite content rarely exceeds 1 volume percent and typically appears in trace amounts. Pyrolusite and cryptomelane exist as compact granular masses commonly infilling vuggy portions of massive vein material.



Figure 22. Vein-infilling, finely crystalline and chalcedonic silica from the Pankey mine displaying crustification textures and fine grained adularia bands (stained yellow).

Manganese oxide abundance varies from trace amounts up to 20 volume percent imparting a black color to the vein material.

Pervasive wallrock silica alteration adjacent to structures varies from thin selvages outward to envelopes 30 m wide within the Vicks Peak rhyolite. However, in the laharic breccia located at Fifty-fifty Hill, pervasive wallrock silicification extends up to 460 m away from the structure (Fig. 21). Intensities generally diminish abruptly from strong to weak replacement over a 100 to 200 m distance outward from the controlling structure. Pervasive silicification results in a dense, extremely brittle lithology which characteristically retains the host rock's original color. Primary textures and structures are preserved to varying degrees depending upon intensity of silica alteration. In the Fifty-fifty Hill area, intense pervasive replacement of the laharic breccia results in a white, fine grained, massive, high silica rock which comprises the majority of the resistant hill. Quartz pseudomorphing calcite occurs locally within intervals of silicification at the Pankey mine in close proximity to the fault. In the vicinity of the Pankey fault, pervasive silica alteration locally encroaches through and overprints previous intermediate argillic alteration.

Quartz veinlet silica alteration occurs peripheral to major structures and varies from poorly developed veinlet networks to weakly developed stockworks. Quartz networks occur as subparallel to randomly oriented veinlets varying from hairline to 5 mm widths. Weak quartz stockworks appear as

multidirectional hairline to 5 mm veinlets and only exist over small areas of the Pankey mine and Indian Trail Canyon areas. Veinlet mineralogy consists of dominant fine grained, massive to drusy quartz with sporadic pyrite and iron oxides. In the Pankey mine area, quartz veinlet networks exist in orientations subparallel to the major structure and occur adjacent to the lower-most exposure levels of the fault (Fig. 23). The veinlet network grades upward to a randomly oriented character and finally increases in intensity to a weak, multidirectional stockwork. The quartz stockwork zone corresponds to the base of the intermediate argillic interval and appears topographically above the intense vein-filling, and pervasive silicification alteration types (Fig. 18).

Silicification commonly grades laterally into intermediate argillic alteration suggesting a close genetic relationship. Silica alteration is in part coeval, but typically postdates argillic alteration. Late stage quartz veinlet networks and stockworks locally exhibit alteration selvages within the argillized host rock; however, earlier quartz veinlet stages do not.

Phyllic Alteration

Phyllic alteration enveloping the Aragon Hill area consists of essential sericite, montmorillonite-chlorite mixed-layer clay, and accessory kaolinite, quartz, pyrite, and late stage calcite. Alteration appears concentrically centered about the

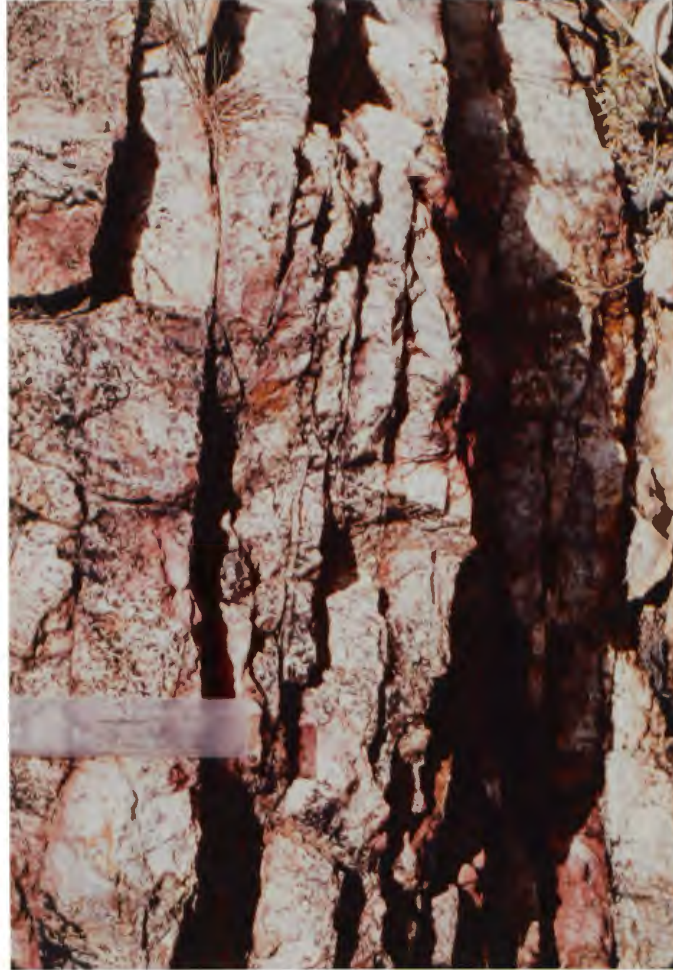


Figure 23. Subparallel quartz veinlet networks peripheral to the Pankey fault in the Pankey mine area; ruler is 15 cm long.

intrusive breccia with intensity gradients diminishing outward into the surrounding rhyolite flow-dome rocks (Plate 1). Controls on intensity include fracture distribution and mineralogical character of the rhyolite, and composition of the intrusive breccia. Alteration within the contrasting rock types differs in both mineralogical and textural signatures.

Phyllic alteration strongly affects the Aragon Hill intrusive breccia and shows ubiquitous continuity throughout all exposures present. The breccia is massive, very friable, and characteristically pale green in outcrop. The heterolithic breccia fragments consistently display differential alteration assemblages. Andesite clasts typically possess dominant montmorillonite-chlorite alteration products, whereas rhyolitic fragments host a sericite, kaolinite, quartz, and pyrite assemblage. The pale green breccia matrix consists of pervasive montmorillonite-chlorite mixed-layer clay and sericite with lesser quartz, kaolinite, pyrite, and calcite and represents intense alteration of the original rock flour matrix (Fig. 24). The montmorillonite poor, chlorite mixed layer clay, confirmed by XRD analysis, imparts the distinctive color. Microscopically it occurs as flake-like microcrystalline intergrowths varying from 45-70 volume percent. Sericite appears as plumose, mosaic-like masses commonly interspersed with kaolinite and the mixed layer clay. Abundances range from 25-30 volume percent. Minor amounts of kaolinite exist as sporadic microcrystalline intergrowths in patchwork masses. Minor quartz occurs as both drusy vug infillings in patchwork masses

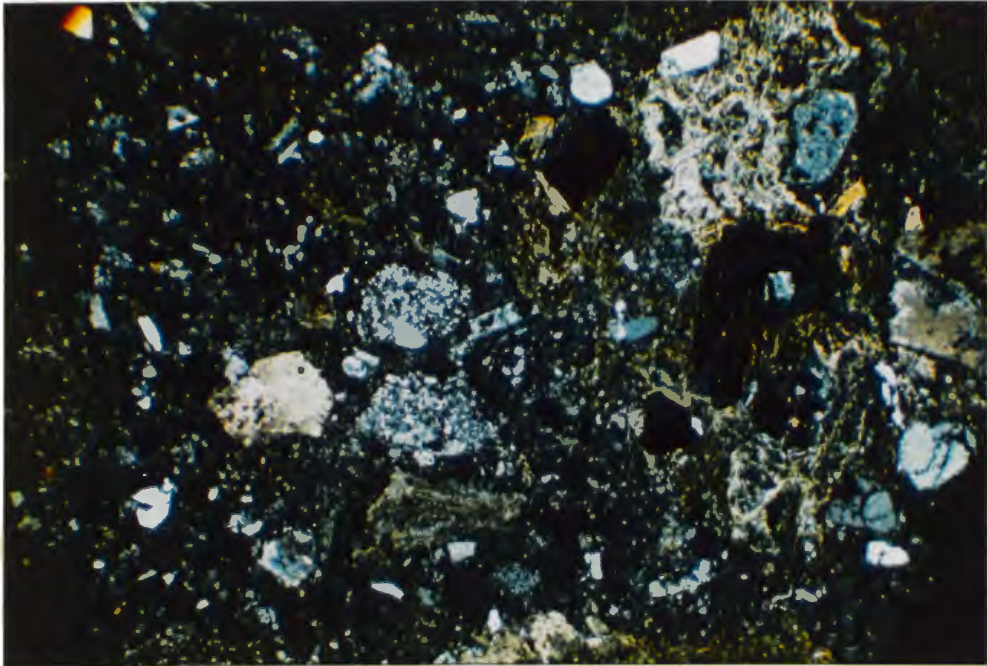


Figure 24. Photomicrograph of the Aragon Hill intrusive breccia matrix material; the scale along the bottom dimension is 11 mm, x-nicols.

and microcrystalline aggregates with fine grained (< 0.05 mm), euhedral, cubic pyrite. Irregular masses of late stage calcite commonly replace kaolinitic alteration material and abraded feldspar crystals within the matrix. Calcite and quartz exist as late stage fracture fillings intergrown with euhedral, bladed barite.

Altered rhyolite flow-dome rocks appear as massive, buff white lithologies varying to pale brownish-red where stained by iron oxides. Alteration intensities vary from weak to moderate and preserve the original porphyritic textures. Moderately developed phyllic alteration consists of 10-25 volume percent sericite occurring as plumose aggregates pervasively replacing feldspar phenocrysts and matrix material (Fig. 25). Kaolinite appears as microcrystalline aggregates pervasively altering plagioclase crystals and constitutes from 4-7 volume percent. Trace amounts of relict pyrite boxworks show alteration to iron oxides. Weakly phyllic altered rhyolite exhibits up to 10 volume percent sericite and less than 4 volume percent kaolinite. Silica generally appears as irregular microcrystalline masses throughout the groundmass and as local veinlet occurrences. Weak phyllic alteration exhibits biotite-stable assemblages; however, sericite commonly replaces biotite within moderate phyllically altered intervals.

Phyllic alteration centered over Aragon Hill is genetically related to and coeval with intrusive breccia emplacement. The diverse alteration types hosted within heterolithic breccia fragments, the ubiquitous distribution of strong phyllic

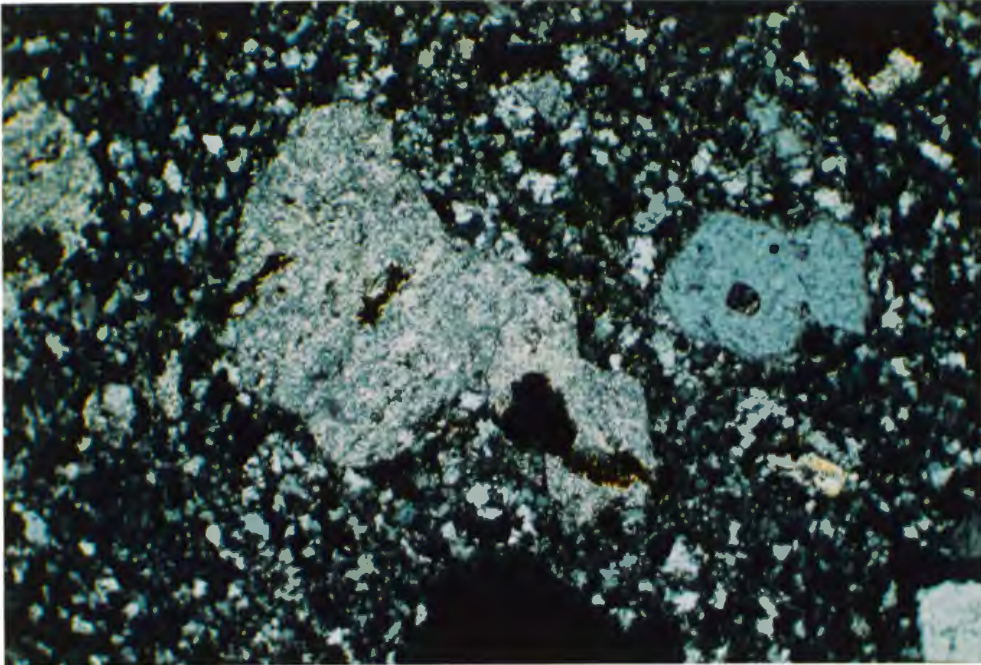


Figure 25. Sericite replacing feldspar phenocryst and groundmass of the rhyolite flow-dome unit; the scale along the bottom dimension is 4.4 mm, x-nicols.

alteration, and the lack of zonation or crosscutting alteration types suggests contemporaneous alteration rather than post-emplacement processes. The single, synchronous alteration episode is postdated by the weakly developed quartz-calcite-barite fracture filling phase.

Supergene Alteration

Supergene weathering effects occur in the majority of rock types exposed in the Nogal Canyon study area and specifically overprint hypogene argillic alteration in the San Jose district area. Supergene kaolinite development appears anomalously located in relation to sequential phyllosilicate zoning patterns. Kaolinite locally occurs far removed from structures where the hypogene argillic alteration grades correspond to montmorillonite development. Supergene kaolinite is erratically confined to the upper intervals of partially welded Vicks Peak Tuff in the Nogal Canyon and Springtime Canyon areas and corresponds to zones of intermediate argillic alteration. Distribution appears primarily influenced by porosity and permeability of the rhyolite tuff and occurrence and abundance of hypogene argillic zone pyrite. The weathering of pyrite, which locally totals 2 volume percent, generated sufficient H_2SO_4 to induce lower pH conditions. Resulting circumstances allowed substantial cation leaching of existing montmorillonite and conversion to kaolinite phases. Supergene kaolinite alteration displays a porous, punky, bleached white appearance and

locally varies to veinlet occurrences. Supergene altered Vicks Peak rhyolite appears similar to unaffected hypogene argillization products and is usually indistinguishable in hand specimen except for veinlet occurrences.

The Pankey mine vein mineral assemblage also reflects weathering effects by the occurrence of supergene carbonates, chlorides, and possible supergene native silver and gold.

CHAPTER VI

MINERALIZATION AND TRACE ELEMENT GEOCHEMICAL STUDIES

Introduction

Previously recognized precious metal mineralization within the southern San Mateo mountains exists within the San Jose and Quartz Hill districts and in the Aragon Hill area. The San Jose and Quartz Hill occurrences constitute volcanic hosted "fissure-type" silver-gold vein associations. The precious metal bearing veins infill and replace steeply dipping, northeast and northwest trending, major structures. Gold-silver occurrences at Aragon Hill appear associated with late stage quartz-barite-calcite bearing fractures that crosscut the Aragon Hill intrusive breccia and are genetically related to igneous activity responsible for breccia emplacement. Ages of mineralization for epithermal occurrences remain unknown. Mining activity in the San Jose district occurred during the early 1930's; however, total production primarily from the Pankey mine amounted to negligible quantities. Lasky (1932) described occurrences at the Rhyolite and Pankey mines in the Noga Canyon area, and Harley (1934) briefly outlines features of the Quartz Hill fissure vein. Of the known mineral occurrences present in the study area, only the Pankey vein cropping out in

Springtime Canyon underwent a broad examination during this study.

A detailed rock sampling program supplemented geologic studies in evaluating the precious metal resource potential of the study area. Two hundred fifty one samples were collected from altered and mineralized areas. All rock samples were analyzed for gold and silver and selected samples were analyzed for arsenic, antimony, copper, molybdenum, lead, and zinc by atomic absorption spectrometry. Sample locations appear on Plate 3 and sample descriptions and analytical results are presented in Appendix A. Geologic mapping, alteration mapping, and mine workings delineated favorable areas of potential mineralization. These areas include the Pankey mine area, the Indian Trail Canyon area, the Indian Peak area, the Taylor Shaft area, the Rhyolite mine area, the Aragon Hill area, and the Seferino, Fifty-fifty Hill area (Plate 1). The sampling program attempted to locate mineralized zones and detect primary leakage haloes in the vicinity of faults, fractures, and alteration zones. Secondary chemical dispersion played a weak to moderate role in affecting trace element abundances and patterns.

Geochemical data interpretation utilized basic statistical techniques to describe trace element distributions and establish anomalous values for further investigation. The cumulative frequency plot method described by Sinclair (1974) and Lepeltier (1969) established threshold values for gold and silver; however, the plots were of limited applicability to other elements due to insufficient population parameters.

Inspection of log histogram plots were inconclusive in partitioning distributions of gold, silver, arsenic, antimony, copper, molybdenum, lead, and zinc; values generally approximate lognormal distributions.

Pankey Mine

The Pankey vein occurrence in the northern portion of the study area crops out as resistant rib-like forms along the northern side of Springtime Canyon and is hosted within the Vicks Peak Tuff. Mineralization at the Pankey mine corresponds with vein-infilling silicification first discovered by prospectors in 1931 (Lasky, 1932).

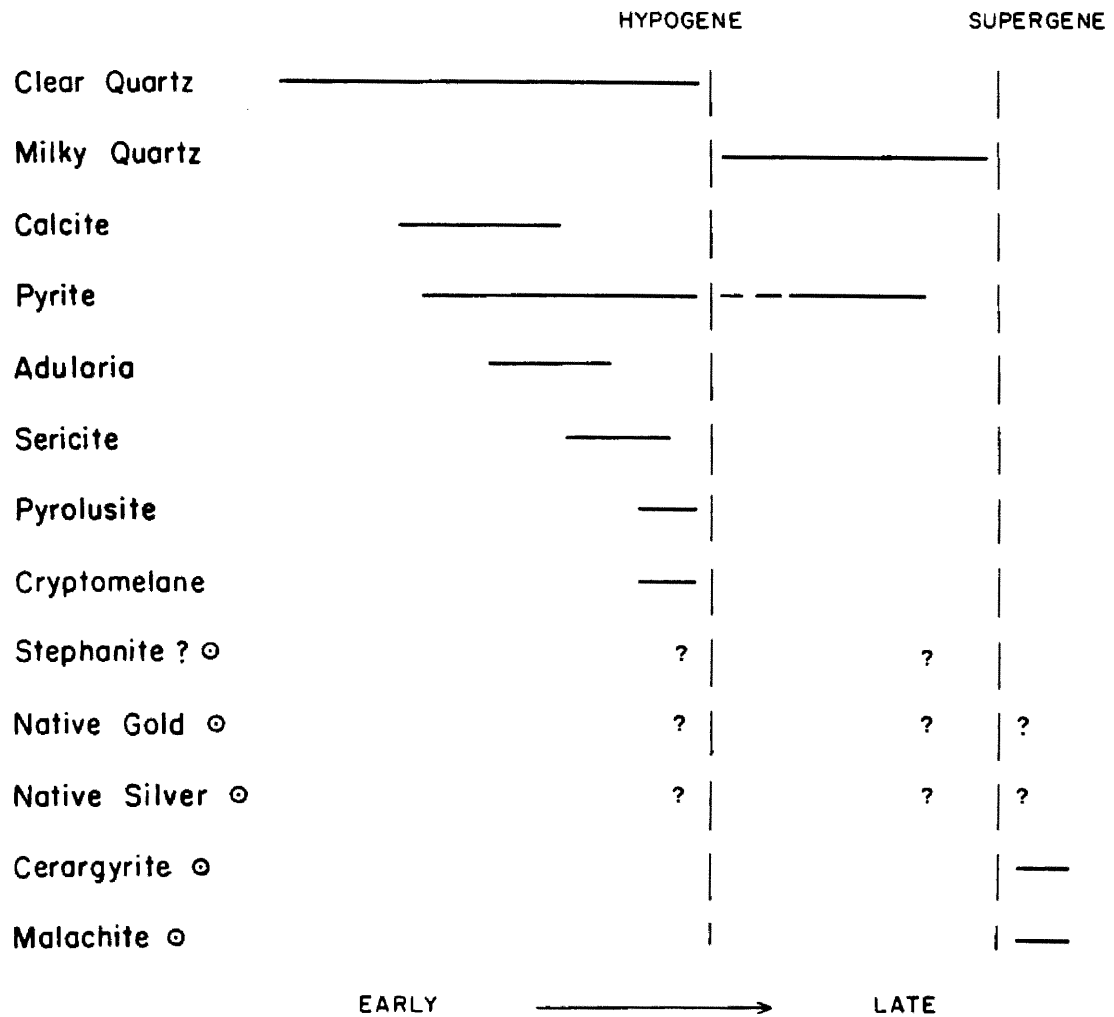
Within the mine area, the Pankey fault strikes N17⁰E and locally exhibits a concave to the west surface trace (Fig. 26). The structure dips from 75 to 79 degrees to the east. The fault's 125 m vertical exposure interval varies from a 12 m wide silicified structure zone at the canyon base upward to a 0.3 m wide uncemented fissure at the hanging wall contact of the Vicks Peak Tuff and Springtime Canyon Quartz Latite.

Vein gangue mineralogy includes early clear quartz and late milky/grey quartz with decreasing amounts of calcite, adularia, sericite, pyrolusite, cryptomelane, and pyrite. A paragenetic diagram depicting age relations appears in Figure 27. The early quartz occurs as crustiform banded and massive vein infillings and to a lesser degree veinlet networks present within or adjacent to the structure zone. The clear quartz veinlet



Figure 26. Exposure of the Pankey fault on the north side of Springtime Canyon. The trace of the N 17° E trending structure is defined by the resistant rib-like outcrops. Where obscured, the fault trace is depicted by the solid white line.

PARAGENESIS



ALL DATA ARE FROM THIS STUDY EXCEPT
FOR ⊙ TAKEN FROM LASKY (1932)

Figure 27. Paragenesis of the Pankey mine mineralization.

networks extend outward sporadically in subparallel arrangements to the structure and are controlled by joints adjacent to the lower exposure levels. Lamellar calcite along with fine grained adularia form thin crustification bands contemporaneously interlayered with early quartz. However, quartz ubiquitously replaces lamellar calcite resulting in fine to coarsely bladed silica pseudomorphs. Fine grained disseminated pyrite, ranging up to 1 volume percent, typically occurs poikilitically enclosed within quartz and calcite. Sericite appearing as random plumose aggregate masses occurs within the interior, massive, vuggy portion of the vein. It locally occurs spatially associated with banded adularia, but typically exists veinward of adularia suggesting a younger paragenesis. Pyrolusite and cryptomelane form discrete granular aggregates infilling the massive to vuggy center portions of the vein indicating a hypogene origin. Manganiferous vein material commonly exhibits significant precious metal contents suggesting either primary precious metal co-existence or supergene adsorption of mobilized metals. Late stage milky/grey quartz appears as veins, veinlets, and late breccia cement commonly exhibiting fine grained, open space textures. Pyritiferous milky quartz infills the lower intervals of the structure forming discontinuous, fine grained masses and ranges from 0.15-0.5 m wide. Late quartz crosscuts the earlier silicification phase and forms an areally more extensive and more abundant quartz veinlet network and stockwork compared to the early quartz veinlet occurrences. A major

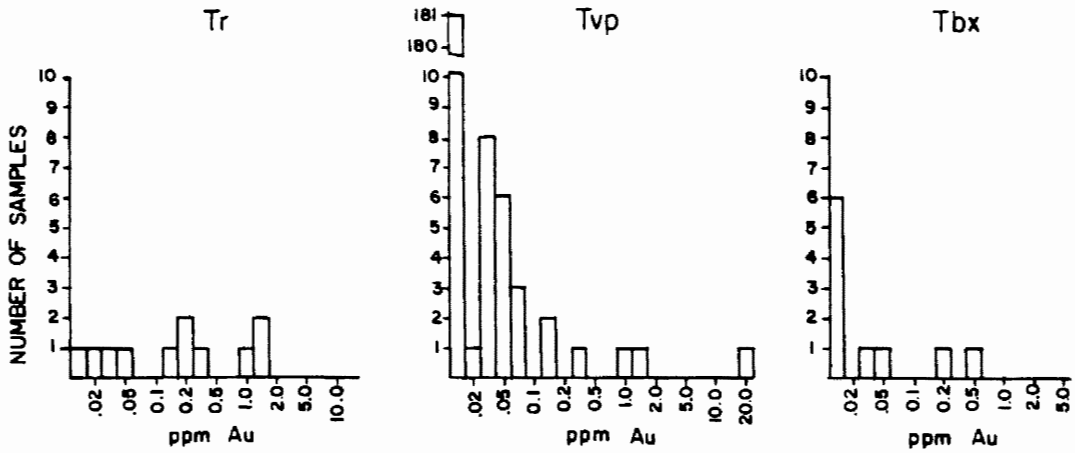
structural episode or series of fracturing events separates the early from the late stage quartz phases allowing for greater distributional extent of the late stage silicification.

Ore minerals documented by Lasky (1932) include native gold, native silver, stephanite?, cerargyrite, and malachite; cursory polished section work during this study did not reveal any precious metal phases. Lasky (1932, p. 109) states that "...stephanite? was observed on polished surfaces of ore as particles of microscopic size almost completely replaced by native gold and silver". Also according to Lasky (1932, p. 109), native gold and silver occurs spatially associated with limonite and "...in certain occurrences strings of gold follow the banding of the limonite and this relationship suggests that gold had been derived from the pyrite". The presence of cerargyrite, malachite, and noted occurrences of gold-silver phases suggests a supergene dominated ore mineralogy at the Pankey mine. Probable silver sulfosalts and auriferous pyrite constituted hypogene ore bearing minerals. The silver to gold ratios as computed from geochemical samples average 100:1.

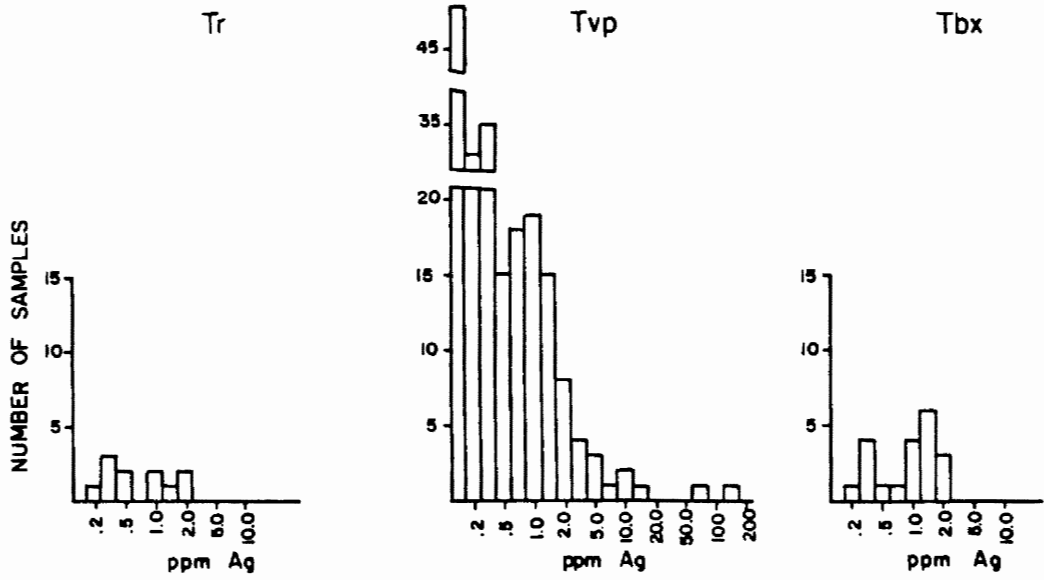
Trace Element Geochemistry

Gold

The range of gold values in rock samples from the study area is summarized in Figure 28. A cumulative frequency plot of Vicks Peak Tuff gold values defines a sigmodal "S" shaped curve denoting a bimodal distribution (Fig. 29). This distribution



	Rx Type	Pop.	Mean	St. Dev.	Threshold	Int. Thres.
Au	Tvp	N=205	0.13	1.6	0.26	0.10-0.26
	Tbx	N=10	0.090	0.19		
	Tr	N=11	0.12	0.088		



	Rx Type	Pop.	Mean	St. Dev.	Threshold	Int. Thres.
Ag	Tvp	N=205	2.1	13.	1.6	1.1-1.6
	Tbx	N=10	1.3	0.34		
	Tr	N=11	0.88	0.70		

Figure 28. Summary of gold and silver population parameters from hydrothermally altered rock samples in the Nogal Canyon study area.

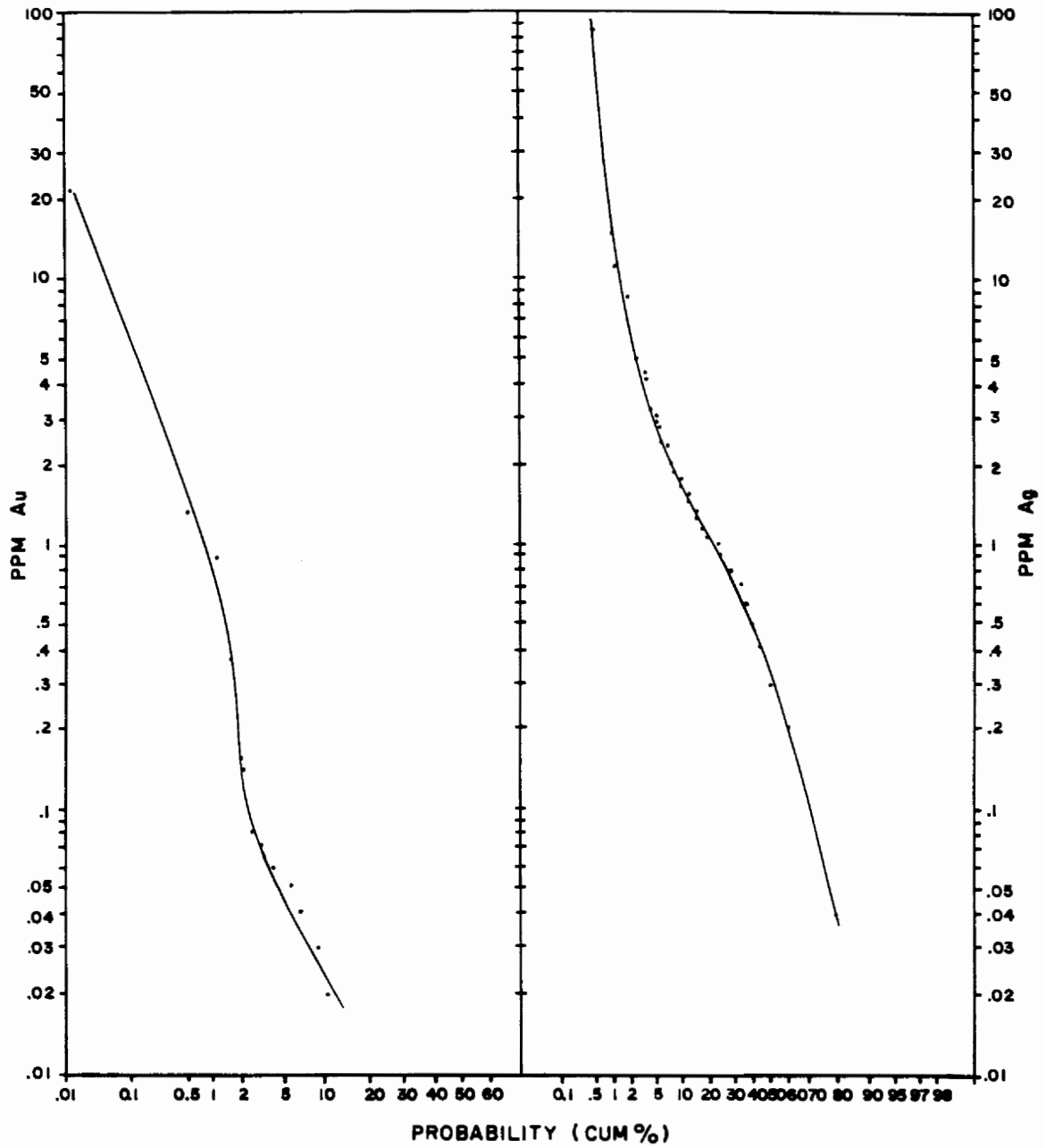


Figure 29. Bimodal cumulative probability plots of gold and silver in hydrothermally altered rocks from the Noyal Canyon study area (N=205).

represents background and anomalous populations, the latter resulting from mineralization. Anomalous gold detected in amounts greater than the threshold (0.26 ppm) in 8 samples represents 3 percent of the distribution. Gold values within the intermediate threshold range (0.10-0.26 ppm) were detected in 8 samples also representing 3 percent of all gold analyses. Samples below the detection limit (0.02 ppm) received a 1.5 ppb value for statistical purposes based on gold abundance for rhyolites (Wedepohl, 1969).

In the Pankey mine area, the areal distribution of anomalous gold samples occurs restricted to silica alteration along the Pankey fault and does not appear disseminated within the wall rock (Fig. 30). Intermediate threshold values in the Rhyolite mine area exist within silicified structure zones and sporadically adjacent to the Rhyolite fault in weakly silicified/ argillized wall rock (Fig. 31). Anomalous gold also occurs confined to the silicified structure zone in the Seferino, Fifty-fifty Hill area (Fig. 32). Significant gold distribution in the Taylor Shaft area appears in silica vein material along structure, and although pervasive silica replacement persists approximately 30 m into the hanging wall, no anomalous samples were detected (Fig. 31). Anomalous gold samples do not occur in the Indian Trail Canyon, Indian Peak, East Aragon Hill, or Red Rock Canyon areas. In the Aragon Hill area, significant gold values occur both in the intrusive breccia and in the rhyolite flow rocks. Anomalous values from the intrusive breccia are erratic, but typically are confined to minor structures with

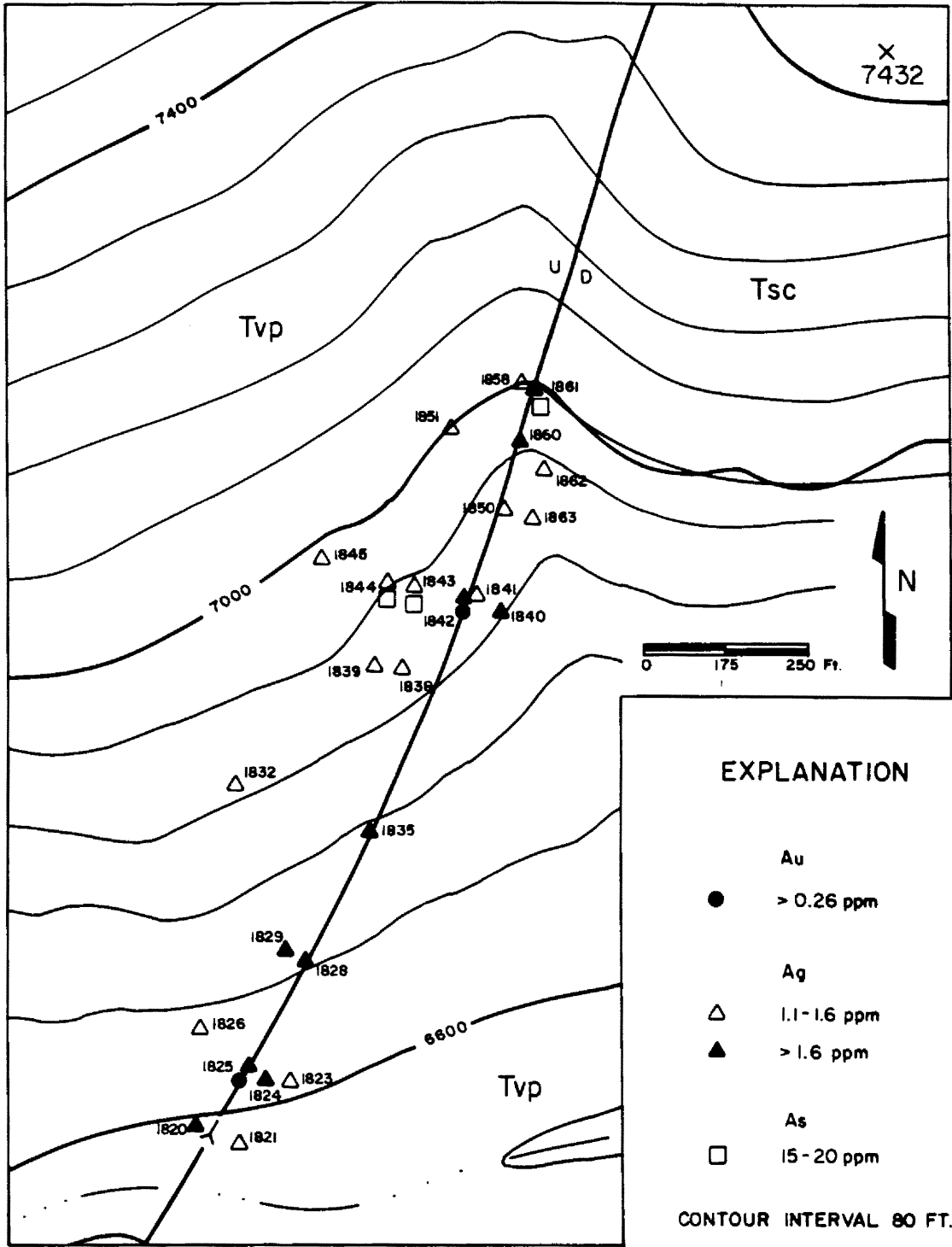


Figure 30. Geochemical distribution of gold, silver, and arsenic in hydrothermally altered rock samples from the Pankey mine area; numbers correspond to sample numbers. Refer to Plate 1 for complete rock type and symbol explanation.

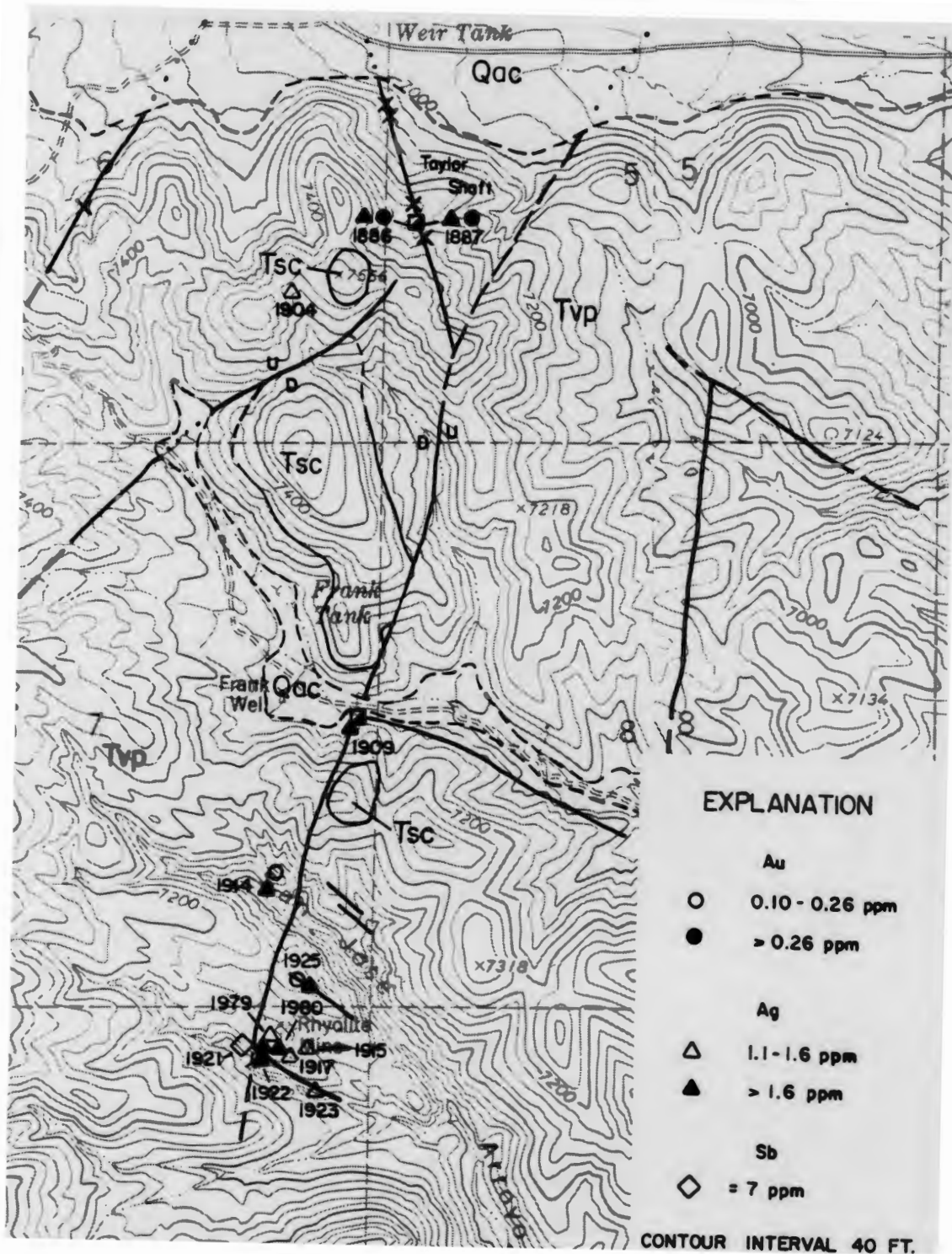


Figure 31. Geochemical distribution of gold, silver, and antimony in hydrothermally altered rock samples from the Taylor Shaft and Rhyolite mine areas; numbers correspond to sample numbers. Refer to Plate 1 for complete rock type and symbol explanation.

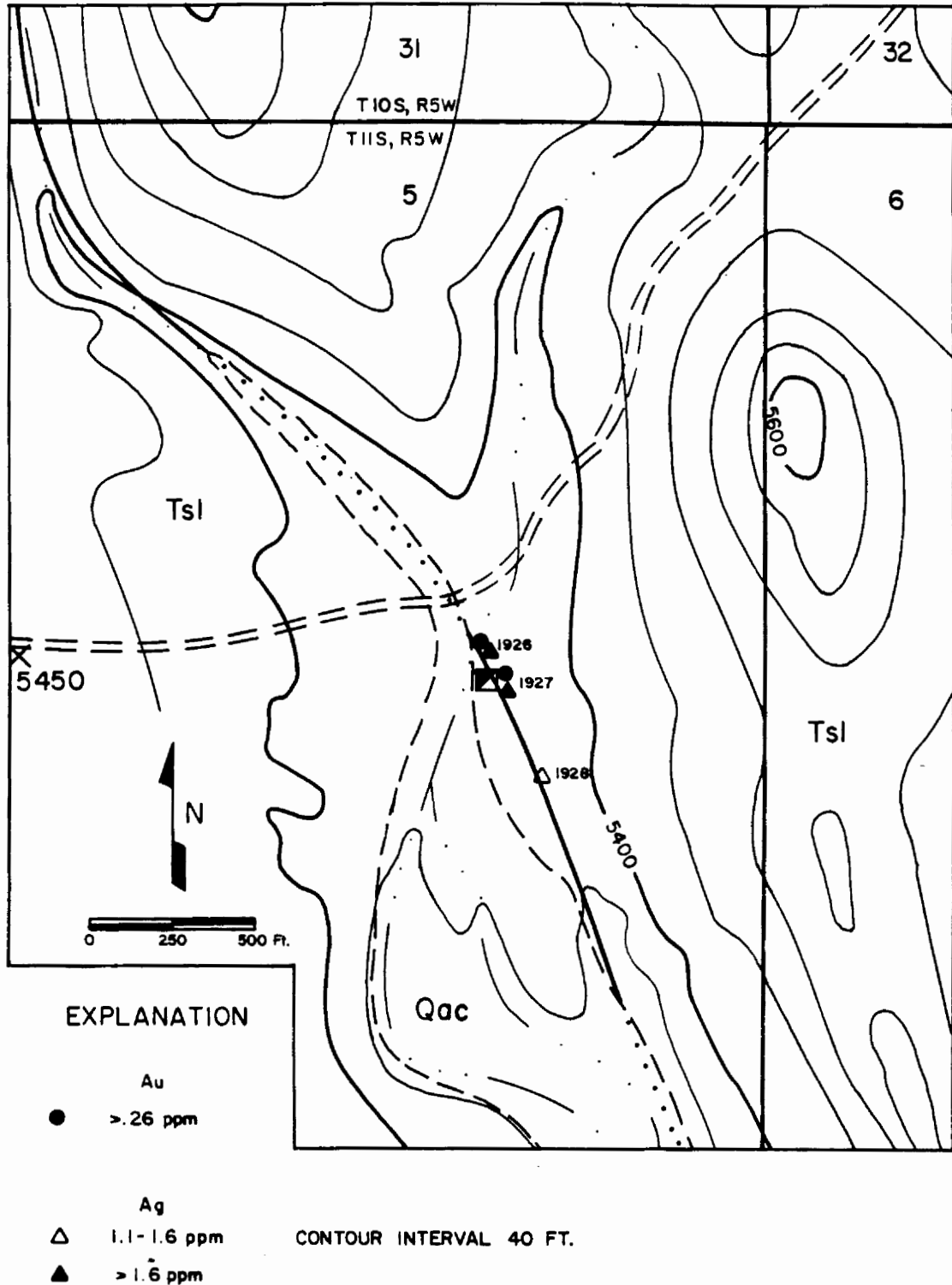


Figure 32. Geochemical distribution of gold and silver in hydrothermally altered rock samples from the Seferino, Fifty-fifty Hill area; numbers correspond to sample numbers. Refer to Plate 1 for complete rock type and symbol explanation.

quartz-barite-calcite infillings (Fig. 33). Gold is probably not hosted within the intrusive breccia matrix. Significant gold values, consistently above detection limit, exist along sericitized, argillized fractures within the rhyolite adjacent to the intrusive breccia contact area (Fig. 34).

Correlation of Vicks Peak Tuff gold and silver samples documents a very strong geochemical association supported by Lasky's (1932) description of native gold and silver intergrowths within the Pankey area (Table 3). Geochemical affinity of gold and silver in the intrusive breccia and rhyolite flow rock contrast poorly with Vicks Peak rhyolite sample results. Gold and copper from the Pankey area show close chemical affinity; however, cursory ore mineral studies have not explained the basis for the relationship.

Silver

Major silver distribution features in rock samples from the study area are displayed in Figure 28. Partitioning of the Vicks Peak Tuff silver distribution utilizing a cumulative probability graph defines bimodal populations interpreted to represent background and anomalous values (Fig. 29). The plot differs from standard bimodal distributions in that negative skewness defines the curve inflection area instead of positive skewness. The negative skewness possibly results from local redistribution during secondary dispersion. Anomalous silver occurs in amounts greater than the threshold (1.6 ppm) in 28 samples representing 11 percent of all samples. An intermediate threshold range

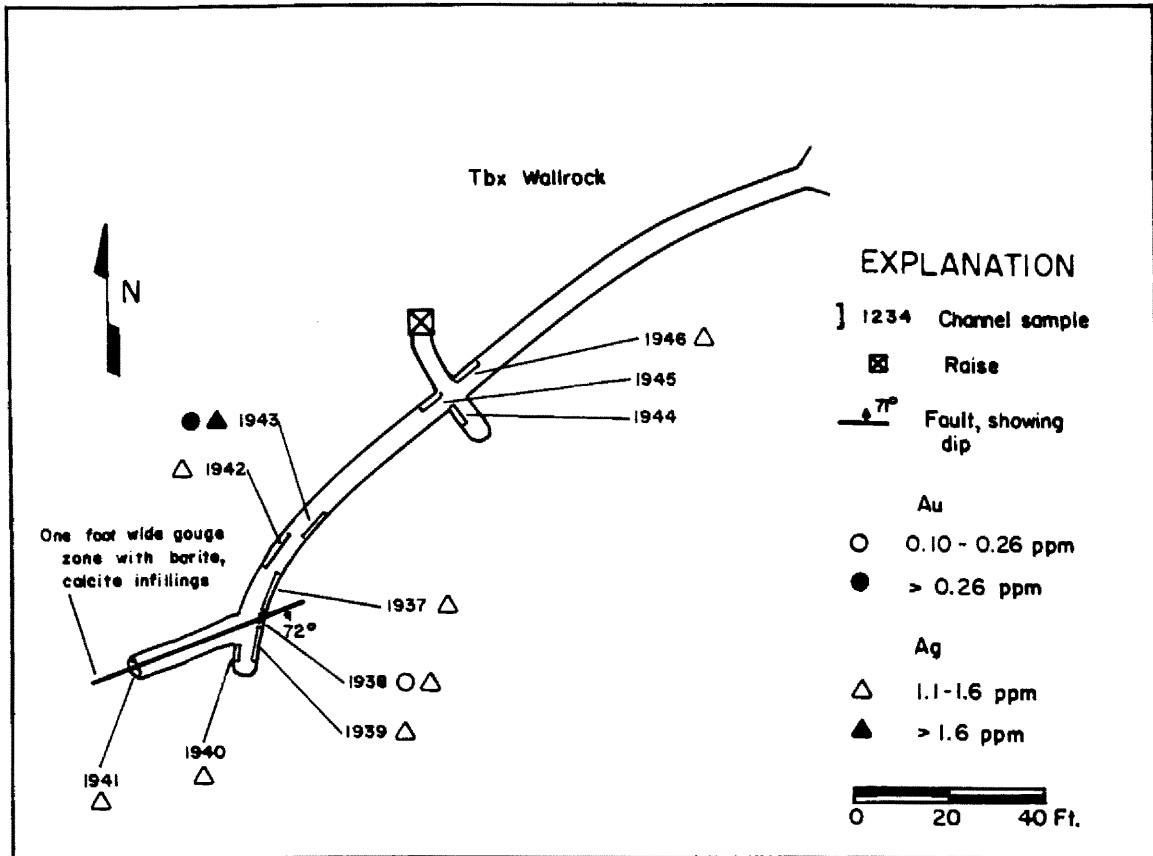


Figure 33. Geochemical distribution of gold and silver in continuous channel samples from the Henckley mine, Aragon Hill; numbers correspond to sample numbers.

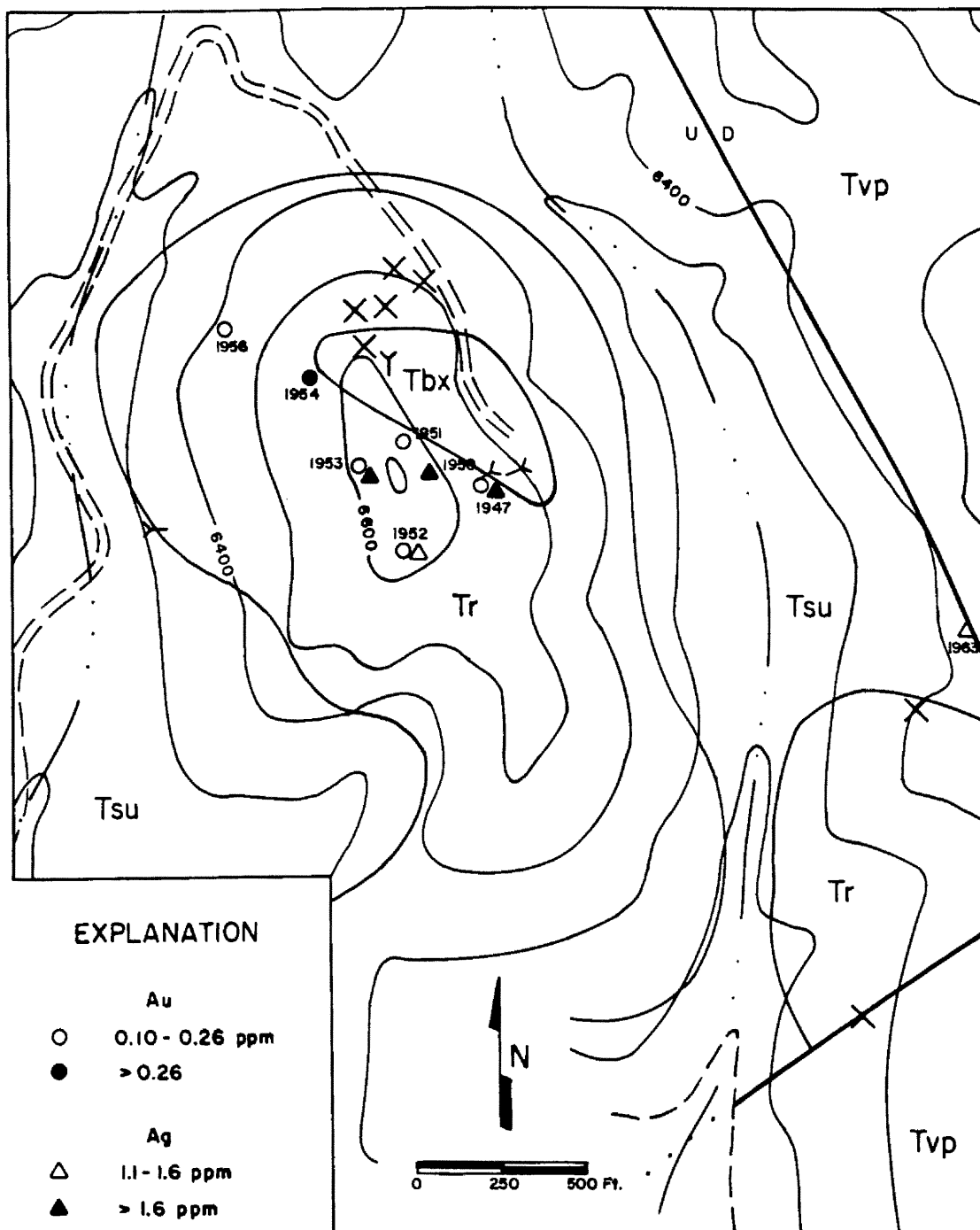


Figure 34. Geochemical distribution of gold and silver in hydrothermally altered rock samples from the Aragon Hill area; numbers correspond to sample numbers. Refer to Plate 1 for complete rock type and symbol explanation.

Table 3. Correlation coefficients from hydrothermally altered Vicks Peak Tuff rock samples in the Nogal Canyon study area, (N for Au and Ag= 205; N for As and Sb=88; N for Cu, Mo, Pb, and Zn=59).

	Au	Ag	As	Sb	Cu	Mo	Pb
Ag	0.92						
As	0.02	0.02					
Sb	0.08	0.04	0.11				
Cu	0.69	0.70	0.18	0.31			
Mo	0.28	0.32	-0.02	0.03	0.58		
Pb	-0.16	-0.19	0.04	0.00	-0.16	-0.12	
Zn	-0.14	-0.14	-0.05	-0.19	-0.12	-0.19	0.05

(1.1-1.6 ppm) contains 35 samples or 14 percent of the distribution. Analytical results below detection limit (0.2 ppm) were assigned a value of 0.04 ppm for statistical calculations based on silver abundance in volcanic rocks (Hamaguchi, 1959).

Distribution of silver values in the Pankey mine area is featured in Fig. 30. Anomalous samples consistently correlate with silica vein material and strong pervasive wall rock silicification immediately adjacent to the structure. Seven samples along structure range from 1.8 ppm to 84.2 ppm averaging 16.4 ppm and span a 125 m vertical interval. Minor amounts of anomalous values exist in weak to moderate pervasively silicified wall rock crosscut by quartz veinlets and argillized wall rock with veinlet silicification grading away from the structure. Intermediate threshold values occur in weak pervasively silicified wall rock with quartz veinlets and in argillized Vicks Peak Tuff with veinlet silica alteration away from the fault. Silver values quickly decrease away from the structure and correlate strongly with the intensity of pervasive and/or veinlet silica alteration. Significant values occur from 3 to locally 60 m away from the fault ranging up to 1.3 ppm. The Indian Trail Canyon and Indian Peak areas exhibit local significant silver values strictly confined to silicified fault zones (Fig. 35). In the Taylor shaft area, anomalous silver is hosted in silica vein material and two samples assayed 15.5 and 173.0 ppm (Fig. 31). No anomalous silver occurs in silicified wall rock adjacent to the structure. Distribution of anomalous silver in the Rhyolite mine area exists within and adjacent to

EXPLANATION

Ag

△ 1.1-1.6 ppm

▲ > 1.6 ppm

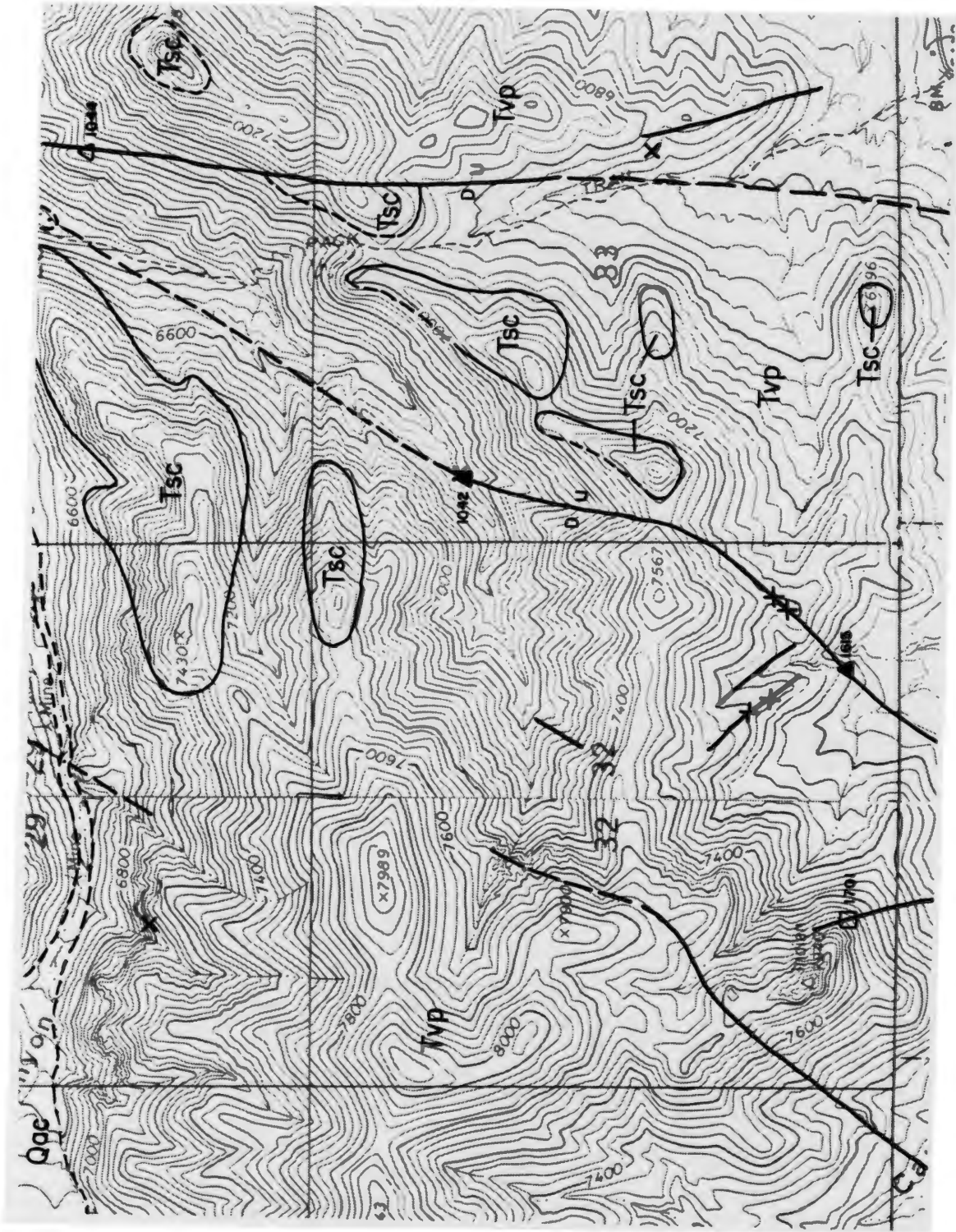
As

□ = 15 ppm

CONTOUR INTERVAL 40 FT.



Figure 35. Geochemical distribution of silver, and arsenic in hydrothermally altered rock samples from the Indian Peak and Indian Trail Canyon areas; numbers correspond to sample numbers. Refer to Plate 1 for complete rock type and symbol explanation.



pervasively silicified structure zones (Fig. 31). Few significant silver values occur outside fault zones. Intermediate threshold values correlate with weakly argillized wall rock crosscut by weak quartz veinletting. In the Fifty-fifty Hill area, significant values also occur strictly within the silicified structural zone and are not dispersed in intense pervasive silica alteration zones within the laharic breccia wallrock (Fig. 32). Significant silver values exist both in the intrusive breccia and rhyolite flow rock of the Aragon Hill area (Figs. 33, 34). Silver consistently ranges between 1-2 ppm and probably occurs within the quartz-sericite-pyrite-clay altered breccia matrix. Important silver values, 1.1 to 2.2 ppm, occur erratically within sericitized- argillized rhyolite flow rock adjacent to the intrusive breccia contact area. Sporadic intermediate threshold values occur along discontinuous structural zones in the Roberts Canyon, East Aragon Hill, and the Red Rock Canyon areas.

Correlation coefficients from the Pankey mine area suggest significant affinity between silver-copper and silver-gold (Table 3). Lasky (1932) discusses the presence of native silver intergrown with native gold, cerargyrite, and malachite in fissure ore from the Pankey vein; however, no primary copper minerals were observed. Silver shows poor correlation with antimony in the vein material sampled which does not substantiate Lasky's (1932) documentation of stephanite (Ag_5SbS_4). Hypogene cerargyrite will not form under 350°C in dilute hydrothermal fluids ranging in pH from 3-8 (Seward, 1976, p. 1339)

suggesting instead a supergene origin. Presence of a secondary copper mineral and a secondary silver chloride illustrates the influence of secondary dispersion processes on primary copper and silver haloes despite occurrence within strong pervasively silicified areas.

Arsenic

The range and distribution of rock chip arsenic values from the study area is presented in Figure 36. According to Wedepohl (1969) and Onishi and Sandell (1955), arsenic abundances in silicic volcanic rocks average 3.5 ppm and range up to 12 ppm in some glassy rocks. Inspection of the arsenic cumulative frequency plot shows a distinct negative skewness above 15 ppm documenting an abundance of 15 to 18 ppm values in the upper portion of the distribution (Fig. 37). The abundance of these low values results from either depletion during chemical weathering, depletion during hydrothermal alteration redistribution, or superimposed mineralization. Based on the available data, differentiation between the above mechanisms is not possible for significant arsenic values (> 15 ppm). Samples below detection limit (1 ppm) were assigned a 0.7 ppm value for statistical purposes (Onishi and Sandell, 1955).

Comparison of arsenic abundances from precious metal systems spatially related to high silica alkali-rhyolite volcanism in the Mogollon-Datil field suggests arsenic in the study area is abnormally low. Ratte et al., (1979) note the restriction of greater than 15 ppm arsenic almost entirely to areas of major

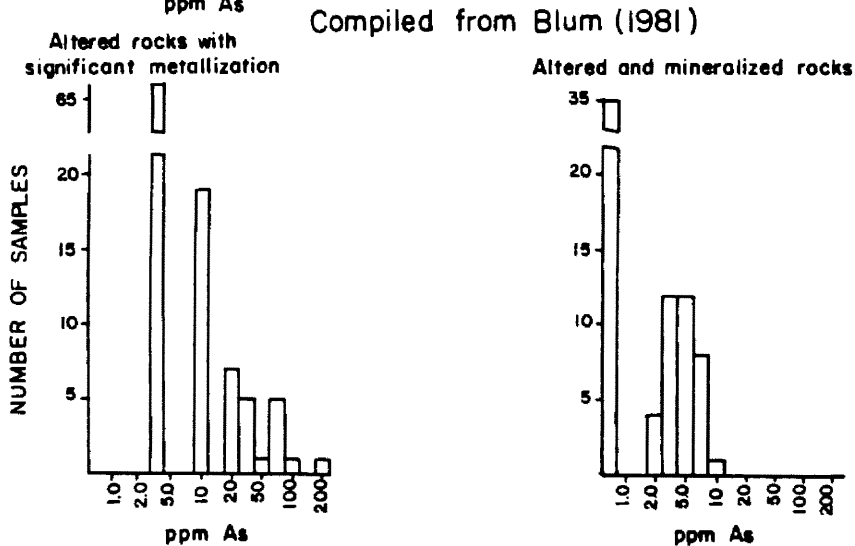
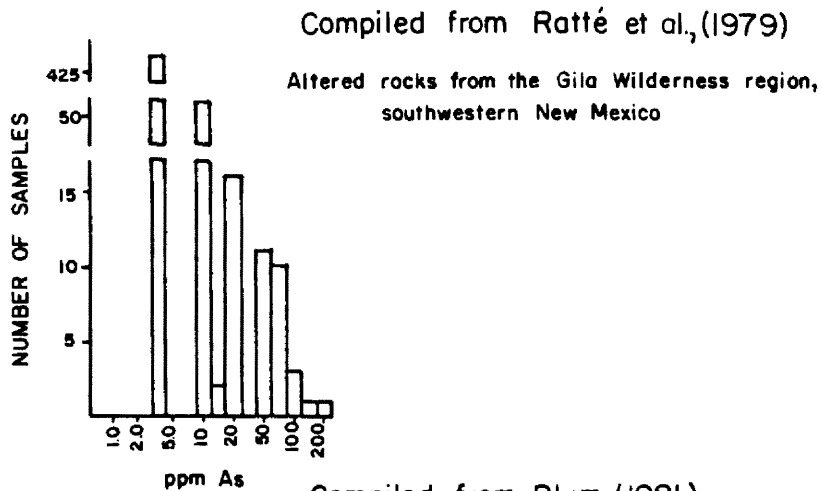
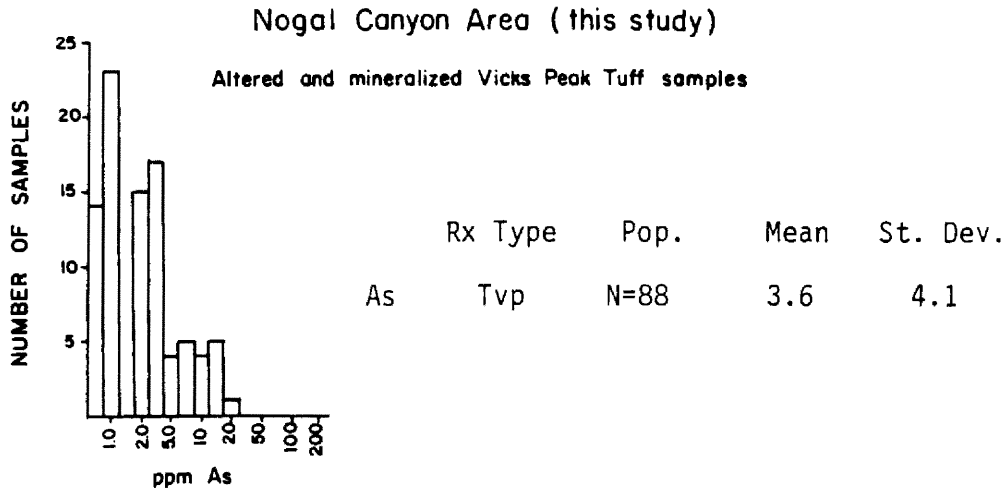


Figure 36. Summary of the arsenic distribution in hydrothermally altered Vicks Peak Tuff rock samples, and comparison to geochemical data from the Gila Wilderness region (Ratte et al., 1979) and from the Wilcox district area (Blum, 1981) within the Mogollon-Datil volcanic field.

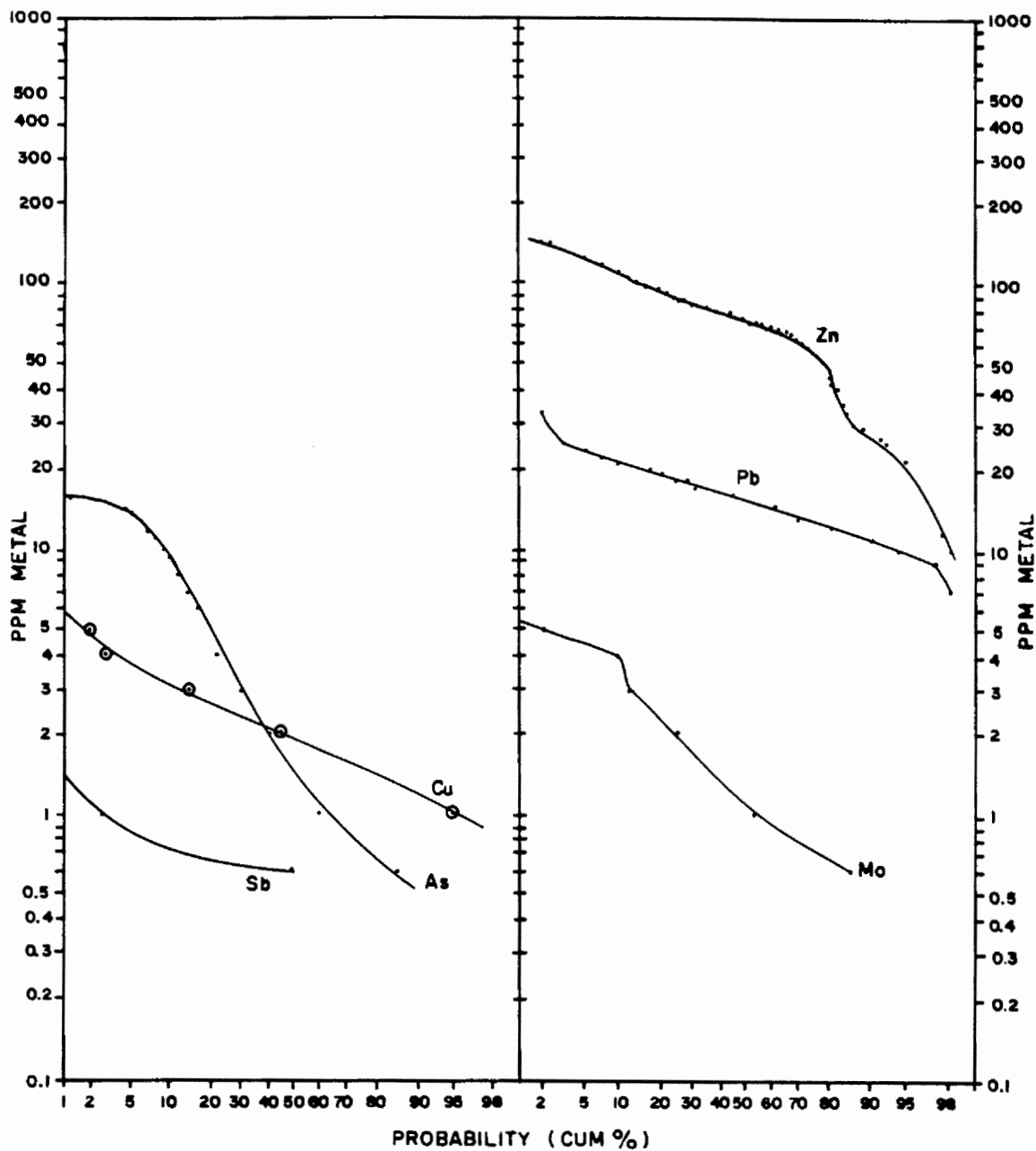
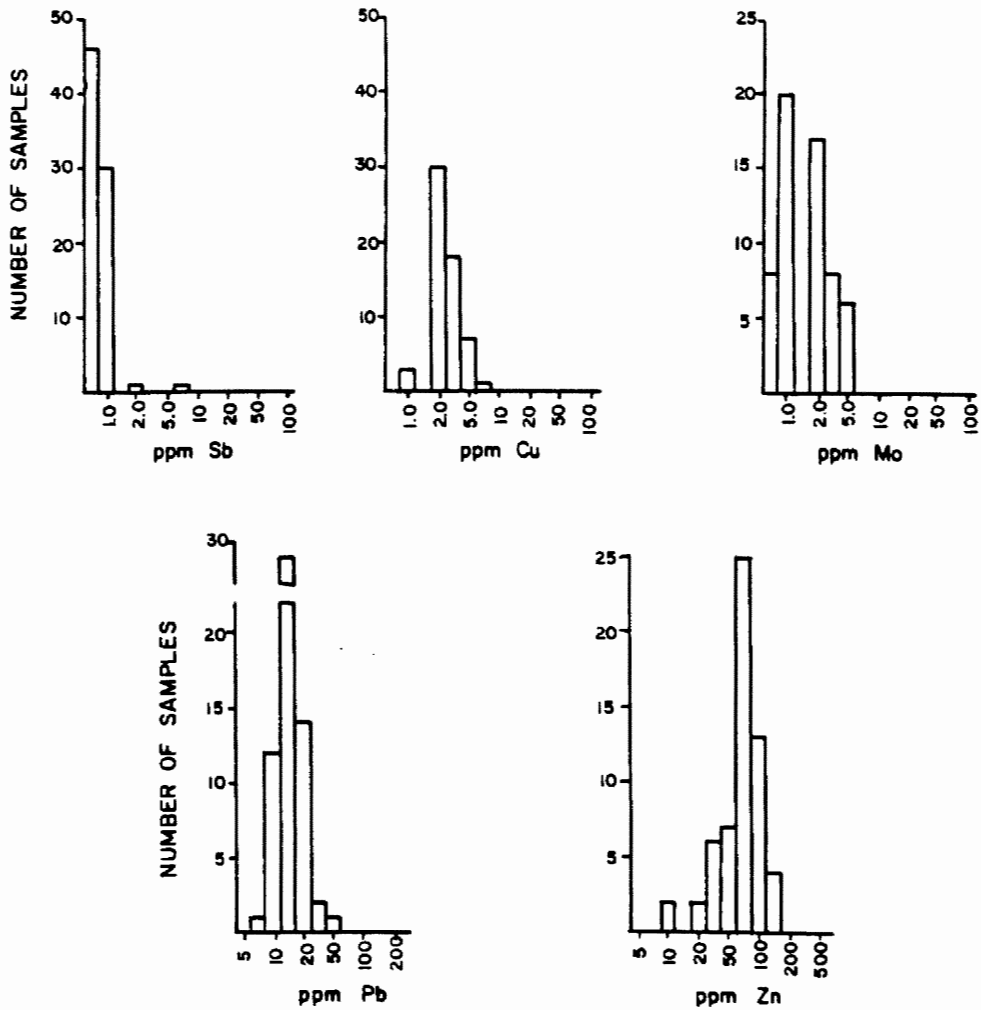


Figure 37. Cumulative probability plots of arsenic, antimony, copper, molybdenum, lead, and zinc in hydrothermally altered Vicks Peak Tuff rock samples from the Nogal Canyon study area, (N for As and Sb=88; N for Cu, Mo, Pb, and Zn=59).

mineralization and alteration in the Gila Wilderness. The Mogollon Au-Ag district located in the Gila region is the only presently recognized area exhibiting major precious metal mineralization associated with high silica alkali rhyolite volcanism. However, recent work by Kent (1983) at the Eberle mine in the Mogollon district documents an approximate 14 m.y. age which is considerably younger than volcanism. Blum's (1981) work in the Wilcox Au-Te district region within the Gila Wilderness documents a high arsenic range "in altered rocks hosting significant metallization" and low arsenic abundances in "hydrothermally altered and mineralized rocks". Comparison of arsenic distribution from Ratte et al., (1979), Blum (1981), and the Nogal Canyon study area appear in Figure 36.

Antimony

The features of the antimony distribution in rock samples from the study area are summarized in Figure 38. A cumulative probability plot is inconclusive in partitioning the antimony distribution (Fig. 37). Samples below detection limit (1 ppm) were assigned a value of 0.6 ppm for statistical purposes based on antimony abundance in high silica rhyolite tuffs (Mahood and Hildreth, 1983). Antimony ranges from 0.4 to 1.1 ppm in high silica rhyolite tuffs; therefore, the Nogal Canyon antimony results are considered approximately average values. Significant values were recorded in only one sample within the Rhyolite mine area (7 ppm Sb)(Fig. 31).



	Rx Type	Pop.	Mean	St. Dev.
Sb	Tvp	N=88	0.86	0.70
Cu	Tvp	N=59	2.6	1.1
Mo	Tvp	N=59	1.9	1.4
Pb	Tvp	N=59	16.	6.3
Zn	Tvp	N=59	74.	32.

Figure 38. Summary of antimony, copper, molybdenum, lead, and zinc population parameters in hydrothermally altered rock samples of Vicks Peak Tuff from the Nogal Canyon study area.

Base Metals

Rock samples from the Pankey mine area were analyzed for copper, molybdenum, lead, and zinc and their distributions appear in Figure 38. Cumulative frequency plots based on 59 samples reveal single populations for copper and lead, a bimodal zinc distribution, and inconclusive results for molybdenum (Fig. 37). Detection limit for all analyzed base metals is 1 ppm.

In acid volcanic rocks, copper ranges from 1 to 34 ppm and averages 6 ppm (Wedepohl, 1969). Distribution of copper values from the Pankey area agree with background copper abundances; however, Laskey (1932) reports malachite and smelter credits of 0.03 percent copper from vein material. Presence of consistently normal copper values defining a single population and secondary copper carbonates probably suggests secondary mobilization and concentration from minor copper bearing primary mineral phases.

Crustal lead abundance, reported by Doe (1967) and Wedepohl (1969), ranges from 8.7 to 55 ppm and averages approximately 25 ppm. There is no appreciable difference between lead concentrations in Nogal Canyon samples and background rhyolite abundances.

In felsic volcanic rocks, zinc ranges from 15 to 210 ppm and averages 56 ppm based on work from Sandell and Goldrich (1943) and Morita (1955). Analyses from high silica rhyolite tuffs (Mahood and Hildreth, 1983) document lead averages 80 ppm and ranges from 29 to 116 ppm. The Pankey samples zinc distribution agrees with normal background values and the bimodal distribution does not

constitute an anomalous relationship. Instead the zinc distribution suggests secondary dispersion or hydrothermal alteration redistribution. Based on empirical evidence, zinc tends toward moderate mobility in an oxidizing surficial environment (Rose et al., 1979).

Molybdenum values from the Pankey area agree closely with background distribution in acid volcanic rocks. Kuroda and Sandell (1954) document a molybdenum in rhyolite range from 0.6 to 5.0 ppm and average 2.2 ppm. High silica rhyolite tuffs studied by Mahood and Hildreth (1983) average 6.9 ppm ranging from 2.9 to 10 ppm.

CHAPTER VII

DISCUSSION AND CONCLUSIONS

Nogal Canyon Area

Volcanic hosted precious metal occurrences in the Nogal Canyon area collectively represent an epithermal "fissure-type" system cropping out at various erosional levels. The occurrences exhibit features characteristic of epithermal associations such as silicification, argillic and advanced argillic alteration assemblages, mineralization localized along thin to large veins, open space gangue textures, gold and silver geochemistry, and evidence of hydrostatic boiling. By analogy with other precious metal systems, the Nogal Canyon occurrences formed at low to moderate temperatures in a near surface environment. Assimilation of alteration and mineralization characteristics exposed throughout the 18 square km area allows for comprehensive explanation and genetic modeling of the system.

Inception of hydrothermal activity and associated mineralization postdates deposition of the Springtime Canyon Quartz Latite and normal faulting in the Nogal Canyon area. Northeast and northwest trending, steeply dipping structures served as fluid channelways for circulating hydrothermal fluids and sites

for mineral deposition. The structures displace a series of downdropped graben-like blocks with intervening horsts which possibly relate to subsidence of the proposed Nogal Canyon cauldron. Cauldron subsidence commonly produces concentric and tensional fracture systems such as medial grabens which may serve as favorable areas for post-cauldron intrusions and related mineralization (Smith and Bailey, 1968). Furthermore, calderas and cauldrons possess inherent prerequisites for the development of hydrothermal deposits and thus represent an important exploration target. These volcano-tectonic features supply the plumbing systems for fluid circulation, a heat source to drive the hydrothermal system, and a source for sulfur and metals. However, due to incomplete documentation of the proposed Nogal Canyon cauldron and lack of age dates on mineralization, the structural fabric and precious metal occurrences do not conclusively correlate to the proposed volcano-tectonic feature and associated magmatism.

The heat source for the Nogal Canyon hydrothermal system is speculated to consist of an unexposed intrusion related to the waning stages of felsic volcanism or a much younger igneous event. Intrusive bodies do not crop out in the San Jose district, but do occur in the southern portion of the map area. Alteration patterns appear primarily controlled by the distribution of fractures and not by an intrusive body close to the present surface. However an undocumented intrusive is the preferred heat source and driving mechanism for hydrothermal features present in the Nogal Canyon area.

Examination of the district wide alteration and mineralization characteristics in the Nogal Canyon area establishes the lateral and vertical zonation patterns of the overall system and also dictates certain genetic aspects of the hydrothermal system. Consistent spatial and temporal relations between intermediate argillic alteration, silicification, and mineralization documents sequentially contemporaneous development during a single hydrothermal episode. Advanced argillic alteration in the Indian Peak area, although representing a differing alteration scheme, appears contemporaneous with the same hydrothermal episode. Intermediate argillic alteration occurring northeast of Indian Peak beneath the quartz-alunite bodies appears continuous with broad argillization below the Vicks Peak-Springtime Canyon contact related to silicic-intermediate argillic occurrences (Plate 1). The Nogal Canyon area lacks pre-ore stage propylitic and potassic alteration assemblages common to other epithermal systems hosting significant mineralization. The absence of abundant mafic components within the rhyolite host rock and lack of Fe and Mg introduction account for the absence of propylitic alteration. Alteration zoning patterns generally consist of structurally controlled silica alteration grading peripherally into intermediate argillic alteration at exposure levels within the Pankey and Indian Creek Trail area. At the Rhyolite mine and Taylor shaft vicinities, vein-infilling silica alteration grades laterally into pervasive wall rock silica flooding suggesting proximity to the lower alteration intervals of the precious metal

system. Exposures at the Pankey mine specifically exhibit decreasing pervasive silica alteration stratigraphically upward along structure grading vertically into pervasive intermediate argillic alteration which envelopes the structure. Weakly developed quartz veinlet networks overlap with the base of argillically altered Vicks Peak Tuff (Fig. 18). Intermediate argillic alteration continues vertically to form broad, blanket-like occurrences beneath the Springtime Canyon Quartz Latite flow where present.

Ascending hydrothermal fluids in the Pankey mine area underwent hydrostatic boiling based on the presence of explosion textures and variable liquid-vapor ratios of stage 1 quartz fluid inclusions. The base of the boiling interval corresponds to a minimum elevation of 2030 m and occurs confined to the structure zone. The lack of rubble breccias, pebble dikes, or hydrothermal breccia features suggests violent boiling probably did not occur. Boiling activity existed below the quartz latite permeability barrier probably initiated by repeated fracturing or tectonic events. Physicochemical changes to the hydrothermal fluid during boiling, specifically partitioning of volatile components into the vapor phase, ultimately developed low pH kaolinitic alteration above the boiling interval. Phyllosilicate zoning within the intermediate argillic alteration zone surrounding the Pankey fault developed due to fluid-wall rock interactions specifically in response to hydrolysis reactions and decreasing temperature away from the fluid channelway. Alteration systematics including chemical parameters are

analogous to descriptions by Hemley and Jones (1964) and Rose and Burt (1979). Argillic alteration extends upward in a funnel-like pattern from the Pankey fault below the limited permeability barrier. Ascending volatile rich, low pH, low density fluids interacted with heavier, cooler liquids of the deep water table within the water saturated, partially welded portions of the Vicks Peak Tuff. The occurrence of the massive, impermeable flow overlying the Vicks Peak rhyolite strongly influenced hydrologic patterns developed during fluid circulation. The limited permeability interface restricted upward fluid movement and channeled fluids laterally resulting in broad, blanket-like argillic alteration. Similarity of alteration types, intensities, and zoning patterns for other vein occurrences in the San Jose district suggests boiling probably occurred on a district wide scale. Local paleotopographic irregularities and lack of uniform isobars in the system's horizontal plane probably led to differing elevations of fluid boiling in separate areas and possibly completely prevented boiling in other areas.

Flat bottomed quartz-alunite replacement deposits overlie unaltered Vicks Peak rhyolite adjacent to the Indian Peak fault. Quartz-alunite alteration represents the stratigraphically uppermost alteration type in the Nogal Canyon area with basal contacts occurring at elevations of 2400 m. The abrupt vertical change from unaltered Vicks Peak Tuff to alunitized Vicks Peak Tuff represents boiling and degassing of structurally confined, ascending fluids intersecting the paleowater table. cursory alunite fluid inclusion observations document highly variable

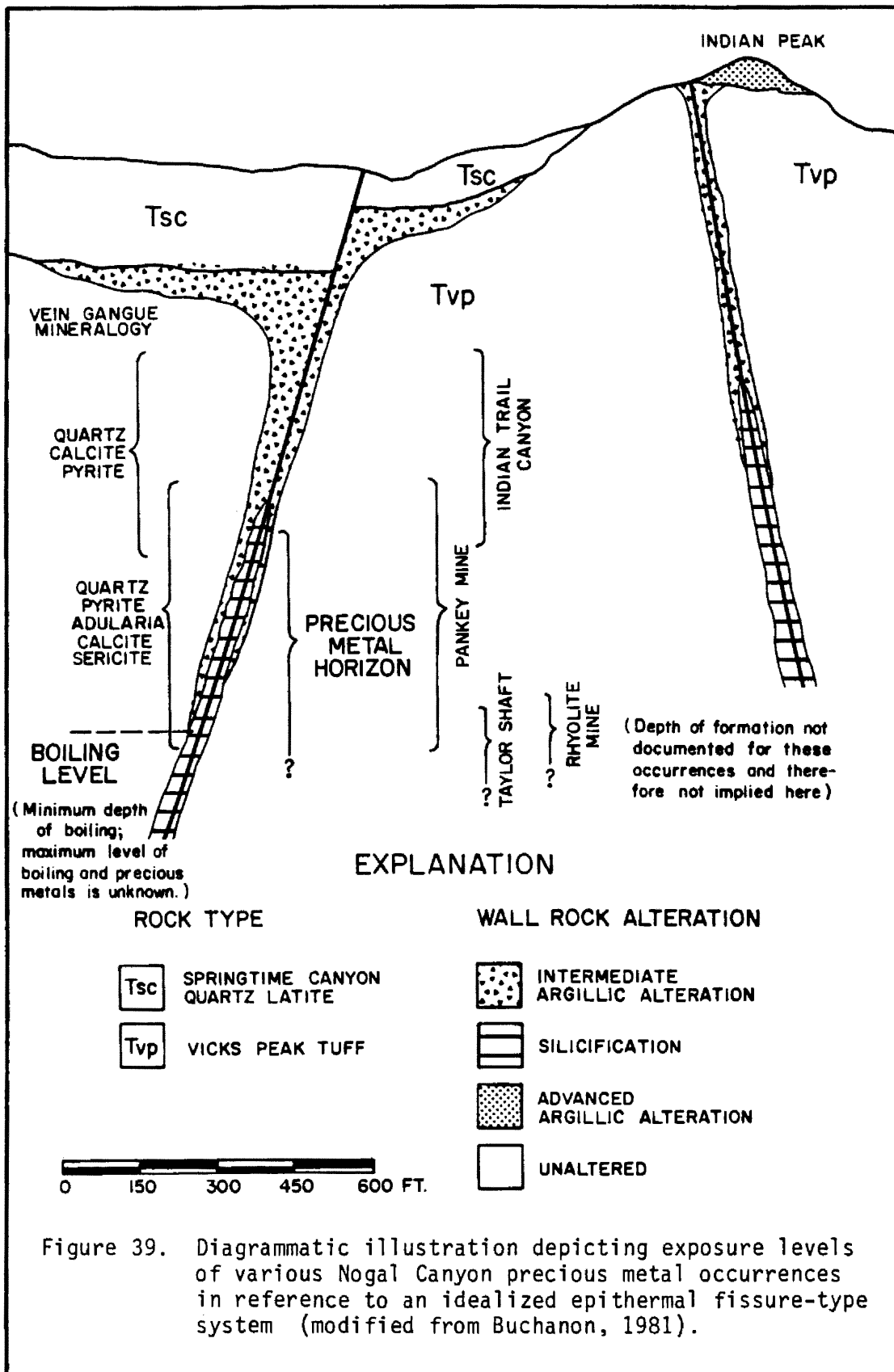
liquid-vapor ratios. The partially welded zone within the Vicks Peak rhyolite provided ample porosity and permeability to host the abundantly oxygenated paleowater table. Fluids which probably boiled at stratigraphically lower intervals ascended along the Indian Peak fault due to the establishment of steady-state upflow conditions. Absence of wall rock permeability within the densely welded Vicks Peak Tuff, favorable pressure gradients, and lack of significant impedance provided by condensate and clays permitted upward propagation of uncondensed fluids along the major channelway until intersection with the paleowater table. Abundant alunite formed above the water table where complete oxidation of the fluids resulted in high sulfuric acid contents and consequently low pH conditions. Potassium availability occurred due to alteration of K-feldspars and subsequent K^+ liberation from the host rhyolite as evidenced by alunite replacing sanidine phenocrysts. The Springtime Canyon flow did not affect hydrologic circulation patterns as elsewhere in the Nogal Canyon area. The quartz latite, if deposited at Indian Peak, would appear at stratigraphically much higher intervals than present levels of exposure.

The two differing alteration schemes in the Nogal Canyon area probably represent a contemporaneous hydrothermal episode differentially situated over an intrusive heat source which accounts for varying H_2S fluid contents. Variation in the lateral and vertical host rock porosity and permeability, specifically the vertical proximity of the quartz latite permeability barrier to the boiling interval, accounts for the

major controls on the distribution and development of alteration types. Alteration in the Indian Peak area may, however, represent a separate event characterized by higher H₂S fluid content which is reflected by the well developed quartz-alunite assemblage.

Assimilation of all available geologic information, particularly alteration and mineralization features, and rock chip geochemistry data allows for evaluation of the gold-silver resource potential of the Nogal Canyon area. The determination of exposure level within the system, and interpretation of geologic features and geochemical results from the levels samples is critical to the evaluation process. Figure 39 is a schematic diagram, modified after Buchanon (1981), which represents exposure levels of various vein occurrences in the San Jose district. Buchanon's (1981) model utilizes a boiling mechanism to generate horizons of precious metal deposition. Although strong boiling did occur at the Pankey mine and probably elsewhere in the district, precious metal precipitation due to boiling is not adequately evidenced as the dominant depositional mechanism. However, the overwhelming resemblance of the Nogal Canyon occurrences to other gold-silver-sulfide epithermal deposits where boiling relates to metal deposition strongly suggests a genetic similarity. Therefore expectations of economic precious metal horizons are discussed in view of work by Buchanon (1981) and Berger and Eimon (1982).

Significant gold-silver mineralization, occurring as either disseminations, stockworks, or fissure deposits, appears



non-existent in the Nogal Canyon area. Insignificant to anomalous precious metal occurrences exist at several localities with irregular pockets of notable mineralization present locally. In the Pankey mine area, erratically important gold-silver values appear confined to the Pankey fault but do not constitute significant mineralization. Sampling peripheral to the structure documents the lack of dissemination into the wall rock and complete absence of mineralization in the quartz network or stockwork zones. Arsenic and antimony values are very low and base metal introduction appears absent at present exposure levels. The potential at depth appears restricted to structurally confined fissures and primary grades would not predictably improve. The Indian Trail Canyon area totally lacks anomalous gold-silver geochemistry except for sporadic occurrences along the silicified fault zone. Exposures display a poorly defined quartz veinlet network zone above a locally exposed silicified structure, and the erosional level conforms to the expected precious metal horizon within the fissure system. However, like the Pankey occurrence, the veinlet zone hosts no precious metal values and fissure samples exhibit unencouraging results. Unattractive depth potential is based on the insignificant geochemical results of the area. In the Taylor Shaft area, geochemical sampling detected mineralization related only to vein-infilling silica introduction; dissemination into the host rock is conspicuously absent. Mineralization occurs in massive, highly manganiferous quartz material varying from 7 to 15 cm wide within the central portion of

the vein. Horizontal continuity of the mineralization appears severely limited due to the lateral restriction of open space silicification presently exposed. Precious metal mineralization may extend at depth; however, continuity would probably depend on degree of structural preparation instead of vertical depth of the precious metal horizon. Significant volumes of mineralized rock appear unlikely for this occurrence. The Rhyolite mine hosts abundant anomalous silver values primarily occurring along the brecciated Rhyolite fault zone and to a greater degree in quartz veinlet networks erratically enveloping the structure. Alteration schemes suggest the present erosional interface should expose the precious metal horizon. However, significant values do not appear at existing exposure levels. Potential at depth would not significantly exceed results observed at the surface based on present data. Although the Indian Peak area lacks anomalous geochemical signatures, alteration schemes suggest present exposures are stratigraphically well above any expected mineralized horizon along the Indian Peak fault. The upper intervals of epithermal systems commonly lack precious metal haloes because of dispersion limitations of boiling and impermeable clay horizons. Fissure or stockwork occurrences may exist at depth whereas the densely welded Vicks Peak host rock precludes disseminated occurrences. However, the consistently weak precious metal intervals present within known Nogal Canyon area occurrences and low pathfinder element abundances suggests the San Jose district

hydrothermal event introduced only insignificant mineralization.

Aragon Hill Area

The intrusive breccia at Aragon Hill occurs along the west-northwest trending Aragon Hill structure zone and is intimately associated with rhyolitic intrusive and extrusive flow-dome rocks. The structure zone may represent the southern portion of the proposed Nogal Canyon cauldron ring fracture zone as interpreted by Deal and Rhodes (1976). Thompson and Giles (1983) cite the favorable setting of epithermal breccia features along major fractures in volcano-tectonic terrains. Intrusive breccias occurring within analogous regional settings exist in the Red Mountain, Galena, and Silver Cliff-Rosita districts of Colorado and are described by Emmons (1895), Burbank (1941;1969), Nash (1975), and Maher (1983). Geologic features exposed at the Aragon Hill intrusive breccia permit interpretation of emplacement processes; an overview of genetic aspects relevant to intrusive breccias will not be discussed here.

Structural, textural, and compositional features of the intrusive breccia suggest a phreatomagmatic process and subsequent fluidization generated breccia emplacement and coeval phyllic alteration. Phreatomagmatic eruptions occur due to the interaction of a heat source and meteoric water in the near surface environment (Williams and McBirney, 1979). The

heating process under essentially constant volume conditions flashes water to steam resulting in a sudden pressure increase. Brecciation events responsible for fragmentation and conduit or channelway development accompany pressure release in the shallow subsurface. A phreatomagmatic brecciation mechanism is suggested by "cold" emplacement features such as the lack of thermal metamorphism of fragments, and relatively low temperature alteration products present within the pipe facies; no juvenile fragments or igneous matrix were recognized. The Aragon Hill structure zone played an important role in the localization of intrusives, and the accumulation and deep penetration of meteoric groundwater. The spatial association of the intrusive breccia with the porphyritic rhyolite intrusives and cross-cutting relations with the rhyolite flow-dome unit implies a close genetic association with subvolcanic igneous activity. The occurrence of pyrite and anomalous silver contents within the breccia matrix suggests possible contribution from a minor proportion of magmatic fluid; however, the appropriate components may have been present within the meteoric water reservoir.

The processes operative during brecciation events proposed by many workers (Barrington and Kerr, 1961; Cornelius, 1967; Bryant, 1968; Watson, 1968) most importantly include fluidization. Wohletz and Sheridan (1979, p. 178) define fluidization as

"a mixture of particles (solid or liquid) suspended in an upward escaping fluid (liquid or gas) so that the frictional force between the fluid and the particles counterbalance the weight of the particles and the whole mass behaves as a fluid."

The mobilization of rock materials by an upward moving, high velocity fluid produces structural features and textural characteristics commonly observed in intrusive breccias, and appear present at the Aragon Hill intrusive breccia. The breccia consists of a heterolithic fragment lithology suspended within an altered rock flour matrix. The strongly mixed, commonly rounded fragments originated from both substantial depth (> 125 m) and close to the point of occurrence supporting an upward transporting, mixing and abrading fluidization process (Reynolds, 1954; Woolsey et al., 1975; Mayo, 1976). Features characteristic of the intrusive breccia margins include friable, clay-gouge material and sheeted shear planes subparallel to the sharp vertical contact. The breccia margin zone is characterized by the notable absence of coarse fragments which exist only toward the central core of the pipe-like intrusive body. Convective particle circulation within fluidized conduits (spouting) is described by Reynolds (1954), Woolsey et al., (1975), and McCallum (in prep.) and appears instrumental in developing annular core-margin segregations within breccia pipes. Along the margin zone, cyclic downward propagation of particle masses results in the generation of several characteristic textural and structural features. A gradient of shear stresses develop in response to particle descent adjacent to the

wallrock and account for the generation of the sheeted breccia margin zone. The deposition of cohesive, finer particles within shear stressed intervals adjacent to the wallrock results in clay-size material segregation and development of pipe margin "smearing". The breccia matrix consists of finely comminuted rock fragments, abraded crystal fragments, and rock flour altered to a dominantly sericite, montmorillonite-chlorite lithology and is identical to alteration in the differing fragment types. Mechanical abrasion and degradation of fragments during the fluidization process accounts for the production of the rock flour matrix (Bryant, 1968). The ubiquity of identical matrix alteration throughout present exposures, and the dissimilar fragment types exhibiting correspondingly different alteration assemblages suggests contemporaneous phyllic alteration occurred during fluidized breccia development by the dominantly meteoric vapor phase. The surrounding rhyolite flow-dome rocks host a phyllic alteration aureole centered about the intrusive breccia. The alteration exhibits decreasing intensity outward from the breccia-rhyolite contact and is contemporaneous with alteration and emplacement of the breccia.

Geochemical sampling indicates weakly anomalous silver values occur consistently throughout the intrusive breccia matrix ranging from 1.0-2.0 ppm. The silver, either derived from vaporized meteoric water or minor magmatic contribution, represents nonsignificant abundances and would not suggest proximity to mineralization. Weakly developed fracture sets

cross-cutting the breccia host quartz-calcite-barite assemblages possessing weak gold mineralization. The textural features of fracture-filling quartz, calcite, and barite are consistent with a hypogene origin; milky supergene calcite postdates the alteration material. Extensive or pervasive epigenetic alteration is undeveloped at present exposure levels. Previous workings at the Henckley mine on Aragon Hill exploited the mineralized quartz-calcite-barite fractures only on a small scale. Sampling along the fractures revealed anomalous gold values (i.e. > 0.6 ppm Au). Sampling along the fractures in the surrounding rhyolite flow-dome unit documents anomalous gold and local silver values adjacent to the rhyolite-breccia contact zone.

The anomalous metal contents in quartz-calcite-barite vein alteration within the breccia and along fractures in the adjacent rhyolite wall rock probably relates to leaching and insignificant metal deposition during the late, waning stages of the breccia-forming thermal episode. However, the geologic and geochemical features may possibly represent subtle expression of epigenetic alteration related to breccia-hosted precious metal mineralization at depth. Further work needed to differentiate between the above possibilities should initially address pathfinder element signatures, and mineralogical and geochemical zoning to gain better insight into the system and depth potential for mineralization.

The Seferino, Fifty-Fifty Hill Area

The Seferino, Fifty-fifty Hill area is located in the southern foothills of the San Mateo mountains (Sec 31, T10S, R5W) and hosts an isolated silver-gold fissure prospect which shares abundant similarities to the Nogal Canyon occurrences. Present erosional levels expose structurally controlled and stratigraphically influenced silica alteration consisting of vein-infilling and pervasive silica introduction. Limited relief precludes the establishment of detailed vertical zoning patterns. Multiple brecciation and silicification events appear confined to the northwest trending structure zone accompanied by finely disseminated pyrite and late stage calcite gangue. Sampling along the structure zone defines significantly anomalous gold and silver values, but continuity is limited and erratic. Pervasive silica alteration, occupying the porous laharc breccia wall rock, extends 450 m away from the structure to the east. However, the intense, pervasive silica replacement is devoid of detectable precious metals. The strong pervasive silicification gradually decreases in intensity grading laterally into quartz-calcite alteration fringes. The Seferino, Fifty-fifty Hill prospect lacks abundantly significant mineralization at present exposure levels, and mineralization would not be expected to increase at depth due to alteration/mineralization characteristics of present erosional levels.

REFERENCES CITED

- Atwood, G.W., 1982, Geology and geochemistry of the San Juan Peak area, San Mateo Mountains, Socorro County, New Mexico: with special reference to the geochemistry, mineralogy, and petrogenesis of an occurrence of riebeckite-bearing rhyolite: Unpub. M. Sc. Thesis, Univ. of New Mexico, Albuquerque, 156 p.
- Bailey, E.H., and Stevens, R.E., 1960, Selective staining of K-feldspar and plagioclase on rock slabs and thin sections: Am. Mineralogist, v. 45, nos. 9-10, p. 1020-1025.
- Barrington, J., and Kerr, P.F., 1961, Breccia pipe near Cameron, Arizona: Geol. Soc. America Bull., v. 72, p. 1661-1674.
- Berger, B.R., and Eimon, P.I., 1982, Comparative models of epithermal silver-gold deposits: American Inst. Mining Eng., Preprint 82-13, 25 p.
- Berry, V.P., Nagy, P.A., Spreng, W.C., Barnes, C.W., and Smouse, D., 1981, National uranium resource evaluation, Tularosa Quadrangle, New Mexico: U.S. Dept. of Energy Pub. GJQ-014(82), 22 p.
- Blum, N., 1981, Zur geologie, petrologie, und geochemie des sudwestrandes der Bursum Caldera zwishcen Lone Pine Hill und Holt Gulch, sw-New Mexico: Unpub. diplomarbeit, Tech. Inst. of Aachen, W. Germany, 181 p.
- Bornhorst, J.T., 1980, Major and trace element geochemistry and mineralogy of Eocene to Quaternary volcanic rocks of the Mogollon-Datil volcanic field, southwestern New Mexico: Unpub. Ph.D. dissertation, Univ. of New Mexico, Albuquerque, 1108 p.
- _____, Jones, D.P., Elston, W.E., Damon, P.E., and Shafiqullah, M., 1982, New radiometric ages on volcanic rocks from the Mogollon-Datil volcanic field, southwestern New Mexico: Isochron/West, no. 35, p. 13-15.
- Brown, D.M., 1972, Geology of the southern Bear Mountains, Socorro County, New Mexico: M.S. thesis, New Mexico Inst. Mining Tech., 110 p; N.M. Bur. Mines and Min. Res. Open File Report 42, 110 p.

- Bryant, D.G., 1968, Intrusive breccias associated with ore, Warren (Bisbee) Mining District, Arizona: *Econ. Geology*, v. 63, p. 1-12.
- Buchanon, L.J., 1981, Precious metal deposits associated with volcanic environments in the Southwest, *In* Dickenson, W.R., and Payne, W.P., eds., *Relations of Tectonics to Ore Deposits in the southern Cordillera*: *Arizona Geol. Soc. Dig.*, v. 14, p. 237-262.
- Burbank, W.S., 1941, Structural controls of ore deposition in the Red Mountain, Sneffels, and Telluride districts of the San Juan Mountains, Colorado: *Colo. Sci. Soc. Proc.*, v. 14, p. 141-261.
- _____ and Luedke, R.G., 1969, Geology and ore deposits of the Eureka and adjoining districts, San Juan Mountains, Colorado: *U.S. Geol. Survey Prof. Paper* 535, 73 p.
- Chapin, C.E., 1971, K-Ar age of the La Jara Peak Andesite and its possible significance to mineral exploration in the Magdalena Mining District, New Mexico: *Isochron/West*, no. 2, p. 43-44.
- _____, 1979, Evolution of the Rio Grande rift - a summary, *In* Riecker, R.E., ed., *Rio Grande rift: Tectonics and magmatism*: Washington, D.C., *Am. Geophysical Union*, p. 1-5.
- Coney, P.J., 1972, Cordilleran tectonics and North America plate motion: *American Jour. Sci.*, v. 272, p. 603-628.
- Cornelius, K.D., 1967, Breccia pipe associated with epigenetic mineralization, Mount Morgan, Queensland: *Econ. Geology*, v. 62, p. 282-285.
- Creasey, S.C., 1966, "Hydrothermal Alteration", *In* *Geology of porphyry copper deposits, southwestern North America*: Univ. of Arizona press, Tuscon, Arizona.
- Dane, C.H., and Bachman, G.O., 1965, *Geologic map of New Mexico*: U.S. Geol. Survey, 2 sheets, scale 1:500,000.
- Deal, E.G., 1973, *Geology of the northern part of the San Mateo Mountains, Socorro County, New Mexico: A study of a rhyolite ash-flow tuff cauldron and the role of laminar flow in ash-flow tuffs*: Unpub. Ph.D. dissertation, Univ. of New Mexico, Albuquerque, 136 p.
- _____ and Rhodes, R.C., 1976, *Volcano-tectonic structures in the San Mateo Mountains, Socorro County, New Mexico*: *New Mexico Geol. Soc. Spec. Pub.* no. 5, p. 51-56.

- Doe, B.R., 1967, The bearing of Pb isotopes on the source of granitic magma: *Jour. Petrology*, v. 8, p. 51-60.
- Eaton, G.P., 1982, The Basin and Range province: Origin and tectonic significance: *Annual Review of Earth and Planetary Science*, v. 10, p. 409-440.
- Elston, W.E., 1976a, Tectonic significance of mid-Tertiary volcanism in the Basin and Range province: A critical review with special reference to New Mexico: *New Mexico Geol. Soc. Spec. Pub. no. 5*, p. 93-102.
- _____, Rhodes, R.C., Coney, P.J., and Deal, E.G., 1976b, Progress report on the Mogollon Plateau volcanic field, southwestern New Mexico, No. 3 - surface expression of a pluton: *New Mexico Geol. Soc. Spec. Pub. no. 5*, p. 3-28.
- _____, Rhodes, R.C., Erb, E.E., 1976c, Control of mineralization by mid-Tertiary volcanic centers, southwestern New Mexico: *New Mexico Geol. Soc. Spec. Pub. no. 5*, p. 125-130.
- _____, 1978, Mid-Tertiary cauldrons and their relationship to mineral resources, southwestern New Mexico: A brief review: *New Mexico Geol. Soc. Spec. Pub. no. 7*, p. 107-114.
- Emmons, W.H., 1895, The mines of Custer County, Colorado: *U.S. Geol. Survey Ann. Report*, 17, pt. 2, 67 p.
- Farkas, S.E., 1969, Geology of the southern San Mateo Mountains, Socorro and Sierra Counties, New Mexico: Unpub. Ph.D. dissertation, Univ. of New Mexico, Albuquerque, 137 p.
- Furlow, J.W., 1965, Geology of the San Mateo Peak area, Socorro County, New Mexico: Unpub. M. Sc. Thesis, Univ. of New Mexico, Albuquerque, 83 p.
- George, W.O., 1924, The relation of the physical properties of natural glasses to their chemical composition: *Jour. Geology*, v. 32, no. 5, p. 353-372.
- Griffitts, W.R., Alminas, H.V., and Mosier, E.L., 1971, Pb, Sn, La, Ag, Be, Zn, Sb, Mo, Au, and Nb distribution in the Vicks Peak, Steel Hill, and Black Hill quadrangles, New Mexico: *U.S. Geol. Survey Open File Reports*, nos. 71-130, 71-134.
- Hamaguchi, H., and Kuroda, R., 1959, Silver content in igneous rocks: *Geochim. et Cosmochim. Acta*, v. 17, p. 44-52.
- Harley, G.T., 1934, The geology and ore deposits of Sierra County, New Mexico: *New Mexico Bur. Mines and Min. Res. Bull.*, 10, 220 p.

- Hemley, J.J., and Jones, W.R., 1964, Chemical aspects of hydrothermal alteration with emphasis on hydrogen metasomatism: *Econ. Geology*, v. 59, p. 538-569.
- Hemley, J.J., Hostetler, P.B., Gude, A.J., and Mountjoy, W.T., 1969, Some stability relations of alunite: *Econ. Geology*, v. 64, p. 599-612.
- Kelly, V.C., and Furlow, J.W., 1965, New control on the lower Paleozoic wedge-edges in south-central New Mexico: *Geol. Soc. America Bull.*, v. 76, p. 689-694.
- Kent, G.R., 1983, Temperature and age of precious-metal vein mineralization and geochemistry of host rock alteration at the Eberle mine, Mogollon Mining District, southwestern New Mexico: Unpub. M.S. Thesis, Michigan Tech. Univ. Houghton, 84 p.
- Kerr, P.F., 1977, *Optical Mineralogy*, McGraw-Hill, New York, 492 p.
- Kesler, S.E., Russell, N., Seaward, M., Rivera, J., McCurdy, K., Cumming, G.L., and Sutter, J.F., 1981, Geology and geochemistry of sulfide mineralization underlying the Pueblo Viejo gold-silver oxide deposit Dominican Republic: *Econ. Geology*, v. 76, p. 1096-1117.
- Kittleman, L.R., Jr., 1963, Glass-bead silica determination for a suite of volcanic rocks from the Owyhee Plateau, Oregon: *Geol. Soc. America Bull.*, v. 74, p. 1405-1410.
- Knewedl, D.A., 1974, Geology of the central Magdalena Mountains, Socorro County, New Mexico: Unpub. Ph.D. dissertation, Univ. of Arizona, Tucson, 218 p.
- Knight, J.E., 1977, A thermochemical study of alunite, enargite, luzonite, and tennantite deposits: *Econ. Geology*, v. 72, p. 1321-1336.
- Kottowski, F.E., 1960, Summary of Pennsylvanian sections in southwestern New Mexico and southeastern Arizona: *New Mexico Bur. Mines and Min. Res. Bull.*, 66, 187 p.
- Kottowski, F.E., 1963, Pennsylvanian rocks of Socorro County, New Mexico: *New Mexico Geol. Soc. Guidebook 14th Field Conf.*, Socorro Region, p. 102-111.
- Kuroda, P.K., and Sandell, E.B., 1954, Geochemistry of Molybdenum: *Geochim. et Cosmochim. Acta.*, v. 6, p. 35-63.
- Lasky, S.G., 1932, The ore deposits of Socorro County, New Mexico: *New Mexico Bur. Mines and Min. Res. Bull.*, 8, 131 p.

- Lepeltier, C., 1969, A simplified statistical treatment of geochemical data by graphical representation: *Econ. Geology*, v. 64, p. 538-550.
- Lipman, P.W., Prostka, H.J., and Christiansen, R.L., 1972, Cenozoic volcanism and plate tectonic evolution of the western United States, Pt. 1, early and middle Cenozoic: *Royal Soc. London Phil. Trans.*, A, v. 271, p. 217-248.
- _____, 1981, Volcano-tectonic setting of Tertiary ore deposits, southern Rocky Mountains, In Dickenson, W.R., and Payne, W.P., eds., *Relations of tectonics to ore deposits in the southern Cordillera: Arizona Geol. Soc. Dig.*, v. 14, p. 199-214.
- Maher, B.J., 1983, Geology, geochemistry, and genesis of the Engineer Pass intrusive complex, San Juan Mountains, Colorado: Unpub. M.S. Thesis, Colorado State Univ., Fort Collins, 226 p.
- Mahood, G., and Hildreth, W., 1983, Large partition coefficients for trace elements in high silica rhyolites: *Geochim. et Cosmochim. Acta.*, v. 47, p. 11-30.
- Mayo, E.B., 1976, Intrusive fragmental rock directly or indirectly of igneous origin: In Wilt, J.C., and Jenny, J.P., eds., *Arizona Geol. Soc. Dig.*, v. 10, p. 348-430.
- McCallum, M.E., in preparation, Experimental evidence for fluidization processes in breccia pipe formation: *Econ. Geology*, v. 80.
- Morita, Y., 1955, Distribution of copper and zinc in various phases of earth materials: *Jour. Earth Sci., Nagoya Univ.*, v. 3, p. 33-48.
- Nash, J.T., 1975, Fluid inclusion studies of Vein, Pipe, and Replacement deposits, northwestern San Juan Mountains, Colorado: *Econ. Geology*, v. 70, p. 1448-1462.
- Onishi, H., and Sandell, E.B., 1955, Geochemistry of As: *Geochim. et Cosmochim. Acta.*, v. 7, p. 1-35.
- Osburn, G.R., and Chapin, C.E., 1983, Nomenclature of Cenozoic rocks of the northeast Mogollon-Datil volcanic field, New Mexico: *New Mexico Bur. Mines and Min. Res., Stratigraphic Chart 1*.
- Ratte, J.C., Gaskill, D.L., Eaton, G.P., Peterson, D.L., Stotelmeyer, R.B., and Meeves, H.C., 1979, Mineral resources of the Gila Primitive area and Gila Wilderness, New Mexico: *U.S. Geol. Survey Bull.*, 1451, 229 p.

- Reynolds, D.L., 1954, Fluidization as a geologic process, and its bearing on the problem of intrusive granites: *American Jour. Sci.*, v. 252, p. 577-614.
- Rhodes, R.C., 1976, Petrologic framework of the Mogollon Plateau volcanic ring complex, New Mexico: Surface expression of a major batholith: *New Mexico Geol. Soc. Spec. Pub. no. 5*, p. 103-112.
- Rose, A.W., and Burt, D.M., 1979, Hydrothermal Alteration: In Barnes, H.L., ed., *Geochemistry of Hydrothermal Ore Deposits*, 2nd ed.: New York, Wiley-Interscience, p. 173-235.
- _____, Hawkes, H.E., and Webb, J.S., 1979, *Geochemistry in Mineral Exploration*, London, Academic Press, 657 p.
- Ross, C.S., and Smith, R.L., 1961, Ash-Flow Tuffs: Their origin, geologic relations, and identification: *U.S. Geol. Survey Prof. Paper 366*, 81 p.
- Sandell, E.B., and Goldrich, S.S., 1943, The rarer metallic constituents of some American igneous rocks: Parts I and II; I. *Jour. Geology*, v. 51, p. 99-112, II. *Jour. Geology*, v. 51, p. 167-176.
- Seager, W.R., Shafiqullah, M., Hawley, J.W., and Marvin, R.F., 1984, New K-Ar dates from basalts and evolution of the southern Rio Grande rift: *Geol. Soc. America Bull.*, v. 95, p. 87-99.
- Seward, T.M., 1976, The stability of chloride complexes of silver in hydrothermal solutions up to 350°C: *Geochim. et Cosmochim. Acta.*, v. 40, p. 1329-1341.
- Simon, D.B., 1973, *Geology of the Silver Hill area, Socorro County, New Mexico*: M. Sc. Thesis, New Mexico Inst. Mining Tech., 101 p; *N.M. Bur. Mines and Min. Res.*, Open File Report 41, 110 p.
- Sinclair, A.J., 1974, Selection of threshold values in geochemical data using probability graphs: *Jour. Geochemical Expl.*, v. 3, p. 129-143.
- Smith, R.L., 1960, Ash Flows: *Geol. Soc. America Bull.*, v. 71, p. 795-842.
- _____, and Bailey, R.A., 1968, Resurgent cauldrons, In Coats, R.R., and others, eds., *Studies in Volcanology*: *Geol. Soc. America Memoir 116*, p. 613-662.
- Thompson, T.B., and Giles, D.L., 1983, Metals exploration workshop: Unpub. shortcourse notes.

- Tonking, W.H., 1957, Geology of Puertecito Quadrangle, Socorro County, New Mexico: New Mexico Bur. Mines and Min. Res. Bull, 41, 67 p.
- Watson, B.N., 1968, Intrusive volcanic phenomena in southern and central Arizona, In Titley, S.R., ed., Southern Arizona Guidebook III: Tucson, Arizona Geol. Soc., p. 147-153.
- Weber, R.H., 1963, Cenozoic volcanic rocks of Socorro County: New Mexico Geol. Soc. Guidebook 14th Field Conf., Socorro Region, p. 132-143.
- Wedepohl, K.H., (1969-1978) ed., Handbook of Geochemistry, (vols. I and II), Springer-Verlag, Berlin.
- Willard, M.E., 1957, Reconnaissance geologic map of the Luera Spring thirty-minute Quadrangle: New Mexico Bur. Mines and Min. Res. Geol. Map 2.
- Williams, H., and McBirney, A.R., 1979, Volcanology, Freeman, Cooper and Co., San Francisco, 397 p.
- Winchester, D.E., 1920, Geology of the Alamosa Creek Valley, Socorro County, with special reference to the occurrence of oil and gas: U.S. Geol. Survey Bull 716-A, p. 1-15.
- Wohletz, K.H., and Sheridan, M.F., 1979, A model for pyroclastic surge: Geol. Soc. America Spec. Paper 180, p. 177-194.
- Woolsey, T.S., McCallum, M.E., and Schumm, S.A., 1975, Diatreme emplacement by fluidization: Physics and Chemistry of the Earth, v. 9, p. 29-42.
- Wright, A.E., and Bowes, D.R., 1963, Classification of volcanic breccias: A discussion: Geol. Soc. America Bull, v. 74, p. 79-86.
- Zoback, M.L., Anderson, R.E., and Thompson, G.A., 1981, Cainozoic evolution of the state of stress and style of tectonism of the Basin and Range province of the western U.S.: Royal Soc. of London Phil. Trans., ser. A., v. 300, p. 407-434.

APPENDIX A

APPENDIX A

Rock Chip Geochemistry and Sample Description Data

All values reported in ppm. Trace element analyses were performed by Cone Geochemical Inc. of Lakewood, Colorado during September, 1982. Atomic absorption spectrometry methods were utilized in all sample analyses. Detection limits for geochem precision methods are as follows:

Au	0.02 ppm	Cu	1. ppm
Ag	0.2 ppm	Mo	1. ppm
As	1. ppm	Pb	1. ppm
Sb	1. ppm	Zn	1. ppm

Outcrop sampling methods included collection of 2 kg of chip material within a 3 m radius of the sample location. Underground samples from the Henckley mine at Aragon Hill consisted of 3.5 kg of continuous chip material taken at waist height. Sample material was manually mixed and split.

Sample No.	Au	Ag	As	Sb	Cu	Mo	Pb	Zn	Rx Type	Location	Alteration	Comments
1801	< 0.02	0.4	--	--	--	--	--	--	Tsc	Roberts Canyon	trace-wk. chlorite, trace-wk. goethite-hematite ± MnO along fractures	
1802	< 0.02	2.1	--	--	--	--	--	--	Tsc	Roberts Canyon	wk.-mod. argillization, trace pyrite casts, wk. goethite along fractures	mod. fractures
1803	< 0.02	0.4	--	--	--	--	--	--	Tvp	Roberts Canyon	mod. argillized-bleached groundmass, mod. fracture controlled goethite-hematite	sample taken along fracture/joint surfaces
1804	< 0.02	0.5	--	--	--	--	--	--	Tvp	Roberts Canyon	mod. argillized, mod. goethite-hematite along fractures	sample taken along fracture/joint surfaces
1805	< 0.02	0.2	--	--	--	--	--	--	Tvp	Roberts Canyon	mod. argillized, mod. goethite-hematite along fractures with local perv. wk. FeO	partially to densely welded, wk. fractured
1806	< 0.02	0.3	--	--	--	--	--	--	Tvp	Roberts Canyon	wk.-mod. argillized, mod. perv. and fracture controlled goethite-hematite	sample taken along fracture/joint surfaces, partially welded
1807	< 0.02	0.2	--	--	--	--	--	--	Tvp	Roberts Canyon	wk.-mod. argillized, trace-wk. goethite-hematite along fractures	
1808	< 0.02	< 0.2	--	--	--	--	--	--	Tvp	Roberts Canyon	mod. argillized, wk. barren hl. qtz. v'lts., mod.-str. goethite hematite along fractures	buff white, partially welded, wk. fractured
1809	< 0.02	4.5	--	--	--	--	--	--	Tvp	Roberts Canyon	wk.-mod. argillized, wk. hl.-1/4" drusy qtz. v'lts., local brecciation, trace-wk. diss. pyrite	prospect pit sample
1810	< 0.02	0.3	--	--	--	--	--	--	Tvp	Roberts Canyon	wk. perv. silicification, wk. argillization, trace diss. pyrite casts, no qtz. v'lts.	
1811	0.06	3.1	--	--	--	--	--	--	Tvp	Roberts Canyon	wk. perv. silicification, trace-wk. hl.-1/2" qtz. v'lts., trace-wk. diss. pyrite casts	

Sample No.	Au	Ag	As	Sb	Cu	Mo	Pb	Zn	Rx Type	Location	Alteration	Comments
1812	<0.02	0.6	--	--	--	--	--	--	Tvp	Roberts Canyon	wk.-mod. perv. silicification, trace diss. pyrite casts	
1813	<0.02	0.6	--	--	--	--	--	--	Tvp	Roberts Canyon	trace-wk. argillization, mod. goethite-hematite along fractures	partially welded, wk. fractured
1814	<0.02	0.4	--	--	--	--	--	--	Tvp	Roberts Canyon	bleached, trace-wk. argillization, wk.-mod. goethite-hematite	sample taken from fracture/joint surfaces
1815	<0.02	0.3	--	--	--	--	--	--	Tvp	Roberts Canyon	trace-wk. argillized, trace perv. silicification, mod. goethite-hematite ± MnO along fractures	densely welded, sample taken along fracture/joint surfaces
1816	<0.02	0.3	--	--	--	--	--	--	Tvp	Roberts Canyon	wk. argillized, trace-wk. pyrite casts, mod. goethite-hematite ± MnO along fractures	sampled along fracture/joints
1817	<0.02	0.3	--	--	--	--	--	--	Tvp	Roberts Canyon	mod. argillized, trace pyrite casts, local hl.-1/8" drusy qtz. v'lts.	buff white, partially welded
1818	<0.02	0.3	--	--	--	--	--	--	Tvp	Roberts Canyon	wk. perv. silicification, trace MnO along fractures, wk. white 1/4"-1" qtz. v'lts.	located along structure zone
1819	<0.02	0.4	--	--	--	--	--	--	Tvp	Roberts Canyon	wk. perv. and v'lt silicification	located along structure zone
1820	0.06	5.0	9	1	4	2	15	55	Tvp	Pankey Mine Area	str. perv. and v'lt silicification, qtz. after lamellar calcite, mod. perv. MnO	located along Pankey structure
1821	<0.02	1.4	2	1	4	5	9	72	Tvp	Pankey Mine Area	mod. perv. and v'lt silicification, trace pyrite casts, trace MnO	no visible sulfides
1822	<0.02	0.7	1	1	3	5	10	75	Tvp	Pankey Mine Area	wk. perv. silicification, trace hl. qtz. v'lts.	pale maroon color, no pyrite
1823	<0.02	1.3	3	1	4	4	16	78	Tvp	Pankey Mine Area	trace-wk. perv. and v'lt silicification	no observed sulfides

Sample No.	Au	Ag	As	Sb	Cu	Mo	Pb	Zn	Rx Type	Location	Alteration	Comments
1824	0.07	4.3	3	<1	5	5	14	51	Tvp	Pankey Mine Area	wk. perv. silicification crosscut by trace-wk. hl.-1/8" drusy qtz. v'lts.	wk.-mod. fractured
1825	1.33	84.2	2	1	8	5	7	42	Tvp	Pankey Mine Area		qtz. vein material from Pankey structure, massive to drusy, finely xtline qtz. with qtz. after lamellar calcite
1826	0.05	1.5	1	<1	4	3	22	78	Tvp	Pankey Mine Area	trace-wk. perv. silicification no qtz. v'lts., no FeO, wk. fracture controlled MnO	densely welded
1827	<0.02	0.9	1	1	3	3	21	86	Tvp	Pankey Mine Area	unaltered, trace MnO dendrites and wad along fractures	densely welded
1828	<0.02	3.0	5	1	4	2	21	55	Tvp	Pankey Mine Area	qtz. cemented breccia crosscut by trace-wk. 1/4-1/2" qtz. v'lts. ± FeO, no sulfides	sample along Pankey structure
1829	0.02	8.6	4	<1	3	3	19	95	Tvp	Pankey Mine Area	trace argillization, wk. hl.-1/2" qtz. v'lts.	pale maroon-grey color
1830	<0.02	0.9	1	1	3	2	13	81	Tvp	Pankey Mine Area	trace-wk. argillization along eutaxitic bands, no qtz. v'lts.	buff white, wk. fractured
1831	<0.02	1.0	<1	1	2	2	20	93	Tvp	Pankey Mine Area	trace-wk. fracture controlled argillization, no qtz. veining	
1832	0.06	1.1	4	<1	4	2	16	82	Tvp	Pankey Mine Area	wk. argillization along eutaxitic bands, trace hl. qtz. v'lts, trace MnO	
1833	<0.02	0.9	4	1	2	2	13	73	Tvp	Pankey Mine Area	trace-wk. argillization, local hl.-1/8" qtz. v'lts. with drusy texture	no sulfides present
1834	<0.02	0.8	2	<1	3	2	14	65	Tvp	Pankey Mine Area	trace-wk. argillization, trace-wk. goethite-hematite along fractures	pale maroon color

Sample No.	Au	Ag	As	Sb	Cu	Mo	Pb	Zn	Rx Type	Location	Alteration	Comments
1835	<0.02	1.8	8	1	3	2	25	65	Tvp	Pankey Mine Area	mod. argillized/brecciated Tvp rehealed with xtlne qtz. cross-cut by multistage hl.-1/4" qtz veining	adjacent of Pankey structure
1836	<0.02	1.0	14	1	3	2	17	83	Tvp	Pankey Mine Area	trace argillization/bleaching, trace hl.-1/2" drusy qtz. v'lts.	partially to densely welded
1837	<0.02	1.4	16	1	3	3	12	68	Tvp	Pankey Mine Area	mod. perv. silicification, trace pyrite, trace-wk. goethite-hematite + MnO	brecciated with multiple stages of qtz.v'lts.
1838	<0.02	1.1	18	1	3	2	15	82	Tvp	Pankey Mine Area	wk. perv. and veinlet silicification, no sulfides observed	locally brecciated, rehealed with very fine grained xtlne qtz.
1839	<0.02	0.8	3	<1	2	2	15	104	Tvp	Pankey Mine Area	wk. fracture controlled argillization, no sulfides	
1840	<0.02	2.9	10	<1	2	1	15	117	Tvp	Pankey Mine Area	trace argillization, trace-wk. pyrite typically as oxidized boxworks	
1841	<0.02	1.6	4	1	3	1	19	85	Tvp	Pankey Mine Area	trace argillization, wk. goethite-hematite + MnO along fractures, trace hl. qtz. v'lts. ± FeO limonites	possible sulfides present in qtz. v'lts.
1842	0.38	7.9	12	1	3	1	19	67	Tvp	Pankey Mine Area	mod. perv. silicification cross-cut by wk. hl.-2" drusy qtz. v'lts., trace goethite-hematite + MnO	relict primary textures preserved
1843	<0.02	1.3	8	1	3	3	12	59	Tvp	Pankey Mine Area	argillized Tvp overprinted by finely xtlne qtz. cement and qtz. v'lts.	mod. brecciated Tvp adjacent to Pankey structure
1844	<0.02	1.1	14	1	3	1	12	85	Tvp	Pankey Mine Area	wk.-mod. perv. argillization with trace diss. pyrite cubes, commonly oxidized, local qtz. v'lts.	

Sample No.	Au	Ag	As	Sb	Cu	Mo	Pb	Zn	Rx Type	Location	Alteration	Comments
1845	<0.02	1.2	4	<1	3	1	21	78	Tvp	Pankey Mine Area	wk. argillization along eutaxitic bands, trace hl. qtz. v'lts.	no sulfides present
1846	<0.02	0.9	<1	<1	2	1	13	82	Tvp	Pankey Mine Area	trace fracture controlled argillization	densely welded
1847	<0.02	0.8	<1	<1	2	2	23	118	Tvp	Pankey Mine Area	wk. perv. argillization, local hl.-1/4" qtz.+sulfide(?) v'lts.	
1848	<0.02	0.8	2	<1	2	1	14	85	Tvp	Pankey Mine Area	mod. argillized, locally brecciated, rehealed with greyish-aphanitic qtz., trace sulfides(?) present	
1849	<0.02	0.8	1	1	2	2	16	82	Tvp	Pankey Mine Area	mod. argillized, trace-wk.diss. pyrite boxwork, wk. goethite-hematite ± MnO along fractures	wk. fractured
1850	<0.02	1.5	4	1	3	5	13	72	Tvp	Pankey Mine Area	mod. perv. silicification overprinting argillization, wk. hl.-1/4" drusy qtz. v'lts.	
1851	0.06	1.3	3	2	3	3	20	79	Tvp	Pankey Mine Area	mod. argillized, wk. fine grained diss. pyrite, wk. stockworks of aphanitic qtz. v'lts, no sulfides	
1852	<0.02	0.9	<1	<1	2	2	14	75	Tvp	Pankey Mine Area	wk.-mod. argillized, 2-3 vol.% very fine grained diss. pyrite casts, wk. perv. MnO	no qtz. v'lts, wk. fractured
1853	<0.02	0.7	3	<1	2	1	11	83	Tvp	Pankey Mine Area	mod. argillized, trace-wk. goethite-hematite after diss. pyrite, trace 1/4-1/2" drusy qtz. v'lts.	local brecciation
1854	<0.02	0.8	2	<1	2	1	15	100	Tvp	Pankey Mine Area	mod. argillized breccia frags rehealed with aphanitic qtz. cement	brecciated texture, no qtz. v'lts.
1855	<0.02	0.7	1	<1	2	1	12	148	Tvp	Pankey Mine Area	mod. argillized, wk. diss. fine grained pyrite, trace -wk. MnO	

Sample No.	Au	Ag	As	Sb	Cu	Mo	Pb	Zn	Rx Type	Location	Alteration	Comments
1856	<0.02	0.5	7	<1	2	1	14	104	Tvp	Pankey Mine Area	mod. argillization, local brecciation rehealed with qtz. cement, trace very fine grained diss. pyrite boxworks	
1857	<0.02	0.7	1	<1	2	<1	18	24	Tvp	Pankey Mine Area	mod.-str. argillized, wk. hl.-1/8" drusy qtz. v'lts. ± FeO, clear aphanitic qtz. breccia cement	no sulfides, local brecciation
1858	<0.02	1.3	6	<1	2	1	13	92	Tvp	Pankey Mine Area	wk. argillized, wk. hl.-1/2" drusy qtz. v'lts., wk. diss. pyrite	wk. fractured
1859	<0.02	0.8	11	1	3	<1	15	63	Tvp	Pankey Mine Area	wk.-mod. argillized, grey aphanitic qtz. cement, sporadic drusy qtz. v'lts., wk. goethite-hematite along fractures	local wk. brecciation
1860	<0.02	11.4	8	1	3	3	12	60	Tvp	Pankey Mine Area	mod. perv. silicification overprinting argillization, brecciation rehealed with aphanitic grey silica	trace goethite-hematite ± MnO
1861	0.03	1.9	16	1	1	2	33	28	Tvp	Pankey Mine Area	wk. perv. silicification overprinting argillization, trace hl.-1/8" qtz. v'lts. crosscut silicification, trace-wk. fine grained pyrite casts	no sulfides
1862	<0.02	1.2	2	<1	2	1	21	165	Tvp	Pankey Mine Area	wk. perv. silicification, wk. argillization, trace hl.-1/8" qtz. v'lts., no sulfides	
1863	<0.02	1.3	2	1	2	1	22	41	Tvp	Pankey Mine Area	mod. argillization, locally wk. perv. silicification, wk.-mod. goethite-hematite ± MnO	
1864	<0.02	0.8	1	<1	2	2	51	69	Tvp	Pankey Mine Area	mod. perv. silicification overprinting wk. argillization, trace-wk. fracture controlled goethite-hematite + MnO	buff white to beige color
1865	<0.02	0.4	1	<1	2	<1	17	88	Tvp	Pankey Mine Area	wk. argillization, wk. sub-parallel hl.-1/8" drusy qtz. v'lts., wk. MnO along fractures	perv. FeO staining

Sample No.	Au	Ag	As	Sb	Cu	Mo	Pb	Zn	Rx Type	Location	Alteration	Comments
1866	<0.02	0.3	<1	<1	1	2	16	10	Tvp	Pankey Mine Area	wk. perv. argillization/silicification, trace hl.-1/8" qtz v'lts.	no sulfides
1867	<0.02	0.8	<1	1	1	1	12	12	Tvp	Pankey Mine Area	wk. argillization, aphanitic grey qtz. breccia cement	local brecciation with minor rotation, no qtz. veinleting
1868	<0.02	0.5	1	<1	2	1	15	29	Tvp	Pankey Mine Area	wk.-mod. argillized, trace 1/4-1/2" qtz. v'lts., no perv. silicification	local brecciation
1869	<0.02	0.5	3	1	2	1	13	22	Tvp	Pankey Mine Area	wk.-mod. argillized, trace 1/4-1/2" qtz. v'lts., wk. fracture controlled FeO	wk. fractured
1870	<0.02	0.7	2	<1	2	1	11	28	Tvp	Pankey Mine Area	trace-wk. argillization, trace diss. pyrite casts, trace 1/4-1/2" qtz. v'lts.	
1871	<0.02	0.9	1	<1	2	1	15	32	Tvp	Pankey Mine Area	wk.-mod. perv. silicification, wk. hl.-1/8" drusy qtz. v'lts., wk. goethite-hematite along fractures	
1872	<0.02	0.6	<1	<1	1	<1	18	147	Tvp	Pankey Mine Area	wk. argillization, wk. perv. silicification, local hl.-1/8" drusy aphanitic qtz. v'lts. + sulfides(?)	trace MnO along fractures
1873	<0.02	1.2	2	<1	2	<1	16	100	Tvp	Pankey Mine Area	wk. argillization with wk. perv. silicification, wk. hl.-1/8" drusy qtz. v'lts. + FeO	wk.-mod. fractured
1874	<0.02	0.8	<1	<1	2	<1	16	126	Tvp	Pankey Mine Area	wk. argillization, wk. perv. silicification, trace hl.-1/8" drusy qtz. + sulfide(?) v'lts.	v'lts oriented in subparallel N-S sets
1875	<0.02	0.7	<1	<1	2	<1	16	78	Tvp	Pankey Mine Area	wk. argillization, trace hl.-1/8" drusy aphanitic qtz. v'lts, trace -wk. goethite-hematite + MnO fracture coatings	v'lts. oriented in subparallel N-S sets
1876	<0.02	0.5	1	<1	2	6	15	35	Tvp	Pankey Mine Area	wk. argillization, trace goethite-hematite along fractures	no qtz. v'lts.

Sample No.	Au	Ag	As	Sb	Cu	Mo	Pb	Zn	Rx Type	Location	Alteration	Comments
1877	<0.02	0.3	<1	<1	2	1	12	90	Tvp	Pankey Mine Area	wk. perv. argillization, trace-wk. goethite-hematite + MnO along fracture surfaces	
1878	<0.02	0.8	<1	<1	2	1	10	26	Tvp	Pankey Mine Area	wk. argillization, local mod. perv. silicification, wk. goethite-hematite along fract.	
1781	<0.02	0.2	--	--	--	--	--	--	Tvp	Indian Trail Canyon	mod. argillization, mod. perv. goethite-hematite, supergene(?) clay v'lts. present	friable, pale brownish-red color
1782	<0.02	0.6	--	--	--	--	--	--	Tvp	Indian Trail Canyon	mod. argillized crosscut by trace-wk. hl.-1/4 " drusy clear qtz. v'lts.	no sulfides or FeO
1783	<0.02	0.3	--	--	--	--	--	--	Tvp	Indian Trail Canyon	wk.-mod. argillized, trace-wk. hl.-1/8" clear aphanitic qtz. v'lts., appear barren	
1784	<0.02	0.4	--	--	--	--	--	--	Tvp	Indian Trail Canyon	wk. perv. silicification crosscut by wk. multidirectional hl.-1/8" qtz. stockwork	no sulfides
1785	<0.02	0.3	--	--	--	--	--	--	Tvp	Indian Trail Canyon	wk. argillized, trace-mod. hl. qtz. v'lt. network without visible sulfides	multiple episodes of qtz. veinletting
1786	<0.02	0.2	--	--	--	--	--	--	Tvp	Indian Trail Canyon	wk. argillized, local hl.-1/2" finely xtline clear qtz. v'lts.	pale red, wk. perv. goethite-hematite
1787	<0.02	0.2	--	--	--	--	--	--	Tvp	Indian Trail Canyon	wk. argillized, wk. perv. goethite-hematite, trace hl.-1/8" drusy finely xtline qtz. v'lts., no sulfides	punky, porous appearance, creamy white to pale pinkish red color
1788	<0.02	0.2	--	--	--	--	--	--	Tvp	Indian Trail Canyon	trace-wk. hl.-1/8" drusy qtz. v'lts., wk. perv. goethite-hematite, finely xtline qtz. breccia cement	local crackle breccia, no sulfides
1789	<0.02	0.3	--	--	--	--	--	--	Tvp	Indian Trail Canyon	wk. argillization, trace hl.-1/2" drusy clear xtline qtz. v'lts., wk. fracture controlled goethite-hematite	

Sample No.	Au	Ag	As	Sb	Cu	Mo	Pb	Zn	Rx Type	Location	Alteration	Comments
1790	0.04	0.2	--	--	--	--	--	--	Tvp	Indian Trail Canyon	wk. argillized, trace hl.-1/8" barren clear qtz. v'lts., multistage v'lts. present	
1791	<0.02	0.3	--	--	--	--	--	--	Tvp	Indian Trail Canyon	wk. perv. argillization	beige to medium brown color
1792	<0.02	0.2	--	--	--	--	--	--	Tvp	Indian Trail Canyon	wk. argillization crosscut by trace qtz. v'lt. stockwork, no sulfides	
1793	<0.02	0.2	--	--	--	--	--	--	Tvp	Indian Trail Canyon	wk.-mod. argillization, wk. brecciated and rehealed with grey aphanitic qtz.	fracturing and silicification post-date argillization
1794	<0.02	0.2	--	--	--	--	--	--	Tvp	Indian Trail Canyon	mod. argillized, local brecciation rehealed with grey aphanitic silica	wk. goethite-hematite ± MnO
1795	<0.02	0.2	--	--	--	--	--	--	Tvp	Indian Trail Canyon	mod. perv. silicification with local hl.-1/4" drusy clear qtz. v'lts., trace goethite-hematite, no MnO	
1796	<0.02	<0.2	--	--	--	--	--	--	Tvp	Indian Trail Canyon	mod. perv. silicification, wk. perv. goethite-hematite, no MnO	
1797	<0.02	<0.2	--	--	--	--	--	--	Tvp	Indian Trail Canyon	mod. argillized, trace diss. pyrite, wk. perv. goethite-hematite limonite	
1798	<0.02	0.3	--	--	--	--	--	--	Tvp	Indian Trail Canyon	wk. argillized, trace hl.-1/8" barren finely xtline qtz. v'lts.	no sulfides within v'lts.
1799	<0.02	0.3	--	--	--	--	--	--	Tvp	Indian Trail Canyon	wk.-mod. argillization, wk. perv. goethite-hematite, no MnO, no sulfides	
1800	<0.02	0.3	--	--	--	--	--	--	Tvp	Indian Trail Canyon	wk.-mod. perv. silicification, no qtz. v'lts., no sulfides	

Sample No.	Au	Ag	As	Sb	Cu	Mo	Pb	Zn	Rx Type	Location	Alteration	Comments
1027	<0.02	0.2	--	--	--	--	--	--	Tvp	Indian Trail Canyon	mod.-str. argillization overprinted by wk. perv. silicification, wk. fracture controlled goethite-hematite + MnO	original textures not discernable
1028	<0.02	0.2	--	--	--	--	--	--	Tvp	Indian Trail Canyon	mod. str. perv. silicification, wk. fracture controlled and perv. goethite-hematite	
1029	<0.02	0.4	--	--	--	--	--	--	Tvp	Indian Trail Canyon	mod.-str. perv. silicification, wk. fracture controlled and perv. goethite-hematite	original textures not recognizable
1030	<0.02	<0.2	--	--	--	--	--	--	Tvp	Indian Trail Canyon	mod. perv. silicification with very fine grained diss. sulfides, no qtz. v'lts., no MnO	original textures not recognizable
1031	<0.02	0.3	--	--	--	--	--	--	Tvp	Indian Trail Canyon	mod. perv. silicification, wk. perv. and fracture controlled goethite-hematite	silicification overprinting argillic alteration
1032	<0.02	<0.2	--	--	--	--	--	--	Tvp	Indian Trail Canyon	wk. argillic alteration, wk.-mod. perv. and fracture controlled goethite-hematite	no sulfides
1033	<0.02	0.2	--	--	--	--	--	--	Tvp	Indian Trail Canyon	wk. argillized, wk. fracture controlled goethite-hematite	
1034	<0.02	0.2	--	--	--	--	--	--	Tvp	Indian Trail Canyon	wk. argillized, porous appearance, wk.-mod. perv. goethite-hematite	pale red to mod. red-brown color
1035	<0.02	0.2	--	--	--	--	--	--	Tvp	Indian Trail Canyon	bleach white, wk. argillized, local mod. perv. goethite-hematite, no sulfides	
1036	<0.02	0.2	--	--	--	--	--	--	Tvp	Indian Trail Canyon	mod. perv. silicification, trace very fine grained diss. pyrite, no qtz. v'lts.	
1037	<0.02	0.2	--	--	--	--	--	--	Tvp	Indian Trail Canyon	wk. argillized, wk. perv. goethite-hematite, local chalcadonic qtz. v'lts.	pale pinkish-red color

Sample No.	Au	Ag	As	Sb	Cu	Mo	Pb	Zn	Rx Type	Location	Alteration	Comments
1038	<0.02	0.2	--	--	--	--	--	--	Tvp	Indian Trail Canyon	trace hl.-1/8" clear xtlne qtz.v'lts., no sulfides, wk.-mod. perv. goethite-hematite	
1039	<0.02	<0.2	--	--	--	--	--	--	Tvp	Indian Trail Canyon	wk. perv. silicification with trace amounts of very fine grained pyrite euhedra, no qtz. v'lts.	
1040	<0.02	<0.2	--	--	--	--	--	--	Tvp	Indian Trail Canyon	wk.-mod. argillized, no silicification, wk.-mod. perv. goethite-hematite limonite	
1041	<0.02	0.2	--	--	--	--	--	--	Tvp	Indian Trail Canyon	wk.-mod. perv. silicification with trace amounts of very fine grained diss. pyrite cubes	no qtz. v'lts.
1042	0.03	2.8	--	--	--	--	--	--	Tvp	Indian Trail Canyon	wk. argillized, crosscut by 2 v'lt. types: 1) hl.-1/8" clear xtlne qtz., 2) hl.-1/4" white barren qtz.,	bleached white color
1043	<0.02	0.2	--	--	--	--	--	--	Tvp	Indian Trail Canyon	wk. argillized, local wk. perv. silicification, no FeO	
1044	<0.02	1.5	--	--	--	--	--	--	Tvp	Indian Trail Canyon	wk. perv. silicification, wk. stockwork of hl.-1/8" white drusy qtz. v'lts.	no visible sulfides
1045	<0.02	0.5	--	--	--	--	--	--	Tvp	Indian Trail Canyon	mod. perv. silicification, wk. fracture controlled MnO, no qtz. v'lts.	
1046	<0.02	0.3	--	--	--	--	--	--	Tvp	Indian Trail Canyon	wk.- mod. perv. silicification, trace hl.-1/8" clear qtz. v'lts. without sulfides, trace perv. FeO limonite	
1047	<0.02	<0.2	--	--	--	--	--	--	Tvp	Northern Nogai Canyon	wk. argillized, trace perv. goethite-hematite, aphanitic qtz. breccia cement	bleach white color, locally brecciated
1048	<0.02	<0.2	--	--	--	--	--	--	Tvp	Northern Nogai Canyon	mod.-str. perv. silicification, with trace diss. pyrite, cross-cut by hl.-1/8" clear xtlne qtz. v'lts.	bleach white to med. grey color

Sample No.	Au	Ag	As	Sb	Cu	Mo	Pb	Zn	Rx Type	Location	Alteration	Comments
1049	<0.02	<0.2	--	--	--	--	--	--	Tvp	Northern Nogal Canyon	unaltered, local hl.-1/8" drusy multidirectional qtz. v'lts., no sulfides	v'lts oriented in subparallel sets, local bleached alt'n selvages
1050	<0.02	<0.2	--	--	--	--	--	--	Tvp	Northern Nogal Canyon	wk. fracture controlled and perv. argillic alteration, wk. fracture controlled goethite-hematite	
1608	<0.02	<0.2	--	--	--	--	--	--	Tvp	Northern Nogal Canyon	wk.-mod. argillic alteration, trace-wk. goethite-hematite ± MnO along fractures	
1609	<0.02	0.2	--	--	--	--	--	--	Tvp	Northern Nogal Canyon	wk. argillized, wk. perv. and fracture controlled goethite-hematite	sampled along fractures
1610	<0.02	<0.2	--	--	--	--	--	--	Tvp	Northern Nogal Canyon	mod. perv. silicification, very fine grained diss. pyrite cubes, sporadic hl. xtline barren qtz. v'lts.	
1611	<0.02	<0.2	--	--	--	--	--	--	Tvp	Northern Nogal Canyon	mod. perv. silicification with trace diss. pyrite, trace-wk. fracture controlled FeO, no MnO	
1612	<0.02	<0.2	--	--	--	--	--	--	Tvp	Northern Nogal Canyon	silica vein material, massive texture varies to sucrosic, no sulfides, late qtz. v'lts, wk. MnO	sampled along structure zone
1613	<0.02	<0.2	--	--	--	--	--	--	Tvp	Northern Nogal Canyon	wk. argillized, wk.-mod. fracture controlled goethite-hematite, trace perv. MnO	bleached appearance
1614	<0.02	<0.2	--	--	--	--	--	--	Tvp	Northern Nogal Canyon	wk.-mod. silicification, locally vuggy texture, trace diss. goethite-hematite after pyrite	
1615	<0.02	2.0	--	--	--	--	--	--	Tvp	Northern Nogal Canyon	str. perv. silicification, no sulfides, crosscut by 1/4-1/2" drusy qtz. v'lts, wk.-mod. FeO along fractures	sampled along silicified zone

Sample No.	Au	Ag	As	Sb	Cu	Mo	Pb	Zn	Rx Type	Location	Alteration	Comments
1616	<0.02	0.2	--	--	--	--	--	--	Tvp	Northern Nogal Canyon	mod. perv. silicification, locally brecciated, trace drusy qtz. v'lts., trace MnO, trace-wk. diss. pyrite	sampled along structure zone, no original texture preserved
1617	<0.02	0.2	--	--	--	--	--	--	Tvp	Northern Nogal Canyon	wk. perv. silicification, trace wk. 1/8-1/4" white drusy barren qtz. v'lts., no sulfides	pale maroon color wk. fracture controlled FeO + MnO
1618	<0.02	0.2	--	--	--	--	--	--	Tvp	Northern Nogal Canyon	trace-wk. fracture controlled argillic alteration, wk. fracture controlled goethite-hematite, no MnO	
1619	<0.02	0.2	--	--	--	--	--	--	Tvp	Northern Nogal Canyon	wk.-mod. perv. silicification with very fine grained diss. pyrite, trace hl.-1/4" qtz. v'lts.	
1620	<0.02	<0.2	--	--	--	--	--	--	Tvp	Northern Nogal Canyon	wk. fracture controlled argillic alteration, trace-wk. goethite-hematite ± MnO	no silicification
1621	<0.02	<0.2	--	--	--	--	--	--	Tvp	Northern Nogal Canyon	wk. perv. argillic alteration, wk. perv. goethite-hematite, trace perv. MnO dendrites	porous bleached texture
1622	<0.02	<0.2	--	--	--	--	--	--	Tvp	Northern Nogal Canyon	wk.-mod argillized overprinted by wk. perv. silicification, wk. FeO ± MnO along fractures	no sulfides
1623	<0.02	<0.2	--	--	--	--	--	--	Tvp	Northern Nogal Canyon	wk. argillized, porous texture with drusy qtz. infillings of vugs and voids	
1624	<0.02	<0.2	--	--	--	--	--	--	Tvp	Northern Nogal Canyon	mod. argillized, wk. perv. goethite-hematite along fractures	
1625	<0.02	<0.2	--	--	--	--	--	--	Tvp	Northern Nogal Canyon	mod. perv. silicification with very fine grained diss. pyrite str. MnO, qtz.+MnO v'lts.	grab sample from prospect pit
1700	<0.02	<0.2	3	1	--	--	--	--	Tvp	Indian Peak	mod. perv. silicification crosscut with multiple stage drusy qtz.+kaol. v'lts, no sulfides	sample along 2-3' wide structure, local mod. brecciation, no relict textures

Sample No.	Au	Ag	As	Sb	Cu	Mo	Pb	Zn	Rx Type	Location	Alteration	Comments
1701	<0.02	<0.2	15	1	--	--	--	--	Tvp	Indian Peak	mod. perv. silicification with wk. hl.-1/8" qtz. v'lts., wk. FeO, no MnO	sampled along 2-3' wide structure zone
1702	<0.02	<0.2	2	<1	--	--	--	--	Tvp	Indian Peak	intense qtz.-alunite replacement, local original textures preserved, no sulfides	buff white color, no FeO
1703	<0.02	<0.2	3	<1	--	--	--	--	Tvp	Indian Peak	intense perv. qtz.-alunite replacement, trace very fine grained diss. pyrite	
1711	<0.02	<0.2	1	<1	--	--	--	--	Tvp	Indian Peak	str. perv. silicification, mod. alunite, dense massive texture, no original textures preserved	
1732	<0.02	<0.2	2	<1	--	--	--	--	Tvp	Indian Peak	intense perv. qtz.-alunite replacement, no sulfides	relict eutaxitic textures preserved, buff white color
1734	<0.02	<0.2	1	1	--	--	--	--	Tvp	Indian Peak	intense perv. qtz.-alunite replacement, trace specularite present	relict eutaxitic textures present
1879	<0.02	0.2	--	--	--	--	--	--	Tvp	Taylor Shaft Area	wk. perv. silicification, trace very fine grained diss. pyrite, wk. fracture controlled goethite-hematite + MnO	
1880	<0.02	0.3	--	--	--	--	--	--	Tvp	Taylor Shaft Area	wk.-mod. perv. silicification, mod. goethite-hematite along fractures	no qtz. v'lts., no sulfides
1881	0.03	0.2	--	--	--	--	--	--	Tvp	Taylor Shaft Area	qtz. material: finely xtline, vuggy boxwork, qtz. pseudo-morphs after lamellar clacite, trace very fine grained sulfides(?)	sampled along 2' structure zone
1882	<0.02	0.4	--	--	--	--	--	--	Tvp	Taylor Shaft Area	wk. argillized crosscut by trace hl. multidirectional qtz. v'lts.	
1883	<0.02	0.3	--	--	--	--	--	--	Tvp	Taylor Shaft Area	mod. perv. and hl.-1/8" qtz. v'lt silicification, wk. FeO + MnO along fractures	sampled along structure zone

Sample No.	Au	Ag	As	Sb	Cu	Mo	Pb	Zn	Rx Type	Location	Alteration	Comments
1884	<0.02	0.2	--	--	--	--	--	--	Tvp	Taylor Shaft Area	wk. perv. argillic alteration, local mod. brecciation, multiple episodes of silica influx	sampled along structure zone, no sulfides
1885	<0.02	0.2	--	--	--	--	--	--	Tvp	Taylor Shaft Area	mod. perv. silicification with very fine grained diss. pyrite, local hl.-1/8" clear drusy qtz. v'lts., wk. FeO + MnO along fractures	
1886	0.87	15.5	--	--	--	--	--	--	Tvp	Taylor Shaft Area	qtz. vein material: white with crustiform and massive-vuggy textures, trace diss. sulfides, trace fracture controlled MnO	dump grab sample
1887	23.20	173.0	--	--	--	--	--	--	Tvp	Taylor Shaft Area	qtz. vein material: limonitic boxwork present, qtz. after lamellar calcite, strong MnO ± sulfides present	dump grab sample
1888	<0.02	0.3	--	--	--	--	--	--	Tvp	Taylor Shaft Area	wk. argillized, trace-wk. 1/8-1/4" drusy clear qtz. v'lts., no sulfides	sample from prospect pit
1889	<0.02	0.2	--	--	--	--	--	--	Tvp	Taylor Shaft Area	mod.-str. perv. silicification, trace qtz. v'lts., trace fine grained sulfides(?), trace fracture controlled MnO	adjacent to Rhyolite fault
1890	<0.02	0.3	--	--	--	--	--	--	Tvp	Taylor Shaft Area	mod.-perv. silicification with trace-wk. very fine grained diss. pyrite, wk.-mod. FeO along fractures	
1891	<0.02	0.6	--	--	--	--	--	--	Tvp	Taylor Shaft Area	mod. perv. silicification, trace perv. FeO after pyrite(?) no MnO, no sulfides	
1892	<0.02	0.2	--	--	--	--	--	--	Tvp	Taylor Shaft Area	wk.-mod. perv. silicified, trace-wk. goethite-hematite ± MnO, no sulfides	
1893	<0.02	0.3	--	--	--	--	--	--	Tvp	Taylor Shaft Area	wk.-mod. argillized, wk.-mod. perv. and fracture controlled FeO and MnO	

Sample No.	Au	Ag	As	Sb	Cu	Mo	Pb	Zn	Rx Type	Location	Alteration	Comments
1894	<0.02	0.2	--	--	--	--	--	--	Tvp	Taylor Shaft Area	trace to wk. argillic alteration bleached appearance, local diss. pyrite casts, wk.-mod. FeO along fractures, no MnO	buff white color
1895	<0.02	<0.2	--	--	--	--	--	--	Tvp	Taylor Shaft Area	trace-wk. argillized, wk.-mod. fracture controlled goethite-hematite, no silicification	
1896	<0.02	0.2	--	--	--	--	--	--	Tvp	Taylor Shaft Area	mod. perv. silicification, trace-wk. very fine grained diss. pyrite, mod. FeO along fract's, no qtz. v'lts.	
1897	<0.02	0.3	--	--	--	--	--	--	Tvp	Taylor Shaft Area	wk. argillized overprinted by mod. perv. silicification, wk.-mod. FeO along fractures	no qtz. v'lts.
1898	<0.02	0.2	--	--	--	--	--	--	Tvp	Taylor Shaft Area	trace-wk. argillization, wk. goethite-hematite along fractures	
1899	<0.02	<0.2	--	--	--	--	--	--	Tvp	Taylor Shaft Area	wk. argillic alteration, trace-wk. diss. pyrite, no qtz. v'lts.	
1900	<0.02	0.3	--	--	--	--	--	--	Tvp	Taylor Shaft Area	wk. argillized, wk.-mod. perv. goethite-hematite present	sampled along fractures
1901	<0.02	<0.2	--	--	--	--	--	--	Tvp	Taylor Shaft Area	trace-wk. argillic alteration, wk.-mod. goethite-hematite along fractures, no qtz. v'lts.	
1902	<0.02	<0.2	--	--	--	--	--	--	Tvp	Taylor Shaft Area	wk. argillized, wk.-mod. perv. and fracture controlled goethite-hematite limonite	no qtz. v'lts., no sulfides
1903	<0.02	<0.2	--	--	--	--	--	--	Tvp	Taylor Shaft Area	mod. argillic alteration, trace diss. pyrite boxwork, wk. fracture controlled FeO	
1904	<0.02	0.2	--	--	--	--	--	--	Tvp	Taylor Shaft Area	wk.-mod. argillization, trace-wk. goethite-hematite ± MnO along fractures	sample taken along fractures

Sample No.	Au	Ag	As	Sb	Cu	Mo	Pb	Zn	Rx Type	Location	Alteration	Comments
1905	<0.02	0.3	--	--	--	--	--	--	Tvp	Taylor Shaft Area	wk.-mod. argillic alteration, mod. hematite along fractures, no sulfides, trace MnO	
1906	<0.02	<0.2	--	--	--	--	--	--	Tvp	Taylor Shaft Area	unaltered to wk. argillized, wk. fracture controlled FeO limonite	
1907	<0.02	0.8	--	--	--	--	--	--	Tvp	Taylor Shaft Area	wk. argillized, wk.-mod. perv. and fracture controlled goethite-hematite	well preserved primary textures
1908	0.03	0.3	--	--	--	--	--	--	Tvp	Taylor Shaft Area	trace-wk. argillic alteration, trace hl.-1/8" drusy white qtz. v'lts., mod. perv. MnO	pale maroon to med. grey-brown color
1909	0.07	1.9	1	<1	--	--	--	--	Tvp	Rhyolite Mine Area	trace-wk. argillization, trace 1/8-1/2" finely xline white qtz. v'lts., mod. perv. FeO + MnO	adjacent to structure zone
1910	<0.02	0.5	2	<1	--	--	--	--	Tvp	Rhyolite Mine Area	wk.-mod. argillized, wk.-mod. goethite-hematite ± MnO along fractures	
1911	<0.02	0.5	4	<1	--	--	--	--	Tvp	Rhyolite Mine Area	trace-wk. argillized, wk.-mod. goethite-hematite along fractures	sample along fractures
1912	<0.02	0.3	1	<1	--	--	--	--	Tvp	Rhyolite Mine Area	trace argillic alteration, wk.-mod. goethite-hematite along fractures, no sulfides present	
1913	<0.02	0.2	4	1	--	--	--	--	Tvp	Rhyolite Mine Area	wk. argillized, wk.-mod. fracture controlled FeO + MnO ± sericite(?)	sample taken along fractures, no sulfides
1914	0.14	2.4	1	1	--	--	--	--	Tvp	Rhyolite Mine Area	wk. argillic alteration, mod-str. goethite-hematite along fractures	sampled along fractures
1914A	<0.02	<0.2	1	<1	--	--	--	--	Tvp	Rhyolite Mine Area	wk. argillized, mod.-str. goethite-hematite ± MnO along fractures	sample from prospect pit

Sample No.	Au	Ag	As	Sb	Cu	Mo	Pb	Zn	Rx Type	Location	Alteration	Comments
1915	<0.02	1.6	<1	<1	--	--	--	--	Tvp	Rhyolite Mine Area	wk. argillized, sporadic hl.-1/8" Qtz. + sulfide v'lts.	
1916	0.05	0.9	1	<1	--	--	--	--	Tvp	Rhyolite Mine Area	unaltered except for trace hl.-1/4" finely xtlne Qtz. v'lts., mod. goethite-hematite along fractures, no sulfides	original textures well preserved
1917	0.04	1.4	1	<1	--	--	--	--	Tvp	Rhyolite Mine Area	bleached appearance, wk. argillized, local hl.-1/4" finely xtlne Qtz. v'lts., wk. perv. goethite-hematite, no sulfides	
1918	<0.02	0.2	2	1	--	--	--	--	Tvp	Rhyolite Mine Area	wk. perv. argillic alteration, mod. fracture controlled goethite-hematite ± MnO, no Qtz. v'lts.	sample taken from prospect pit exposure
1919	<0.02	0.9	5	1	--	--	--	--	Tvp	Rhyolite Mine Area	wk. argillic alteration, mod. goethite-hematite along fractures, local chalcadonic fracture fillings	bleached appearance
1920	0.04	0.2	1	1	--	--	--	--	Tvp	Rhyolite Mine Area	wk. argillic alteration, trace wk. fracture controlled goethite-hematite limonite, no Qtz. v'lts.	
1921	0.08	1.9	3	7	--	--	--	--	Tvp	Rhyolite Mine Area	wk. perv. silicified, mod. goethite-hematite + MnO along fractures	sample located adjacent to structure
1922	<0.02	1.7	7	1	--	--	--	--	Tvp	Rhyolite Mine Area	locally brecciated, wk.-mod. silicified including Qtz. cement, sporadic finely xtlne Qtz. v'lts.	sample from prospect pit exposure adjacent to Rhyolite Mine portal
1923	<0.02	1.2	2	1	--	--	--	--	Tvp	Rhyolite Mine Area	wk. argillized, mod. perv. goethite-hematite limonite ± MnO along fractures, no Qtz. v'lts.	sample taken along fractures

Sample No.	Au	Ag	As	Sb	Cu	Mo	Pb	Zn	Rx Type	Location	Alteration	Comments
1924	<0.02	0.5	1	1	--	--	--	--	Tvp	Rhyolite Mine Area	wk. argillized/bleached, mod.-str. goethite-hematite-jarosite (?) along fractures	no silica introduction
1925	0.17	2.4	6	1	--	--	--	--	Tvp	Rhyolite Mine Area	mod. perv. and v'lt silicification, mod. goethite-hematite + MnO along fractures,	locally brecciated, sample along structure zone
1978	<0.02	<0.2	1	<1	--	--	--	--	Tvp	Rhyolite Mine Area	wk. perv. and fracture controlled argillic alteration, wk. goethite-hematite along fractures	
1979	0.03	1.5	<1	<1	--	--	--	--	Tvp	Rhyolite Mine Area	structural breccia: silicified fragments healed in white finely xtlined qtz. cement, wk. MnO, no qtz. v'lts.	sample along Rhyolite fault zone
1980	<0.02	2.3	2	1	--	--	--	--	Tvp	Rhyolite Mine Area	wk. argillized, crosscut by trace hl.-1/8" finely xtlined qtz. v'lts., wk.-mod. FeO along fractures	adjacent to Rhyolite fault zone
1981	<0.02	0.2	1	1	--	--	--	--	Tvp	Rhyolite Mine Area	wk. argillic alteration, trace very fine grained diss. pyrite boxwork, fracture controlled goethite-hematite	
1926	0.69	11.1	--	--	--	--	--	--	Ts1	Seferino Hill Area	high silica vein material: str. perv. silicification, multiple episodes of silica influx and brecciation, no sulfides wk. FeO	laharic breccia host rock, sample taken along structure zone
1927	1.62	14.0	--	--	--	--	--	--	Ts1	Seferino Hill Area	high silica vein material: str. perv. silica influx with multiple episodes of brecciation, wk. perv. FeO	sample taken along structure zone
1928	0.02	1.3	--	--	--	--	--	--	Ts1	Seferino Hill Area	mod-str. perv. silicification, vuggy boxwork texture infilled with late white qtz., trace-wk. FeO	sample taken along structure zone
1929	<0.02	0.8	--	--	--	--	--	--	Ts1	Seferino Hill Area	mod. perv. matrix silicification of laharic breccia, local calcite v'lts., no qtz. v'lts.	sample taken adjacent to structure zone

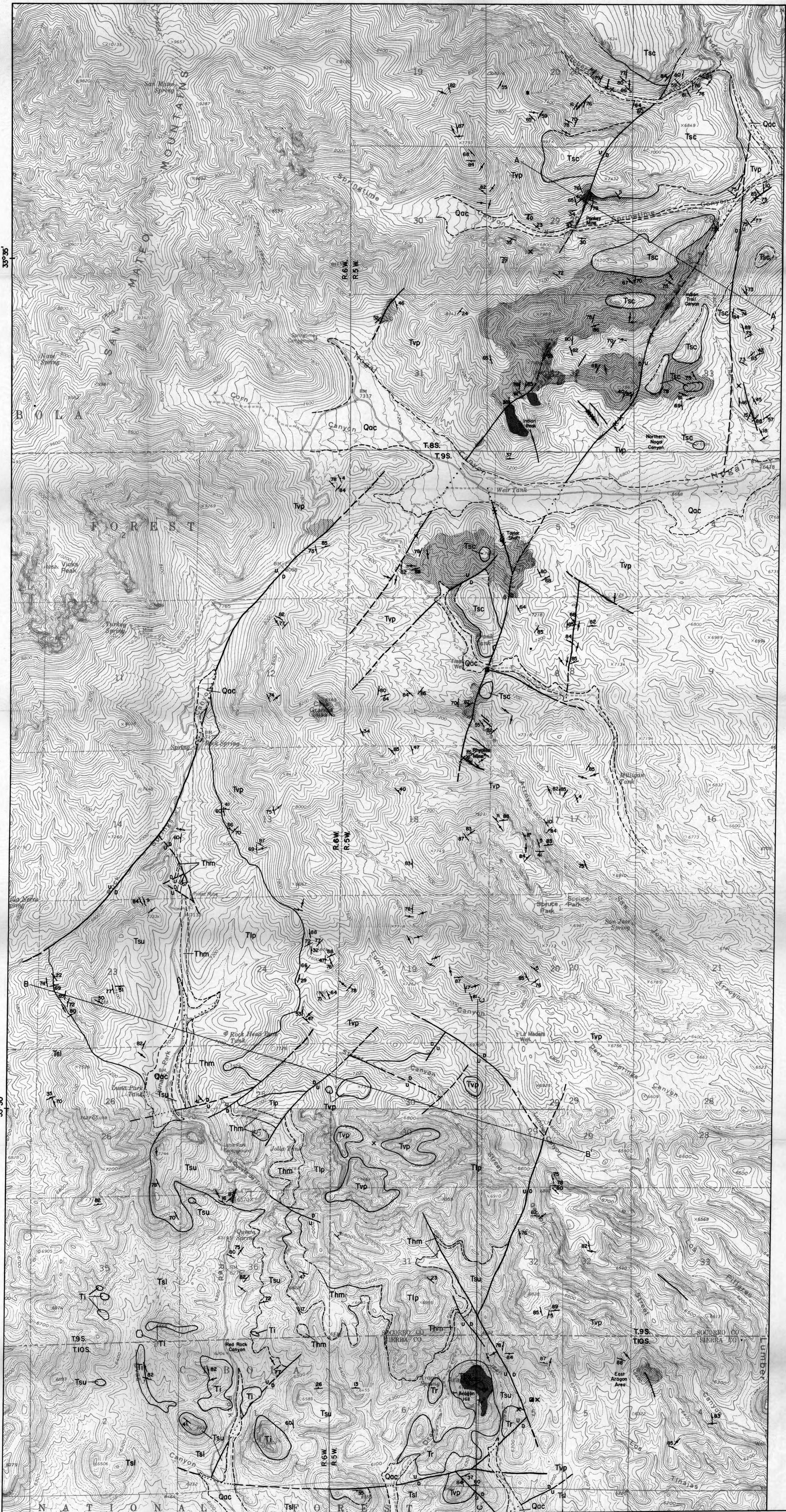
Sample No.	Au	Ag	As	Sb	Cu	Mo	Pb	Zn	Rx Type	Location	Alteration	Comments
1930	<0.02	<0.2	--	--	--	--	--	--	Tsl	Seferino Hill Area	breccia matrix is mod. silicified, trace-wk. FeO along fractures, trace diss. pyrite, no qtz. v'lts.	sample adjacent to structure zone
1931	<0.02	0.3	--	--	--	--	--	--	Tsl	Seferino Hill Area	mod. perv. breccia matrix silicification, local relict unaltered laharc breccia present, no qtz. v'lts.	
1932	<0.02	0.2	--	--	--	--	--	--	Tsl	Seferino Hill Area	mod. perv. breccia matrix silicification, trace-wk. MnO, no qtz. v'lts.	
1933	<0.02	<0.2	--	--	--	--	--	--	Tsl	Seferino Hill Area	intense perv. silica replacement of breccia resulting in vuggy finely xtline high silica rock, no qtz. v'lts.	
1934	<0.02	<0.2	--	--	--	--	--	--	Tsl	Seferino Hill Area	intense perv. white finely xtline qtz. replacement, no MnO, no sulfides, trace FeO	no qtz. v'lts.
1935	<0.02	<0.2	--	--	--	--	--	--	Tsl	Seferino Hill Area	mod. perv. silica replacement of breccia matrix, frags typically unaltered, no qtz. v'lts.	
1936	<0.02	<0.2	--	--	--	--	--	--	Tsl	Seferino Hill Area	wk. breccia matrix silica replacement, drusy/cockade xtline qtz. growths on breccia fragments	
1937	<0.02	1.5	--	--	--	--	--	--	Tbx	Henckley Mine Aragon Hill	mod. sericitized breccia matrix, wk. FeO ± barite-calcite fracture fillings	10 ft. underground channel sample
1938	0.23	1.6	--	--	--	--	--	--	Tbx	Henckley Mine Aragon Hill	structure zone gouge material: sericite-clay alteration, wk. FeO + MnO along fractures, abundant qtz.-barite-calcite	2 ft. underground channel sample along fracture zone
1939	<0.02	1.4	--	--	--	--	--	--	Tbx	Henckley Mine Aragon Hill	mod. breccia matrix sericite alteration, wk. FeO + MnO, no qtz. v'lts., no sulfides	8 ft. underground channel sample

Sample No.	Au	Ag	As	Sb	Cu	Mo	Pb	Zn	Rx Type	Location	Alteration	Comments
1940	<0.02	1.6	--	--	--	--	--	--	Tbx	Henckley Mine Aragon Hill	mod. breccia matrix sericite alteration, sericite/chlorite fragment alteration, trace diss. pyrite, wk. FeO + MnO	3 ft. underground channel sample
1941	<0.02	1.3	--	--	--	--	--	--	Tbx	Henckley Mine Aragon Hill	str. sericite alteration, abundant FeO + MnO along fractures	3 ft. channel sample along structure zone
1942	<0.02	1.3	--	--	--	--	--	--	Tbx	Henckley Mine Aragon Hill	mod. breccia matrix sericite alteration, trace diss. pyrite, variable fragment alteration, no silica influx	8 ft. underground channel sample
1943	0.58	1.9	--	--	--	--	--	--	Tbx	Henckley Mine Aragon Hill	mod. breccia matrix sericite alteration, no sulfides or qtz. v'lts., trace FeO +MnO along fractures	9 ft. underground channel sample
1944	0.05	1.0	--	--	--	--	--	--	Tbx	Henckley Mine Aragon Hill	mod. breccia matrix sericite alteration with varialbe frag alteration types, trace very fine grained diss. pyrite	5 ft. underground channel sample
1945	<0.02	0.7	--	--	--	--	--	--	Tbx	Henckley Mine Aragon Hill	mod. breccia matrix sericite alteration, wk. fractured, no sulfides, wk. fracture controlled MnO wad and dendrites	5 ft. underground channel sample
1946	0.03	1.2	--	--	--	--	--	--	Tbx	Henckley Mine Aragon Hill	mod. matrix sericitization with sericite and chlorite alteration of breccia clasts, trace-wk. MnO dendrites and wad, no FeO	6 ft. underground channel sample
1947	0.15	2.2	--	--	--	--	--	--	Tr	Aragon Hill	wk. argillized, wk.-mod. goethite-hematite along fractures	buff white color
1948	0.09	0.5	--	--	--	--	--	--	Tr	Aragon Hill	wk. argillized with local 1/4-1/2" drusy qtz. v'lts., wk. FeO along fractures	
1949	0.02	0.2	--	--	--	--	--	--	Tr	Aragon Hill	wk. argillized, wk.-mod. goethite-hematite along fract. no silica influx	

Sample No.	Au	Ag	As	Sb	Cu	Mo	Pb	Zn	Rx Type	Location	Alteration	Comments
1950	0.05	1.6	--	--	--	--	--	--	Tr	Aragon Hill	trace-wk. argillic alteration, mod. goethite-hematite along fractures, no sulfides present	no silica influx
1951	0.14	0.4	--	--	--	--	--	--	Tr	Aragon Hill	wk. argillic alteration, trace diss. pyrite(?), mod. goethite-hematite along fractures	no silicification
1952	0.20	1.1	--	--	--	--	--	--	Tr	Aragon Hill	trace-wk. argillic alteration, trace very fine grained diss. pyrite(?) with FeO alteration	
1953	0.16	1.8	--	--	--	--	--	--	Tr	Aragon Hill	trace-wk. argillic alteration, mod. goethite-hematite along fractures, no v'lt or perv. silica influx	
1954	0.27	0.3	--	--	--	--	--	--	Tr	Aragon Hill	unaltered to wk. argillic alteration, wk. perv. goethite-hematite, no qtz. v'lts.	
1955	0.04	0.4	--	--	--	--	--	--	Tr	Aragon Hill	wk. argillic alteration, trace very fine grained FeO xtls after pyrite(?), wk. perv. FeO	no v'lt. or perv. silicification
1956	0.22	0.3	--	--	--	--	--	--	Tr	Aragon Hill	trace to wk. argillic alteration local fracture controlled FeO, trace hl. qtz. v'lts.	
1964	<0.02	0.9	--	--	--	--	--	--	Tr	Aragon Hill	wk.-mod. argillized, mod. goethite-hematite ± MnO along fractures	sample from exposure in prospect pit
1957	<0.02	<0.2	--	--	--	--	--	--	Tvp	East Aragon Area	mod.-str.perv. silicification, trace diss. pyrite(?), trace hl.-1/8" finely xtline qtz.v'lts.	
1958	<0.02	0.2	--	--	--	--	--	--	Tvp	East Aragon Area	incipient bleaching, wk. perv. FeO limonite staining, no qtz. v'lts.	
1959	<0.02	<0.2	--	--	--	--	--	--	Tvp	East Aragon Area	incipiently to wk. argillized, wk. fracture controlled FeO	
1960	<0.02	0.5	--	--	--	--	--	--	Tvp	East Aragon Area	wk. argillized, mod. goethite-hematite along fractures	sample taken along joint and fracture sets

Sample No.	Au	Ag	As	Sb	Cu	Mo	Pb	Zn	Rx Type	Location	Alteration	Comments
1961	<0.02	0.2	--	--	--	--	--	--	Tvp	East Aragon Area	wk. argillized, irregular FeO staining, no silica influx	
1962	<0.02	0.8	--	--	--	--	--	--	Tvp	East Aragon Area	wk.-mod. argillized, wk. goethite-hematite ± jarosite(?) along fractures	sample from prospect pit
1963	<0.02	1.1	--	--	--	--	--	--	Tvp	East Aragon Area	structural breccia: argillized fragments set in aphanitic qtz. cement, no sulfides	
1965	<0.02	<0.2	--	--	--	--	--	--	Ti	Red Rock Canyon	incipient argillic alteration, bleaching	
1966	<0.02	<0.2	--	--	--	--	--	--	Ti	Red Rock Canyon	wk. clay-sericite groundmass alteration, trace-wk. MnO no silica introduction	
1967	<0.02	1.4	--	--	--	--	--	--	Tsl	Red Rock Canyon	wk. propylitic alteration of andesite flow, wk. fracture controlled MnO	
1968	<0.02	0.2	--	--	--	--	--	--	Ti	Red Rock Canyon	incipient to wk. clay alteration, trace amounts of diss. hematite after (?), trace MnO	
1969	<0.02	0.2	--	--	--	--	--	--	Tsl	Red Rock Canyon	wk.-mod propylitic alteration, wk. fracture controlled MnO	
1970	<0.02	0.2	--	--	--	--	--	--	Ti	Red Rock Canyon	wk. argillized Ti groundmass, trace very fine grained diss. pyrite euhedra, wk. perv. FeO	
1971	<0.02	0.2	--	--	--	--	--	--	Tsl	Red Rock Canyon	wk. chlorite + clay ± sericite (?), sporadic calcite v'lts., no sulfides	
1972	<0.02	<0.2	--	--	--	--	--	--	Ti	Red Rock Canyon	wk. argillized, wk.-mod. goethite-hematite along fractures, trace diss. pyrite casts no silicification	
1973	<0.02	<0.2	--	--	--	--	--	--	Ti	Red Rock Canyon	wk. Ti groundmass argillic alteration, wk. perv. FeO no pyrite, no silica influx	

Sample No.	Au	Ag	As	Sb	Cu	Mo	Pb	Zn	Rx Type	Location	Alteration	Comments
1974	<0.02	1.4	--	--	--	--	--	--	Ts1	Red Rock Canyon	wk. perv. chlorite alteration, wk. calcite-epidote fracture filling within andesite	
1975	<0.02	<0.2	--	--	--	--	--	--	Tvp	Red Rock Canyon	incipient clay alteration, wk. MnO along fractures	
1976	<0.02	0.2	--	--	--	--	--	--	T1p	Red Rock Canyon	wk. argillic alteration, trace very fine grained diss. pyrite boxwork, wk.-mod. perv. FeO no silicification	
1977	<0.02	0.2	--	--	--	--	--	--	T1p	Red Rock Canyon	unaltered with mod. goethite-hematite along fractures	sample from prospect pit



EXPLANATION

EXTRUSIVE & SEDIMENTARY ROCKS INTRUSIVE ROCKS

Qac

ALLUVIUM AND COLLUVIUM DEPOSITS

Tbx

INTRUSIVE BRECCIA

Ti

PORPHYRITIC RHYOLITE ROCKS

Tr

RHYOLITE FLOW-DOME ROCKS

Crystal rich, massive lava flows

Tsc

SPRINGTIME CANYON QUARTZ LATITE

Crystal rich, massive lava flows

Tvp

VICKS PEAK TUFF

Multiple flow, densely to partially welded, crystal poor, rhyolite ash flow tuff

Tip

UNIT OF LUNA PARK

Interbedded andesite flows, heterolithic breccia flows, and volcanic conglomerates

Thm

HELLS MESA TUFF

Crystal rich, rhyolite ash flow tuff

Tsu

UPPER MEMBER

Lafite and andesite flows, flow breccias, and latitic ash flows

Tsl

LOWER MEMBER

Andesite flows and flow breccias

SPEARS FORMATION

ALTERATION



QUARTZ, ALUNITE ALTERATION

Pervasive replacement occurrences with trace amounts of koolinite, specularite, and pyrite



SILICIFICATION

Pervasive and veinlet occurrences of crystalline quartz ± pyrite ± adularia ± sericite ± calcite ± pyroxene ± cryptomelane



KAOLINITE, MONTMORILLONITE-ILLITE, MONTMORILLONITE QUARTZ, PYRITE ALTERATION

Weak to moderate pervasive argillization typically adjacent to fault zones but locally of regional extent



SERICITE, QUARTZ, PYRITE, KAOLINITE, MONTMORILLONITE-CHLORITE, CALCITE ALTERATION

Weak to moderate pervasive alteration of Ti, Tr, and Tbx

--- CONTACT; DASHED WHERE APPROXIMATELY LOCATED

U --- FAULT; SHOWING RELATIVE MOVEMENT, DASHED WHERE APPROXIMATELY LOCATED, DOTTED WHERE CONCEALED

78 STRIKE AND DIP OF ASH FLOW COMPACTION FOLIATION

→ STRIKE OF VERTICAL COMPACTION FOLIATION

56 STRIKE AND DIP OF JOINTS

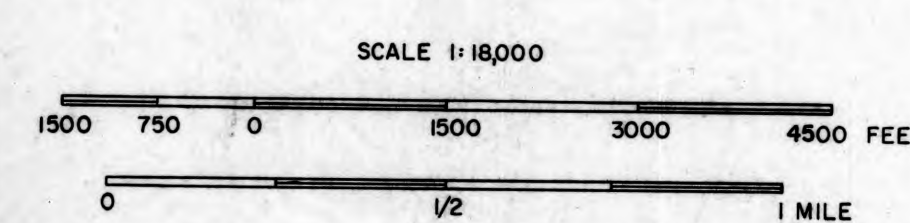
→ STRIKE OF VERTICAL JOINTS

12 STRIKE AND DIP OF BEDDING

X PROSPECT PIT

■ SHAFT

➤ ADIT



RECONNAISSANCE GEOLOGIC AND ALTERATION MAP OF THE NOGAL CANYON AREA

SOUTHERN SAN MATEO MOUNTAINS SOCORRO AND SIERRA COUNTIES, NEW MEXICO

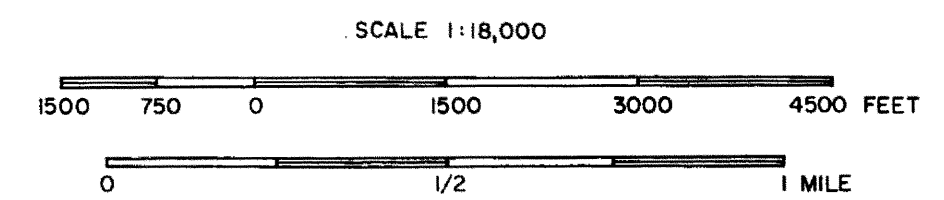
JON FORURIA COLORADO STATE UNIVERSITY 1984

PLATE I

QUATERNARY
OLIGOCENE
TERTIARY

GENERALIZED
CROSS SECTIONS
A-A', B-B', C-C'
OF THE NOGAL CANYON AREA

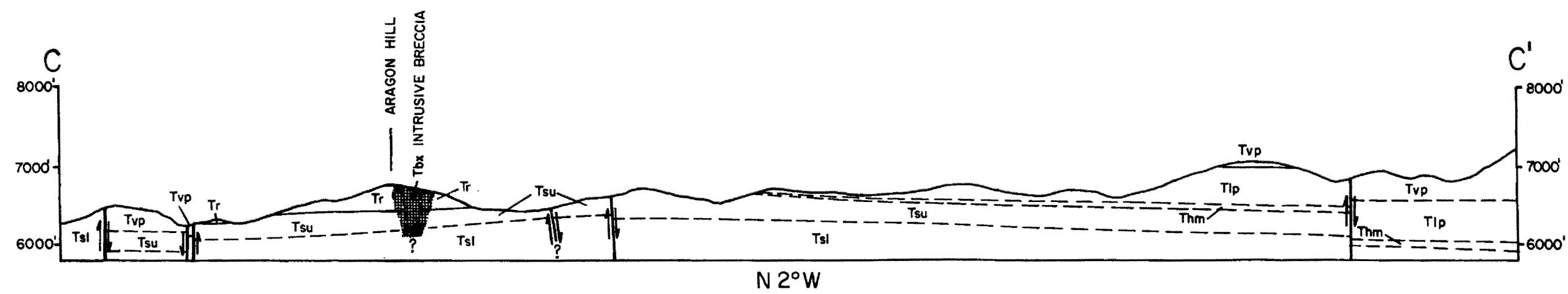
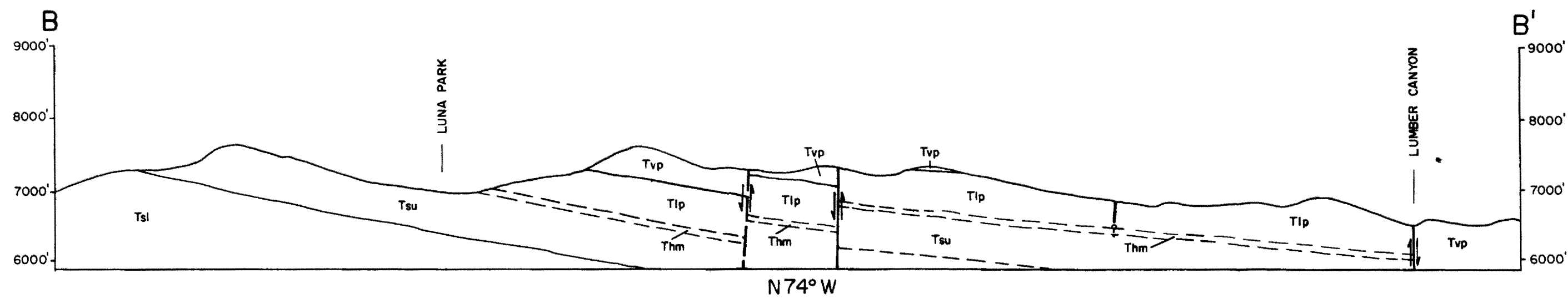
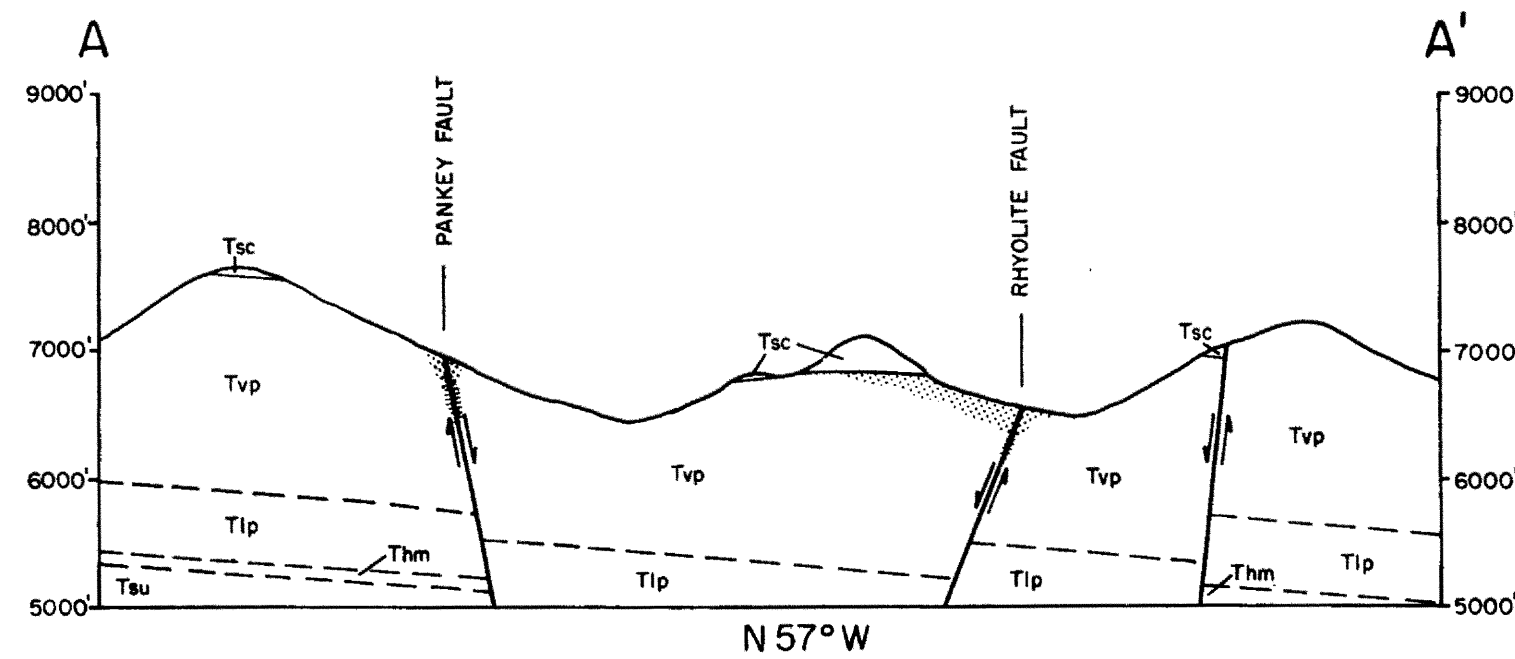
Refer to Plate I for Explanation
and Cross Section locations

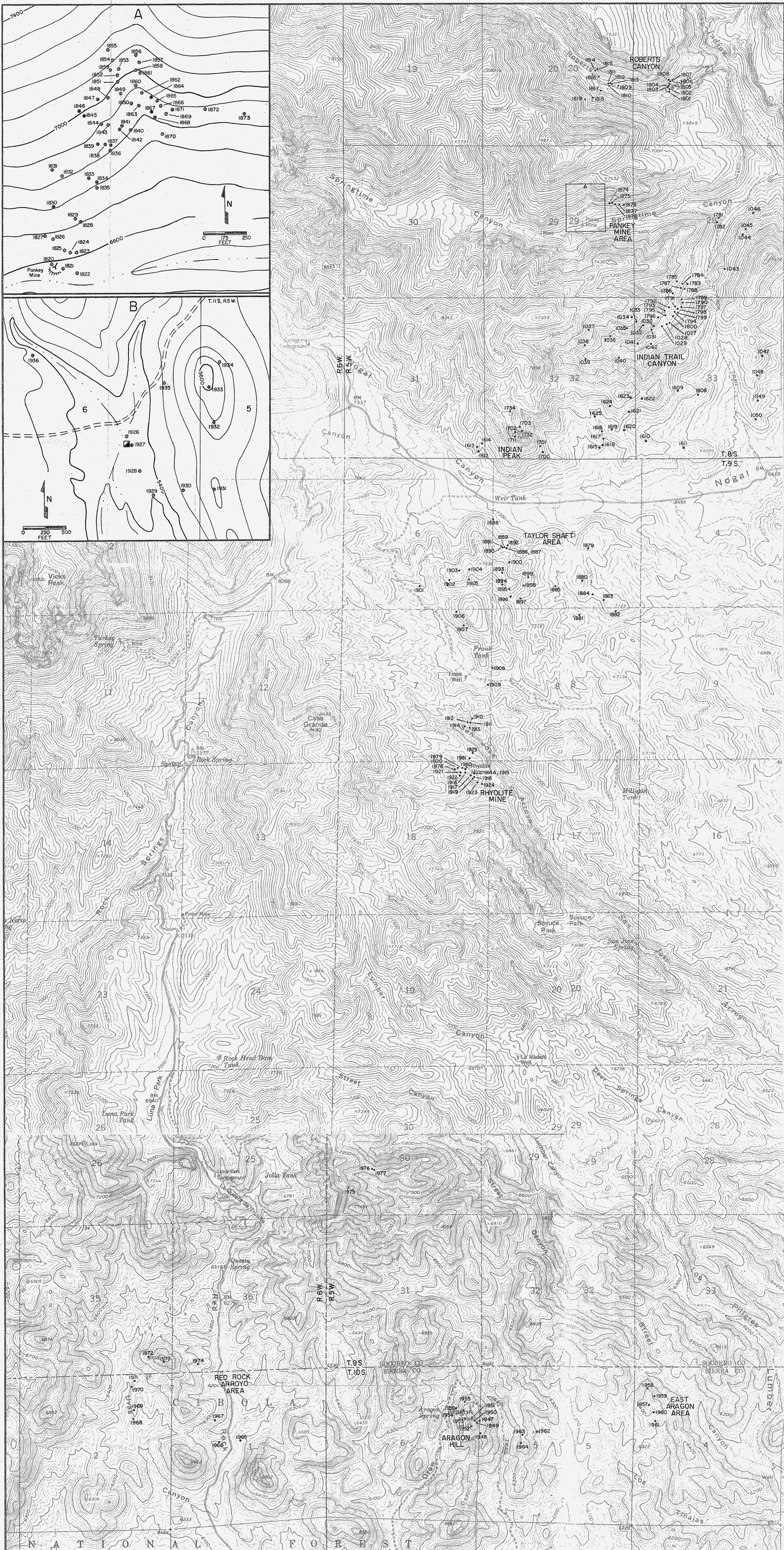


JON FORURIA
COLORADO STATE UNIVERSITY
1984

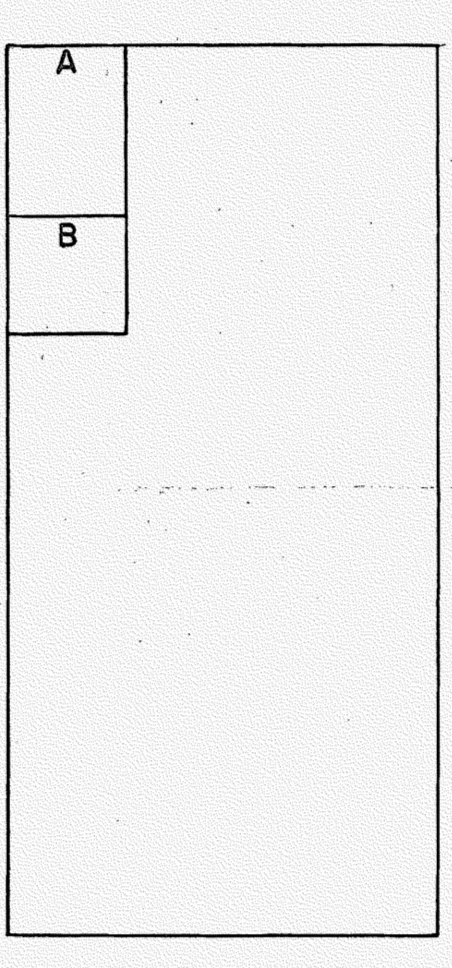
PLATE 2

DE 144
SG3FG7
1984
THESIS





EXPLANATION



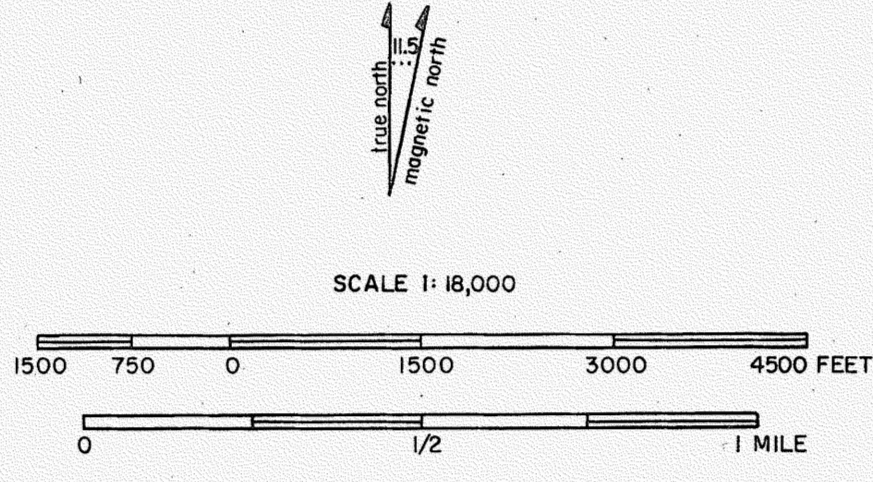
INSET (A) DEPICTS PANKEY MINE AREA ROCK CHIP SAMPLE LOCATIONS

INSET (B) DEPICTS SEFERINO, FIFTY-FIFTY HILL AREA ROCK CHIP SAMPLE LOCATIONS

UNDERGROUND SAMPLE LOCATIONS AT THE HENCKLEY MINE, ARAGON HILL APPEAR ON FIGURE 33.

1867
SAMPLE NUMBER AND LOCATION

REFER TO APPENDIX A FOR GEOCHEMICAL RESULTS AND SAMPLE DESCRIPTIONS



ROCK CHIP SAMPLE LOCATION MAP OF THE NOGAL CANYON STUDY AREA

SOUTHERN SAN MATEO MOUNTAINS
SOCORRO AND SIERRA COUNTIES, NEW MEXICO

JON FORURIA
COLORADO STATE UNIVERSITY
1984

PLATE 3

QE 144
.S 6367
1984
76515